

Doctoral thesis

Doctoral theses at NTNU, 2023:148

Yoko Arteaga

Material Appearance for Conservation and Restoration

Capturing and modelling the appearance of
gilded surfaces

NTNU
Norwegian University of Science and Technology
Thesis for the Degree of
Philosophiae Doctor
Faculty of Information Technology and Electrical
Engineering
Department of Computer Science



Norwegian University of
Science and Technology

Yoko Arteaga

Material Appearance for Conservation and Restoration

Capturing and modelling the appearance of
gilded surfaces

Thesis for the Degree of Philosophiae Doctor

Trondheim, April 2023

Norwegian University of Science and Technology
Faculty of Information Technology and Electrical Engineering
Department of Computer Science



Norwegian University of
Science and Technology

NTNU

Norwegian University of Science and Technology

Thesis for the Degree of Philosophiae Doctor

Faculty of Information Technology and Electrical Engineering
Department of Computer Science

© Yoko Arteaga

ISBN 978-82-326-7001-7 (printed ver.)
ISBN 978-82-326-7000-0 (electronic ver.)
ISSN 1503-8181 (printed ver.)
ISSN 2703-8084 (online ver.)

Doctoral theses at NTNU, 2023:148

Printed by NTNU Grafisk senter

Abstract

The human visual system is extremely efficient at identifying and recognising different materials. Rarely do humans mistake one material for another, and the appearance of a material tells us many important cues about the environment we live in. However, the mechanisms behind material appearance and perception are not fully understood.

Cultural heritage objects exist in a wide range of materials, each with its own particular appearance. While it is common to evaluate the colour of cultural heritage objects before and after restoration, this is not always representative of perceptual differences that the restoration may cause. Gilding is a form of polychromy commonly used in the Middle Ages which poses many technical challenges to acquire its appearance. The gold leaf, of metallic nature, creates a particular appearance which changes depending on the fabrication method and has a strong angular-dependence.

This thesis aims to address some of these issues, by acquiring, modelling and analysing the appearance of complex cultural heritage materials. Focus is given to gilded surfaces since they exhibit interesting appearance properties such as gloss, metallicity, and in some cases even translucency. The research is divided into two sub-objectives, one concerning methods for appearance capture, and the second deals with applying material appearance analysis for conservation and restoration.

The first research domain of this PhD thesis deals with methods for material appearance capture. First, the challenges and limitations of using conventional methods for appearance capture are explored. As an alternative, an imaging-based methodology is developed and evaluated for bi-

directional reflectance measurements, catered for cultural heritage materials of challenging appearance. This method is then applied to satisfy the second sub-objective.

The second research domain concerns the application of material appearance analysis for conservation. For this, the appearance of different types of gilding is acquired, modelled and evaluated. By using perceptual gloss metrics the different types of gilding can be described and characterised in terms of perceptual differences. Moreover, varnish removal methods are evaluated in terms of appearance change, to guide the conservation of a 15th century painted panel.

Acknowledgements

The research presented in this thesis was carried out as part of the CHANGE-ITN project¹; and as so, I have had the pleasure of spending my time at C2RMF, in the Louvre palace, and at NTNU, right next to lake Mjøsa. I could not have asked for a better experience, and for that reason I wish to acknowledge the people who have helped me along the way, and without whom this thesis would not have been possible.

First of all, I would like to express my gratitude to my supervisors Clotilde and Jon. Thank you for your guidance, support, and endless opportunities throughout this project.

I would like to extend my thanks to Nicolas for showing me around when I had just arrived at C2RMF, and for letting me work with so many interesting objects. I also have to include Angèle in these thanks, who brought me to INP, where I was given the opportunity to work alongside some great people.

I want to take this opportunity to thank my colleagues from C2RMF, and specially the *groupe imagerie*. Of course, I am deeply appreciative of my friends and colleagues from the Colourlab, at NTNU, for always making me feel welcome whenever I came to visit. Moreover, I would like to thank my co-authors Stéphanie and Diane, thank you for introducing me to the world of gilding, and Aditya, for helping me with everything BRDF related.

My heartfelt thanks go out to my fellow friends from CHANGE. The past three years would not have been the same without you. We have gone

¹This thesis has received funding from the European Union's Horizon 2020 research and innovation program under the Marie Skłodowska-Curie grant agreement No. 813789.

through so much and I wish you all the best for the future.

Finally, I am grateful for my friends and family who have supported me all this time. I am sure you are all tired of hearing me say I am writing my thesis, but I promise it is done now.

Contents

Abstract	iii
Acknowledgements	v
Contents	ix
I Introduction	1
1 Introduction	3
1.1 Motivation	4
1.2 Materials and Objects Investigated	6
1.3 Research Objectives and Questions	8
1.4 List of Contributing Papers	11
1.5 Research Framework and Scope	12
2 Background	15
2.1 Introduction	15
2.2 Theory of Conservation	15
2.3 Material Appearance and Perception	19

2.3.1	Colour Perception	21
2.3.2	Gloss Perception	21
2.3.3	Texture Perception	22
2.3.4	Translucency Perception	23
2.3.5	Metallicity Perception	23
2.4	Appearance Capture and Modelling	24
2.4.1	Bidirectional Reflectance Distribution Function Models	24
2.4.2	Multiangle Reflectance Measurements	28
2.4.3	Multispectral HDR Imaging	29
2.4.4	Perception-Based Evaluation of Appearance Models	32
2.5	Surface Microtopography	32
2.5.1	Topography Measurements	33
2.5.2	Typology of Surface Defects	34
2.6	Applications in Conservation Restoration	35
3	Summary of Articles	37
3.1	Introduction	37
3.2	Article A: Characterising appearance of gold foils and gilding in conservation and restoration	38
3.3	Article B: Image-based goniometric appearance characterisation of bronze patinas	40
3.4	Article C: HDR multispectral imaging-based BRDF measurement using flexible robot arm system	43
3.5	Article D: Appearance-based evaluation of varnish removal methods in gilded surfaces	46
3.6	Article E: Quantifying the appearance of gilded surfaces	50
4	Discussion	53

4.1	Research Contributions	54
4.1.1	Capture and model the appearance of complex cultural heritage materials	54
4.1.2	Apply material appearance analysis to guide conservation	59
4.2	Scope of the Research	62
4.2.1	Breadth of the Research	62
4.2.2	Research Impact	63
5	Conclusions and Future Perspectives	65
5.1	Conclusions	65
5.2	Future Perspectives	67
II	Original Papers	81
	Article A: Characterising appearance of gold foils and gilding in conservation and restoration	83
	Article B: Image-based goniometric appearance characterisation of bronze patinas	103
	Article C: HDR multispectral imaging-based BRDF measurement using flexible robot arm system	111
	Article D: Appearance-based evaluation of varnish removal methods in gilded surfaces	119
	Article E: Quantifying the appearance of gilded surfaces	143

Glossary

appearance the aspect of visual perception by which objects are recognised, described by colour, gloss, translucency and texture.

ASTM American Society for Testing and Materials.

BRDF bidirectional reflectance distribution function, describes the angular distribution of incoming and outgoing radiation for a surface or material. Here, it is considered the physical, measurable property of a material linked to its appearance.

BSDF bidirectional scattering distribution function, describes the angular distribution of scattering within a material.

burnishing mechanical action used in *water gilding* and *imitation gilding*, in which an agate stone is in sliding contact with the metal leaf, smoothing the surface and making it shinier.

C2RMF Centre of Research and Restoration of the Museums of France.

CCD charged coupled device.

CCS chromatic confocal sensing.

CFA colour filter array.

CHANGE-ITN Cultural Heritage Analysis for New Generations - Innovative Training Network.

CIE *Commission Internationale de l'éclairage [International Commission on Illumination]*.

CIE XYZ standardised three-dimensional, device independent colour space.

cleaning in the context of this thesis, cleaning refers to the removal of superficial layers of varnish.

colorimetry the discipline that quantifies and physically describes human colour perception.

colour appearance attribute related to the perception of the light-matter interaction ruled by the material's spectral absorbance.

conservation treatments applied to cultural heritage objects for their better understanding, to restore and preserve (also see *restoration* and *preservation*).

contrast gloss perceived relative brightness of specularly and diffusely reflecting areas.

CT Cook-Torrance.

CTF camera transfer function.

cultural heritage in the context of this thesis, it denotes tangible cultural artefacts, which have been passed on by past generations.

diffuse reflection reflection of light from a surface at many angles, caused by back-scattering at the surface.

DOI distinctness-of-image (see *DOI gloss*).

DOI gloss distinctness-of-image gloss, the perceived sharpness of images reflected on a surface.

gilding form of polychromy where a gold leaf is attached to a surface by different means (see *water gilding*, *oil gilding*, and *imitation gilding*).

gloss appearance attribute related to the perception of the light-matter interaction caused by the material's ability to reflect light with an angular distribution (also see *DOI gloss* and *contrast gloss*).

glossmeter device which captures the intensity of the reflected light at the mirror angle for specific angles of incidence, values are given in gloss units (also see *gloss* and *mirror angle*).

goniochromaticity ability of a material to show strong angular-dependent reflectance properties, causing a significant appearance change.

goniospectrophotometer device which captures the bidirectional spectral reflectance of a material at a range of angles of incidence and reflection.

HDR high dynamic range, where dynamic range is a measure of light intensity in an image from the highlights to the shadows.

HVS human visual system, part of the central nervous system, which gives humans the ability to detect and process visible light, as well as interpreting this information to form a representation of the surrounding environment.

imitation gilding form of polychromy where a burnished silver leaf is covered with a yellow resin to imitate the appearance of gold (see *gilding* and *resin*).

INP *Institut National du Patrimoine [National Heritage Institute]*.

light part of electromagnetic spectrum which is perceived by the human visual system, between 380 nm and 780 nm.

metallicity appearance attribute related to the perception of the light-matter interactions specific to metals.

mirror angle angle of reflection equal to that of incidence.

multiangle spectrophotometer device which captures the bidirectional spectral reflectance of a material at a fixed number of angles of incidence and reflection.

NTNU Norwegian University of Science and Technology.

patina form of metal polychromy used to decorate metallic artworks.

PCA principal component analysis, dimensionality reduction method.

preservation to maintain an object in its present form, avoiding further deterioration.

resin see *varnish*.

restoration to reveal an object's original form at some point in the past.

RMS root mean square.

SFA spectral filter array.

SNR signal-to-noise ratio.

sparkle angular-dependent texture visual effect where the surface exhibits points of high specular reflection.

specular reflection reflection of light from a surface at the mirror angle (see *mirror angle*).

surface reflectance light-matter interactions at the surface of the material which exhibits angular and spectral variations.

surface roughness three-dimensional variation of the material's surface.

texture appearance attribute related to the perception of the light-matter interaction caused by spatial variations on a material's surface. Can be related to *topography* or *surface roughness* of the material.

topography see *surface roughness*.

translucency appearance attribute related to the perception of the light-matter interaction caused by the material's ability to transmit light, where scattering is present.

varnish clear, translucent protective coating.

Part I

Introduction

Chapter 1

Introduction

The origin of conservation of cultural heritage in the Western world can be traced back to the 19th century, when ideas related to the Enlightenment gained popularity. Romanticism spread the notion that art, ancient objects, and sites, were worthy of recognition; public access to art and culture became widespread; and scientific practice became the primary form of investigation to access and avail truth. As a result, various schools of thought and conservation theories came to light. In current times, conservation is a collaborative effort relying heavily on scientific analysis.

Cultural heritage objects are composed of a variety of materials, each with its own unique, complex appearance. Analysing the material appearance of an object helps to understand the object's condition, value, and purpose, guiding conservation efforts. However, the mechanisms that allow the human visual system ([HVS](#)) to recognise the appearance of different materials is little understood ([Adelson, 2001](#); [Fleming, 2014](#)). Given that cultural heritage objects are made of a combination of materials with unique appearance properties, complex measurements are required to characterise their appearance.

This thesis has been written as part of a Ph.D. program in the [CHANGE-ITN](#) (Cultural Heritage Analysis for New Generations - Innovative Training Network) project and as a result of a collaboration between the Centre of Research and Restoration of the Museums of France ([C2RMF](#)) in Paris, France, the French National Centre for Scientific Research (CNRS), PSL-PCMTH UMR8247, and the Colourlab at the Norwegian University of Science and Technology ([NTNU](#)) in Gjøvik, Norway. It aims to develop ima-

ging techniques for appearance capture and modelling of cultural heritage materials to guide conservation efforts.

This chapter presents an introduction to the research work done as part of the Ph.D. It is sectioned into Motivation (Sec. 1.1), Materials and Objects Investigated (Sec. 1.2), Research Objectives and Questions (Sec. 1.3), List of Contributing Papers (Sec. 1.4), and Research Framework and Scope (Sec. 1.5).

1.1 Motivation

The integration of scientific methods into the field of conservation dates back to the early 19th century, and has had a significant impact on the discipline. These methods enable the evaluation of an object's condition, provide knowledge concerning its history, and warrant conservation techniques. Additionally, these practices are employed for monitoring weathering effects (Papanikolaou, Dzik-Kruszelnicka and Kujawinska, 2022), supporting restoration efforts (Cutajar et al., 2022), and advancing our understanding of material degradation processes (Martínez Domingo et al., 2019) and manufacturing methods (Arteaga, Mélard et al., 2022).

The recent increase in the use of digital imaging technologies in conservation has led to a wide range of applications, including the digitisation of cultural heritage objects for documentation (MacDonald et al., 2017), analysis (Deborah and Mandal, 2022), and digital restoration (Callet, Zymła and Mofakhami, 2002). No matter its application, it is vital that the digital copy of the cultural heritage object is representative of the real state of the object. Spectral imaging has been explored as a method for capturing the physical property of the object, its spectral reflectance, and by means of colorimetry, visualisations can be rendered which correspond to human perception. However, this approach is only feasible for flat objects with a relatively matte surface (Mandal et al., 2021), such as paintings.

Appearance is defined as “the aspect of visual perception by which objects are recognised” (ASTM, 2012), and it encompasses various visual attributes, as identified by the *Commission Internationale de l'éclairage [International Commission on Illumination]* (CIE). These include colour, gloss, translucency, and texture (Eugène, 2008). While it is common to describe and characterise materials based on these individual attributes, it has been proven that they influence each other (Ho, Landy and Malo-

ney, 2008; Vangorp, Laurijssen and Dutré, 2007). In conservation, surface appearance is traditionally described by colour and gloss. While the former may be sufficient to perceptually describe diffuse materials such as paint (CIE, 2004), complex materials with varying roughness exhibit different appearance (Simonot and Elias, 2004; Elias, Rie et al., 2006). The latter has proven unable to identify perceptual cues on which gloss appearance relies (Leloup et al., 2014; Ji et al., 2006; Obein, Leroux and Vienot, 2001). Moreover, these measurements are insufficient to characterise a wide range of materials which present interesting appearance properties such as goniochromaticity, translucency, and metallicity, to name a few.

Composite materials, such as gilding, are commonly present in many objects, including illuminated manuscripts, paintings, altarpieces, and sculptures. While it is challenging to create an accurate digital copy of an object containing gilded areas (Toque et al., 2010), it is possible to do so using spectral imaging techniques (MacDonald et al., 2017; Martinez et al., 2019). However, the resulting image will look flat, the gilding will not look golden, but brown, as the gold leaf's ability to reflect light is lost. In the same way that ageing of an object hinders the reading of its purpose and value (Kollandsrud, 2017), appearance changes between the object and its digital copy can also hinder its understanding and hence its value.

Bidirectional reflectance measurements are recommended to characterise the reflectance properties of goniochromatic ¹ materials so they can correlate to our perception of their appearance (Hunt and Pointer, 2011). Recommendations based on the material optical properties have been made by ASTM International (ASTM, 2012) and the CIE (Eugène, 2008). Commercial multiangle spectrophotometers measure the reflectance at a fixed combination of illumination and viewing angles and have been used for flake paints such as in the automotive industry (Ferrero et al., 2013). Goniospectrophotometers measure a broad range of illumination and viewing angles and then the bidirectional reflectance distribution function (BRDF) of the surface can be modelled (Nicodemus and Richmond, 1977).

The limitations of goniospectrophotometers are that the material must lie flat on the surface, while either the illumination or the acquisition

¹Goniochromatic materials are those which show strong angular-dependent reflectance properties. Normally, they present a change in hue. Although the materials investigated here do not change in hue, their reflectance has a strong angular-dependence which causes a significant appearance change.

sensor moves to perform the measurements (Sole, Farup et al., 2018). This can be time consuming and expensive, and moreover, this equipment is not widely available in cultural heritage institutions. As a solution, imaging-based measurements could be favoured. They have been widely used in the computer graphics field (Marschner et al., 1999; Guarnera et al., 2016), for human skin measurements (Lu, Koenderink and Kappers, 1998; Marschner et al., 1999), and for packaging print materials (Sole, Guarnera et al., 2021).

The aim of this thesis is to:

Explore material appearance analysis, with focus on evaluating the appearance of gilded surfaces, to guide conservation and restoration treatments.

More specifically, the aim is to acquire, model, and evaluate the surface appearance of challenging materials, specifically patinated bronze and gilded wood. These materials have been chosen because they present complex appearance properties which vary goniometrically. The intention of this research is to apply material appearance analysis in the context of conservation and restoration, by using this framework to guide conservation treatments. Given that the acquisition of the material appearance of these surfaces is not a banal task, it is favourable to use an imaging-based method as an alternative to commercial devices. Moreover, the acquisition of surface appearance is a current problematic in many industries and research areas, not only cultural heritage. For this reason, a secondary aim of this PhD project is to:

Evaluate the suitability of an imaging-based method for appearance capture of goniochromatic materials.

1.2 Materials and Objects Investigated

In order to achieve the aims of this thesis two materials, each with their own problematic, have been chosen: gilded wood and patinated bronze. These materials are representative cultural heritage objects, and serve to investigate surface modifications and their impact on surface appearance.

Gilded wood Gilding is a form of polychromy where a gold leaf is attached to a surface. Frequently used in the Middle Ages (Courtier and

Dubost, 2021), gilding has a complex surface appearance due to the metallic nature of gold. Due to its metallic properties, it is insufficient to characterise its appearance with traditional methods such as colorimetry and gloss measurements.

Often times, gilding can be varnished to protect its surface and modify its appearance (Neven, 2016; Kollandsrud and Plahter, 2019; Chaban et al., 2021; Sandu, Busani and Sá, 2011). Varnish being an organic material, changes aspect over time and a common conservation practice is to clean it or remove it, to reveal the original aspect of the gilding. While the chemical removal of varnish is a widely studied practice in the field of painting conservation (Learner et al., 2007; Wolbers, Stavroudis and Cushman, 2020; Mecklenburg, Charola and Koestler, 2013), there is little knowledge of its effects on gilded wood. Moreover, the appearance and perception of gilding has not been thoroughly investigated, resulting in a lack of dedicated technical vocabulary leading to misconceptions and misunderstandings.

As part of a collaboration with the *Institut National du Patrimoine [National Heritage Institute]* (INP) in Paris, a 15th century painted panel and its 19th century gilded frame were restored as part of a final year conservation studies project (Marchioni, 2021). The painting in question, named after its iconography, the *Vierge de douleur [Virgin of Sorrows]* (Fig. 1.1), went through a restoration campaign. In order to guide the conservation treatments, gilding mock-ups were fabricated to evaluate chemical varnish removal methods. This research focused on the evaluation of appearance changes caused by the conservation treatments. This material concerns **Article A, D and E**.

Another form of gilding, called “imitation” gilding (Kollandsrud, 2017), popular in Norway in the 13th century is also investigated. This gilding is produced by applying a yellow pine resin over a burnished silver leaf creating a glossy appearance imitating that of gold. While it has been argued this material was used as an alternative to gold leaf, its peculiar appearance might contest this hypothesis. Moreover, the composite nature of the “imitation” gilding implies different light-matter interactions take place at the surface of the material. Samples of “imitation” gilding, produced in 2017 at the Cultural History Museum, University of Oslo, Norway, have also been investigated, and its appearance is evaluated in **Article E**.



Figure 1.1: Unknown. *Vierge de douleur* [Virgin of sorrows]. 15th century. Painted panel. 36.8 x 34.0 cm (62.3 x 43.0 cm with frame). Jacquemart-André Museum, Paris. **a** Before restoration. **b** After restoration. ©Angèle Dequier/Inp

Patinated bronze Patinas are a form of metal polychromy where the surface of a metal is modified chemically to alter its appearance. Different recipes give the metal a different colour (Edelson, 2000). In this thesis, patinas from the Coubertin foundry in Paris, famous for making Rodin's sculptures, were used as samples to evaluate the feasibility of using an imaging-based method for appearance capture.

The patinas chosen are present in three colours: red, green and black; and two surface finishes: smooth and rough. The patinas were chosen because of their variability in both hue and roughness. They have a metallic, goniochromatic appearance and a slight specular gloss. This material concerns **Article B** and **C**.

1.3 Research Objectives and Questions

As described in the previous section, the aim of this thesis is to analyse the material appearance of cultural heritage objects for conservation, with emphasis on acquisition and modelling. Due to the specular nature of the surfaces and the fragility of the samples, non-contact imaging techniques are favoured for the acquisition of material appearance.

In order to achieve this aim, two sub-objectives have been defined. The first sub-objective is closely related to the technical domain and deals with methods for appearance measurement. The second sub-objective

deals with cultural heritage conservation and restoration and focuses on gilded surfaces. For each sub-objective, a set of research questions have been formulated.

Sub-objective 1: *Capture and model the appearance of complex cultural heritage materials*

Appearance, as previously defined, is “the aspect of visual perception by which objects are recognised” (ASTM, 2012). Due to the perceptual nature of appearance, goniochromatic materials pose a technical challenge as their appearance cannot be described by solely by individual measurements. Previous research has shown that the perception of the four appearance attributes, colour, gloss, translucency, and texture, influence each other (Eugène, 2008). Thus, more complex measurements such as the BRDF are necessary. Here, the BRDF of the surface is considered the physical, measurable property of the material which is linked to appearance.

Commonly, the BRDF of different materials is measured using goniospectrophotometers. These devices measure the reflectance of a surface at a wide combination of viewing and illumination directions. However, these devices are expensive and the measurements are time consuming. Since the context of this research work is in the field of conservation, it is favourable to choose acquisition devices which can be easily implemented in museums or conservation workshops. Thus, imaging-based solutions and hand-held commercial devices are favoured due to their flexibility. Finally, different analytical BRDF models exist (Guarnera et al., 2016) which have been proven successful at estimating the appearance of different materials. However, as previously explained, their application to real cultural heritage surfaces is very limited with the few examples being paint (Chen, Taplin and Berns, 2011) and glazes (Simonot, Elias and Charron, 2004).

For this sub-objective, the following research questions have been formulated:

- RQ1** What are the challenges and limitations of measuring the appearance of gilded surfaces using portable, commercially available devices?
- RQ2** Is it possible to perform material appearance measurements of goniochromatic, cultural heritage materials using imaging devices?
- RQ3** How reliable are the measurements obtained from an imaging setup

in comparison to a commercially available goniospectrophotometer?

Sub-objective 2: *Apply material appearance analysis to guide conservation*

Conservation treatments pose many ethical issues. Caple (2012), proposed the “RIP” model, where conservation is guided by three principal opposing goals: revelation, investigation, and preservation.

Revelation, aims to reveal the objects original form at some point in the past. “The visual form can be restored to give the observer, (...) a clear visual impression of the original form or function of the object (...)”. Investigation, on the other hand, are “forms of analysis which uncover information about the object, from visual information (...) to completely destructive analysis (...)”. Finally, preservation, is “the act of seeking to maintain the object in its present form, without any deterioration”. Considering conservation as the balance of these three activities, material appearance analysis should address all of them.

To address this sub-objective, the research work will focus on the appearance of gilding. To solve the “revelation” question, a collaborative work has been carried out with the INP to guide the restoration of a 15th century painted panel. For this aim, different varnish removal methods were tested on gilding mock-ups. The different methods are evaluated in terms of appearance change. A desirable quality of the chosen method (amongst others) is its ability to restore the original appearance of the gilded wood.

On the other hand, “investigation”, requires both qualitative and quantitative observations to evaluate an object. The concepts of material appearance and perception are not fully understood and correlated. Colorimetry is the most advanced of the material appearance fields, with efforts being made in gloss (Chadwick and Kentridge, 2015), translucency (Gigilashvili, Thomas et al., 2021), and texture (Conni, 2022). However, gilded surfaces present a metallic appearance that falls in an ambiguous category (Toscani et al., 2020). Thus, it is important to use more complex measurements which describe more accurately the appearance of the objects investigated. For this purpose, the appearance of three types of gilding, water gilding, oil gilding, and “imitation” gilding, will be “investigated”.

Finally, digital models and reconstructions could offer an alternative solution for the task of “preservation”, at least for digitally preserving the ap-

pearance of an object at a given point in time. For the digital models to be accurate, perceptually faithful appearance models are necessary.

With these three concepts in mind, the final research question is formulated:

RQ4 Is it possible to use BRDF models to perceptually evaluate the appearance of gilded surfaces for conservation purposes?

1.4 List of Contributing Papers

The research that constitutes this thesis is presented in five core research papers, **Article A** to **E** covering the research questions discussed in Sec. 1.3. Four of them have been published through peer-reviewed publication channels, whereas the remaining one is under revision and to be published in a book. The publications are listed in the order that corresponds to the thesis narrative. The related papers are part of the work carried out during the PhD period but do not contribute to the main research work.

Core Papers:

Article A: *Characterising appearance of gold foils and gilding in conservation and restoration*

Arteaga, Y., Sole, A., Hardeberg, J. Y. & Boust, C.

Proceedings of the 11th Colour and Visual Computing Symposium, September 8-9, 2022, Gjøvik, Norway

Article B: *Image-based goniometric appearance characterisation of bronze patinas*

Arteaga, Y., Boust, C., Déquier, A. & Hardeberg, J. Y.

Proceedings of the 29th Color and Imaging Conference, November 1-4, 2021, Virtual

Article C: *HDR multispectral imaging-based BRDF measurement using flexible robot arm system*

Arteaga, Y., Boust, C., & Hardeberg, J. Y.

Proceedings of the 30th Color and Imaging Conference, November 13-17, 2022, Scottsdale, USA

Article D: *Appearance-based evaluation of varnish removal methods in gilded surfaces*

Arteaga, Y., Marchioni, D., Courtier, S., Boust, C. & Hardeberg, J. Y.

Heritage Science, **11**, 31 (2023)

Article E: *Quantifying the appearance of gilded surfaces*

Arteaga, Y., Boust, C. & Hardeberg, J. Y.

To appear in: *Cultural Heritage Analysis for New Generations*, Degrigny, C., George, S., Hardeberg, J.Y. & Østlien, A., editors, Routledge, 2023

Related Papers:

- *Semiautomatic Toolmark Classification in Chased Metals Using Surface Microtopography*
Arteaga, Y., Mélard, N., Boust, C., Hardeberg, J. Y. & Robcis, D.
Heritage, 2022; **5**(4):2922-2943.
- *Multi-scale Painter Classification*
Ciortan, I. M., **Arteaga, Y.**, George, S., & Hardeberg, J. Y. Proceedings of the International Conference Florence Heri-Tech: the Future of Heritage Science and Technologies, 2022, Florence, Italy.
- *SHREC'20 Track: Retrieval of digital surfaces with similar geometric reliefs*
Thompson, E. M., (...), **Arteaga, Y.**, et al.
Computers & Graphics, 2020; **91**:199-218.

1.5 Research Framework and Scope

A visual rationale is provided in Fig. 1.2, to aid the narrative of the thesis and how each paper is related to each other, to the research objectives and questions, and to the materials analysed.

To answer the primary and secondary aims of this thesis, defined in Sec. 1.1, two sub-objectives have been defined. Sub-objective 1, deals with methods for appearance measurement, where the relevant research questions are **RQ1**, **RQ2**, and **RQ3** answered by **Article A**, **B**, and **C**. The results from **Article C** are considered the culmination of the secondary aim. The imaging system presented there is used in the second sub-objective, which deals with applying material appearance analysis to conservation and restoration of gilded surfaces. It is related to **RQ4**, and answered by **Article D** and **E**.

Article A discusses the challenges and limitations of using commercial hand-held multiangle spectrophotometer to capture the bidirectional re-

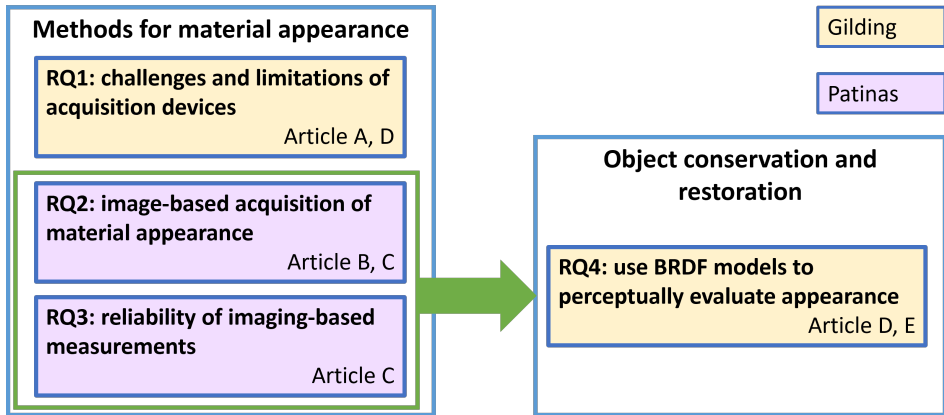


Figure 1.2: Overview of the research objectives and their relationship to the core publications and objects studied.

flectance of gold leaves commonly used for gilding, and gilding mock-ups.

Article B and **C** present imaging-based setups for capturing the goniochromatic appearance of bronze patinas. In both articles, the appearance of the patinas is correlated to the surface roughness of the samples. **Article B** discusses a modified method commonly used for the characterisation of sparkle based on a charged coupled device (CCD) camera, a light source, and a tilting platform. **Article C** evaluates the accuracy of an in-house built system compared to that of a commercial goniospectrophotometer. The system is composed of a robotic arm used to move the light source, a multispectral snapshot camera, and a tilted stage.

Article A and **D** aim at modelling the BRDF of gold leaves and gilding mock-ups. **Article A** uses data acquired by a commercial handheld multi-angle spectrophotometer. In **Article D**, the imaging system presented in **Article C** is used to acquire the bidirectional reflectance of the mock-ups and their BRDF is modelled. The gilded surfaces are classified depending on their fabrication method and conservation treatment.

Article D and **E** use the data obtained from the setup in **Article C** to visualise and evaluate the appearance of gilded samples in terms of perceptual gloss attributes. **Article D** poses the question of evaluating chemical varnish removal methods, while **Article E** compares two types of gilding and a third imitation gilding.

Here it must be noted that throughout the thesis, the **BRDF** is considered to be the physical property of materials linked to appearance. While appearance encompasses colour, gloss, translucency and texture, the materials investigated here have a strong angular-dependence which requires goniometric measurements.

Chapter 2

Background

2.1 Introduction

This chapter provides an overview of the foundations on which this thesis lies. It starts with a review of basic concepts on conservation and restoration practice and the needs from the community (Sec. 2.2). The next section defines material appearance and perception (Sec. 2.3), and the following section, how to capture and model it, and how to evaluate appearance models (Sec. 2.4). Next, surface microtopography is introduced, acquisition systems and the analysis of microtopographic data (Sec. 2.5). The final section presents research on material appearance applied to cultural heritage (Sec. 2.6).

2.2 Theory of Conservation

Currently in France ¹, there are three major criteria underlying the practice of conservation: the stability of the materials used, the reversibility of their application, and the legibility of the resulting work. Any addition to a heritage object during conservation and restoration must meet these three criteria to be acceptable. The stability of the materials is essential and they cannot have an impact on the original object.

The theory of conservation began to take shape during the 18th century, when François-Toussaint Hacquin, painter and relining artist, wrote:

¹Unlike hard scientific disciplines which are universal, conservation practice follows criteria which vary amongst different countries, cultures, and time periods. This thesis was conducted in France; and thus, follows French criteria for conservation.

“Given that we are far from being infallible, it is prudent to leave to our successors the means of resolving any accidents that our lack of foresight or our self-esteem may occasion” (Philippe, 2008).

Hacquin was concerned about the stability of materials, and aware of the need to be able to “reverse” a restoration; he also documented in detail all the cases entrusted to him. A revealing example of the thoughts at the time is the “varnish quarrel” that took place at the end of the 18th century. Philip Hackert advocated for the use of a turpentine-based varnish which is reversible, and ages better than the usual oil varnish. Its opponents maintained that such a varnish, of a different nature from that of the components of ancient canvases, would distort the artworks (Philippe, 2008). This is still a debatable subject.

Classical theorists act according to the pursuit of *Truth*; truth must be preserved or revealed. This *Truth* is defined differently by different classical theories², and there are various factors affecting *Truth*: the history of the object, artistry, material components, documentary efficiency, and material function to name a few.

In the 19th century, the architect and theoretician Viollet-le-Duc insisted above all on stability, and the absence of reversibility. He recommended the use of the same materials as in the original object, and even higher quality materials if the originals showed weaknesses. “To restore a building is not to maintain, repair or redo it, it is to restore it to a complete state that may never have existed at a given time” (Viollet-le-Duc, 1875).

Viollet-le-Duc is the apostle of the theory of reinvention. For him an object’s true nature was the producer’s intent and the object’s aesthetic qualities. These interventions, often criticised today, have had the merit of bringing certain major sites back to life, such as Carcassonne or the Château de Pierrefonds. As an extreme opponent of Viollet-le-Duc’s philosophy, John Ruskin advocates for non-restoration: “What is called restoration means the most complete destruction that a building can undergo” (Ruskin, 2008).

For Ruskin, any restoration should be banned, a work of art only has meaning through the modifications it has undergone over time. Ruin is its final state, and authenticity is the primordial factor which should not

²Classical theorists may have very different philosophies, but they share the common principle of the pursuit of *Truth*. Here *Truth* is the notion of truth as the key value in conservation and a goal in itself (Muñoz-Viñas, 2002).

be intervened with. This point of view is more aesthetic than realistic.

In the later 19th century, Boito's *restauro scientifico* [*scientific restoration*] gained popularity (Muñoz-Viñas, 2012). His theory retained truth as a guiding principle, but advocated for an objective method to achieve truth. Camillo Boito insisted on the fact that a restoration must allow the conservation of the works, as well as the respect of their authenticity. Consequently, the modern consolidation and restoration must be distinguished from the ancient object. Boito recommends the use of materials with different appearance from the original, and the addition of inscriptions or explanatory plaques of the intervention. The readability criterion includes two notions:

- How to read the original work? In particular, if the work has been heavily modified over the centuries, should it be de-restored to return it to its original state?
- The readability of modern restoration interventions. This is a major point, the restoration should not be the creation of a fake.

Today, *Teoria del Restauro* [*Theory of Restoration*] by Cesare Brandi (Brandi, 2001), is one of the major texts which serves as the philosophy of restoration in France. Brandi details three principles: readability, stability and reversibility. He emphasises that the restoration must save the work at the time it is considered, and facilitate any future restorations so the work is made to last. In practice, restorers have to make a choice between what is possible to do on an artwork to preserve it and what is the best thing to do, according to the philosophy of restoration. The collection manager and the conservator have the responsibility to decide which interventions are carried out.

"It is a challenge to the restorer's sense of responsibility to decide how much of what it is possible to do through science and technology should in fact be used and done. In a philosophy of abstinence there is scope for placing what is feasible at a subsidiary level and one's own attitude under higher aspects" (Althöfer, 1981).

The notion of reversibility poses a problem, as it assumes that any action performed on the artwork is completely reversible, which in practice is not always possible. Conservators now favour reprocessability, any future intervention must remain possible, or removability, any added material must be able to be removed (Bertholon, 2017).

Scientific conservation, or material theory of conservation, establishes how the restored object should be, by determining precisely how it was at a given moment. It also determines which conservation techniques and materials are more efficient, and monitors the development of a given conservation process.

There are four main objectives to scientific conservation (Clavir, 2012), or material theory of conservation:

- Attempt to preserve the true nature of objects. This is common to all classical theories of conservation.
- An objects true nature relies on its material constituents. This risks falling under material fetishism³.
- Techniques and target state of the conservation should be determined by scientific means.
- Scientific conservation produces results that are better than non-scientific techniques.

The scientific conservation approach is a contested philosophy. The Nara document notes that authenticity and value cannot be judged within fixed criteria since they are linked to “the worth of a great variety of sources of information”. These sources of information include “form and design, materials and substance, use and function, tradition and techniques, location and setting, and spirit and feeling, and other internal and external factors” (UNESCO World Heritage Committee, 1994).

Moreover, there is great controversy as scientific conservation is grounded on the assumption that it improves conservation practice from a technical point of view (Muñoz-Viñas, 2012).

Some limiting factors which create a lack of pragmatical relevance for conservation are the lack of communication between conservators and scientists, the irrelevance of some scientific conservation research to actual conservation practice, and the inability of science to cope with complex material problems such as those of conservation objects (Bradley, 1997). These are mostly based on practical consideration. Nevertheless,

³Material fetishism is a term coined by Petzet (1999). He says that for most Western people, there is a *belief* that the conservation of the material components of an object, even when the result of the conservation is unperceived, is a worthwhile endeavour.

scientific practice in conservation allows and facilitates to assess an objects condition, know an objects history, and warrants a given conservation technique.

Caple (2012), proposes a RIP approach, which stands for revelation, investigation, and preservation. Revelation entails cleaning and exposing to reveal the objects original form at some point in the past. This lies in the visual form to give the observer a visual impression and interpretation of the object. Investigation is the analysis which uncovers information about the object. Multiple forms of analysis fall under this category including destructive analysis. Finally, preservation seeks to maintain the object in its current state.

Since there are many truths within an object, Muñoz-Viñas (2012), suggests seeking meaning rather than truth by preserving or improving the scientific meaning of an object, its social and symbolic meaning for a large group, and its sentimental or symbolic meaning for small groups or individuals. An object has value and function, where its function could be related to political, economic, or social aspects, its value is what people place upon the object.

Throughout this PhD thesis, ethical and philosophical questions around conservation have been considered. The contribution of this research is meant to serve as a tool to support conservators and restorers. For this reason, the research work has been carried out in close collaboration with conservators and restorers from different specialities, at different institutions, to avoid falling into a "non-pragmatical" research framework.

2.3 Material Appearance and Perception

Appearance is defined as "the aspect of visual perception by which objects are recognised" (ASTM, 2012), and it encompasses various visual attributes. The CIE identified four main features (Eugène, 2008): colour, gloss, translucency, and texture. Here, the appearance of a surface is defined as the physical, optical structure of a material which under a certain illumination, is perceived by the HVS in the form of an appearance response. The material itself is a distal stimulus, which requires illumination for it to be observed. The interaction of the light with the physical properties of the material creates a stimulus which is perceived by the observer. The retinal and neural characteristics of the HVS convert the stimulus into an appearance response (Hutchings, 1995). The HVS is capable of interpreting the appearance response and inferring the material prop-

erties as well as the lighting conditions. By using (hard) metrology, the structure and physical properties of the material can be measured and modelled (Pointer, 2003; Choudhury, 2014). In turn, these can then be reproduced (Elkhuizen et al., 2019; Dorsey, Rushmeier and Sillion, 2010). However, the physical properties of the material alone cannot predict the perception of the material. Although the HVS interacts and recognises multiple materials constantly, the mechanisms which relate the physical properties of surfaces and our perception of them is not well understood.

Pointer (2003), defined the concept of soft metrology as “the measurement of parameters that, either singly or in combination, correlate with attributes of human response”. Soft metrology aims to develop measurement techniques and models which enable to quantify properties of materials which are determined by human responses (Eugène, 2008). This is mainly based on psychophysics which is defined as “the study of the functions relating the physical measurements of stimuli and the sensations and perceptions the stimuli evoke” (ASTM, 2012).

While a lot of attention has been given to the perception of objects, material perception has been investigated rather little. Adelson (2001), claims we tend to talk about “things” rather than “stuff”. Where “things” are objects that can be counted such as chairs, “stuff” are materials of unspecified extent such as snow. The HVS is extremely efficient at perceiving and recognising different materials. However, the perceptual mechanisms that underlie this are still poorly understood. The perception of materials are generally grouped according to appearance attributes such as colour, gloss, translucency and texture (Anderson, 2011; Eugène, 2008). Intuitively, perceptual attributes can be linked to specific physical material properties. For example linking spectral absorbance to colour perception, or surface reflectance to gloss perception. However, research has shown that generally, there is no one-to-one correspondence between single physical properties and perceptual attributes.

Moreover, multiple studies have found that the perception of a single appearance attribute influences another one. For example, the perception of gloss and surface topography influence each other (Ho, Landy and Maloney, 2008; Vangorp, Laurijssen and Dutré, 2007; Olkkonen and Brainard, 2011; Wijntjes and Pont, 2010). It has also been found that illumination characteristics influence the judgement of glossiness (Doerschner, Boyaci and Maloney, 2010; Fleming, Dror and Adelson, 2003; Olkkonen and Brainard, 2010; Obein, Knoblauch and Viénot, 2004; Te Pas and Pont, 2005), and that sub-surface scattering plays a role in glossiness

perception (Gigilashvili, Shi et al., 2021). This implies that the study and characterisation of surface appearance is a complex task which cannot focus on a single appearance attribute.

The following sub-sections will focus on the perception mechanisms of the four appearance attributes, colour, gloss, translucency, and texture, as well as metallicity.

2.3.1 Colour Perception

Colour appearance and perception is the most successful and advanced application of soft metrology. Colorimetry was standardised in 1931 by the CIE, with the definition of the CIE XYZ tristimulus space (Smith and Guild, 1931). Recently, more advance and complete models are being presented, which take into account finer aspects of colour appearance (Fairchild, 2013).

2.3.2 Gloss Perception

Gloss perception is a field which is subject of study and discussion (Chadwick and Kentridge, 2015). Hunter (1937), defined six perceptual dimensions of gloss:

- specular gloss: related to the perceived shininess or brilliance of highlights;
- contrast gloss (or luster): associated with the contrast between specularly reflecting areas and diffusely reflecting areas;
- distinctness-of-image gloss: the distinctness and sharpness of the observed reflected image;
- absence-of-bloom gloss (or haze): related to the presence of a haze or a milky appearance adjacent to reflected highlights;
- absence-of-surface-texture gloss: surface evenness, or the absence of visible texture;
- sheen: the perceived gloss at grazing angles of otherwise matte surfaces.

Using a set of achromatic painted samples in which at least three of the gloss attributes defined by Hunter could be perceived simultaneously, O'Donnell and Billmeyer Jr (1986) and Billmeyer Jr and O'Donnell (1987),

found that observers could not distinguish more than one gloss dimension. Using computer renderings Ferwerda, Pellacini and Greenberg (2001) and Wills et al. (2009), investigated gloss perception and found two perceptual dimensions of gloss, contrast gloss and distinctness-of-image gloss.

Ferwerda, Pellacini and Greenberg (2001), present a psychophysically-based model for gloss perception. The authors define contrast gloss and distinctness-of-image gloss as perceptual dimensions of gloss, and define these as metrics that relate changes in apparent gloss to variations in the physical parameters of the isotropic version of Ward's light reflection model (Eq. 2.4).

Optical instruments, namely glossmeters, have been used by many industries for the physical measurement of specular gloss. Glossmeters measure the flux reflected from a material compared to the flux reflected from a standard under the same measurement conditions. The primary standard is defined to be a perfectly polished material with a refractive index of 1.567 at 589.3 nm (Budde, 1980). Materials such as metals, with higher refractive index can show gloss units (GU) higher than 100. Since these devices were originally intended to judge gloss differences of surfaces with similar appearances, their results are not reliable to estimate the gloss appearance of a surface.

Leloup et al. (2014), provide an overview of aspects that play a role in gloss perception, namely: illumination, object properties, and viewing conditions (including binocular vision and motion). Most importantly, this research highlights that gloss measurements relate poorly with gloss perception. Moreover, a non-linear relationship between gloss measurements and gloss perception was found using achromatic and chromatic painted samples (Obein, Knoblauch and Viénot, 2004; Ji et al., 2006).

2.3.3 Texture Perception

The perception of texture is highly related to the surface topography of a material. According to Anderson (2011), the perception of three-dimensional shape variations belongs to three categories: the microscopic scale, which plays a significant role in surface reflections although indistinguishable with the naked eye; mesoscale, describes the coarseness of the surface and can be called topography; and the macroscopic scale which generally describes the shape of an object. Research has suggested that the microscale and mesoscale roughness influence the per-

ception of the gloss of a surface (Qi et al., 2012), where microscale roughness had a linear relationship, and mesoscale roughness a non-linear relationship to the perceived glossiness.

2.3.4 Translucency Perception

The perception of translucency is related to the transmission of light in materials. Translucency is caused by the scattering of light in the volume of the material which gets reflected back into the first medium. At opposite ends of the scale lie a transparent material where no light is reflected to the first medium, and an opaque material where light is only reflected from the first interface.

Research has focused on the effect of light refraction (Fleming, Jäkel and Maloney, 2011), suggesting the HVS uses the degree of distortion of the background for estimating the refractive index of a material. Also, varying lighting conditions show that the illumination and phase function relates to our translucency perception (Fleming and Bülthoff, 2005; Xiao et al., 2014). The study of translucency perception is starting to accumulate an important amount of literature (Gigilashvili, Thomas et al., 2021), and standard perceptual models are being developed (Urban et al., 2019).

2.3.5 Metallicity Perception

Metallicity is not formally defined as an aspect of material appearance. However, it has been identified as one of the perceptual dimensions for specular and diffuse reflection (Toscani et al., 2020). The perception of metallic surfaces falls in an ambiguous category. Metals do not have diffuse reflection, because their high extinction index prevents back-scattering. While polished metals have a flat surface microgeometry which causes sharp specular reflection, rough metals have a diffuse-like appearance due to scattering at the surface. The appearance of non-achromatic metals such as gold and copper, has commonly been described as a combination of colour and gloss (Todd and Norman, 2018; Komatsu et al., 2013). However, as illustrated by Harvey and Smithson (2021), this comes from an incomplete consideration of gloss as specular reflectance.

While the HVS accurately judges an object as metallic rather than shiny such as porcelain or glass (Fleming, Wiebel and Gegenfurtner, 2013; Sharan, Rosenholtz and Adelson, 2014; Tamura, Higashi and Nakauchi, 2018; Vangorp, Barla and Fleming, 2017), computer vision systems find these distinctions problematic (Bell et al., 2015; Liu et al., 2010). How-

ever, in the case of achromatic polished metals, there is a perceptual overlap between the appearance of metallic and transparent stimuli. When observers are left without motion cues from dynamic stimulus, mirror objects are qualified as glass up to 40 % of the time, depending on the object's geometry (Tamura, Higashi and Nakauchi, 2018). Toscani et al. (2020), suggest that the perception of achromatic reflection is based on a three-dimensional space where "lightness" relates to diffuse reflection, "glossiness" to the presence of high contrast, sharp specular highlights, and "metallicity" to spread out specular reflections.

2.4 Appearance Capture and Modelling

As defined in the previous section, the appearance of a surface is the physical, optical structure of a material, which creates an appearance response when exposed to a certain illumination. While the appearance of a surface can be described by its colour, gloss, translucency, and texture (Eugène, 2008), research has shown that the perception of these four attributes is linked, and in the case of real materials they cannot be individually studied⁴. For this reason, it is relevant to characterise the appearance of a surface by considering how it interacts with light, not only spectrally but also angularly. For this reason, in this research the BRDF of the surface is considered the physical, measurable property of the material which is linked to its appearance.

2.4.1 Bidirectional Reflectance Distribution Function Models

The reflectance $\beta(\lambda)$ of a material is defined as following:

$$\beta(\lambda) = \frac{\Phi_r(\lambda)}{\Phi_i(\lambda)}, \quad (2.1)$$

where Φ_r and Φ_i are the light flux reflected by the surface and the flux incident on it, respectively (Hecht, 2012). $\beta(\lambda)$ is thus, a function that describes the effectiveness of the material in reflecting radiant energy. Given a detector with a set of sensitivities $\tau_i(\lambda)$, the signal acquired by its i th channel can be calculated as (Lapray et al., 2017):

$$\phi_i = \int_{\Lambda} E(\lambda)\tau_i(\lambda)d\lambda = \int_{\Lambda} \beta(\lambda)S(\lambda)\tau_i(\lambda)d\lambda. \quad (2.2)$$

⁴With the exception of particular materials such as matte, Lambertian surfaces, commonly used for colour perception experiments, or digitally rendered surfaces in the case of gloss perception.

Here, $E(\lambda)$ is the spectral irradiance emitted by the sample under analysis, $\beta(\lambda)$ is its reflectance, $S(\lambda)$ is the spectral irradiance of the illumination source and Λ is the spectral domain of interest⁵. The reflectance can be calculated by dividing the emitted irradiance, $E(\lambda)$, over the irradiance of the light source, $S(\lambda)$, incident on the sample (Pedrotti, Pedrotti and Pedrotti, 2017).

The bidirectional reflectance of a material can be modelled using the **BRDF** (Nicodemus and Richmond, 1977). The **BRDF** describes how light is reflected off a surface. It is defined by the ratio between the differential irradiance along \mathbf{l} at point x and the differential outgoing radiance along \mathbf{v} :

$$f(x, \mathbf{l}, \mathbf{v}) = \frac{dL_r(x, \mathbf{v})}{dE(x, \mathbf{l})} \quad (2.3)$$

For a **BRDF** model to be physically valid it must obey two properties: be energy conserving and reciprocal. Due to the law of conservation of energy, the radiant energy reflected at a surface must not be greater than the energy incident on the surface. The second property is known as Helmholtz reciprocity, which dictates that the **BRDF** must be symmetrical. This means that reversing incoming and outgoing light does not change the **BRDF** outcome. Moreover, the **BRDF** ignores sub-surface scattering, assuming that the incident light on an opaque homogeneous surface is reflected from the same point (Nicodemus and Richmond, 1977).

The **BRDF** of a material can be further divided into isotropic and anisotropic. Regular surfaces with a rotational symmetry are called isotropic and the **BRDF** is expressed as $f(x, \theta_i, \theta_r)$, following the notation in Figure 2.1. Anisotropic surfaces exhibit a change in **BRDF** when rotated around the surface normal, giving $f(x, \theta_i, \phi_i, \theta_r, \phi_r)$.

A number of empirical and physical reflectance models have been defined to model different types of materials to digitally simulate the appearance of a surface (Guarnera et al., 2016). The following sub-sections will present some **BRDF** models used in this work. However, this list is not exhaustive.

⁵In this case, the wavelength domain Λ corresponds to the visible spectrum, i.e. $\Lambda \in [380, 740]$ nm (Hunt, 1995).

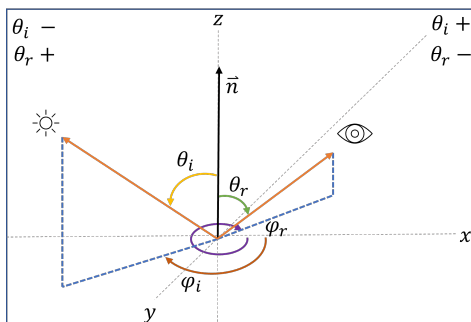


Figure 2.1: BRDF measurement and notation.

Ward's BRDF:

Ward (1992), proposes a light reflection model given by:

$$\rho(\theta_i, \phi_i, \theta_r, \phi_r) = \frac{\rho_d}{\pi} + \rho_s \frac{\exp[-\tan^2 \delta / \alpha^2]}{4\pi \alpha^2 \sqrt{\cos \theta_i \cos \theta_r}}. \quad (2.4)$$

The Ward model uses three parameters to describe the BRDF. ρ_d is the object's diffuse reflectance, ρ_s is the energy of the specular component, and α is the spread of the specular lobe. This model has been used to describe glossy paints (Chen, Taplin and Berns, 2011).

Cook-Torrance BRDF:

Cook and Torrance (1982), developed a reflectance model based on the decomposition of a surface into a succession of microfacets, where each microfacet is assumed to be flat. The Cook-Torrance model, is a well established physical model and is used extensively to model specular materials like gold (Sole, Guarnera et al., 2021; Cook and Torrance, 1982; Sole, Farup et al., 2018).

Cook-Torrance (CT) is a physical model based on the microfacet theory (Cook and Torrance, 1982). The CT model consists of specular and diffuse reflection components and mathematically is defined as follows:

$$f = k_d R_d + k_s R_s, \quad (2.5)$$

In Eq. 2.5, k_d and k_s are weighting parameters and $k_d + k_s = 1$. The specular term is based on microfacet theory, which dictates that only the microfacets on the surface with orientations in between the viewing vector

and the incident vector, called half-vector $\mathbf{h} = \mathbf{l} \cdot \mathbf{v}$, will contribute to the reflected light (Heitz, 2014).

The general form of the CT specular term is:

$$R_s = \frac{1}{\pi} \frac{FDG}{(\mathbf{n} \cdot \mathbf{l})(\mathbf{n} \cdot \mathbf{v})}, \quad (2.6)$$

where F is the Fresnel term (Torrance and Sparrow, 1967), G is the geometrical attenuation factor accounting for shadowing and masking of microfacets, and D is the distribution of normals facing \mathbf{h} .

Beckmann distribution The distribution of microfacets normals, D , describes the statistical distribution of surface normals over the microsurface. The Beckmann distribution for rough surfaces follows a Gaussian model and it is given by:

$$D = \frac{1}{m^2 \cos^4 \alpha} e^{-[\tan \alpha / m]^2}, \quad (2.7)$$

where m is a measure of roughness and α is the angle between the surface normal \mathbf{n} and the half vector \mathbf{h} .

The bidirectional shadowing and masking effects are described by the geometrical attenuation factor, G . It describes what fraction of the microsurface normals is visible in incidence and viewing directions. Originally Cook and Torrance (1982), used the V-cavity masking function. The V-cavity microsurface model computes scattering on separate microspheres and averages their contributions. It is defined as:

$$G = \min \left\{ 1, \frac{2(\mathbf{n} \cdot \mathbf{h})(\mathbf{n} \cdot \mathbf{v})}{(\mathbf{v} \cdot \mathbf{h})}, \frac{2(\mathbf{n} \cdot \mathbf{h})(\mathbf{n} \cdot \mathbf{l})}{(\mathbf{v} \cdot \mathbf{h})} \right\}. \quad (2.8)$$

GGX distribution Walter et al. (2007), proposes a bidirectional scattering distribution function (BSDF) called GGX. This GGX BRDF is inspired by the microfacet model proposed by Cook and Torrance. The general form of the GGX is given by:

$$R_s = \frac{1}{4} \frac{FDG}{(\mathbf{n} \cdot \mathbf{l})(\mathbf{n} \cdot \mathbf{v})}, \quad (2.9)$$

which is the same as the general form of the CT in Eq. 2.6, except that the normalisation factor for the Fresnel term is changed to 4. The Fresnel

term in the GGX distribution is the same as the one proposed by Cook and Torrance but the distribution of microfacets normals, and the attenuation factor is based on the Smith shadowing and masking approximation. The GGX normal distribution function of microfacets is given by:

$$D = \frac{\alpha_g^2 \chi^+(\mathbf{h} \cdot \mathbf{n})}{\pi \cos^4 \theta_h (\alpha_g^2 + \tan^2 \alpha_h)^2}, \quad (2.10)$$

where α_g is a width parameter for the specular lobe, θ_h is the angle between the half-vector, \mathbf{h} , and the surface normal, \mathbf{n} , and χ^+ is a positive characteristic function which equals to one if its parameter is greater than zero and zero if its parameter is lesser or equal to zero. The GGX distribution has stronger tails than the Beckmann distribution; and thus, tends to have more shadowing.

The geometrical attenuation factor which describes the shadowing and masking effects in the GGX is derived from D (Eq. 2.10). This is given by the Smith monodirectional shadowing term. The Smith microsurface profile assumes the microsurface is not autocorrelated and thus, implies a random set of microfacets rather than a continuous surface. It is defined as:

$$G_1(\mathbf{v}) = \chi^+ \left(\frac{\mathbf{v} \cdot \mathbf{h}}{\mathbf{v} \cdot \mathbf{n}} \right) \frac{2}{1 + \sqrt{1 + \alpha_g^2 \tan^2 \theta_v}}, \quad (2.11)$$

where θ_v is the angle between the viewing vector \mathbf{v} and the surface normal \mathbf{n} .

2.4.2 Multiangle Reflectance Measurements

Reflectance measurements typically involve a light source, to uniformly illuminate the surface of the material, and a detector, which measures the amount of light reflected from the surface. When measuring spectral reflectance, as the physical property related to colour, the CIE recommends different geometries, based on spheres and single bidirectional measurements (CIE, 2004). While the spectral distribution of the reflectance is related to colour, directional changes dictate other appearance attributes such as gloss and texture. Multiangle spectrophotometers measure the reflectance of a surface for a fixed combination of illumination geometries, where goniospectrophotometers do so over a broad range of angles (ASTM, 2008).

Goniospectrophotometers can be classified into two categories, scanning based and imaging based devices. Scanning based devices normally measure the ratio of reflected to incident power. The sample is measured lying flat and either, the light source and the detector rotates, or the sample does. These measurements are very accurate but time consuming. Typically, a broadband illumination is used as a light source, and a spectroradiometer is used as a detector. The spectroradiometer captures the radiance at the surface in the visible range, from 400 nm to 700 nm, at a given interval step, usually ranging from 1 to 10 nm.

Imaging-Based Reflectance Measurement Setups

Due to the complexity and limited availability of goniospectrophotometers, imaging-based setups are presented as an alternative to perform multi-angle reflectance measurements. Previous research has been done using imaging-based setups to perform bidirectional reflectance measurements of human skin (Marschner et al., 1999), velvet cloth materials (Lu, Koenderink and Kappers, 1998), and packaging print materials (Arney, Heo and Anderson, 2004; Sole, 2019). Imaging-based setups have also been used for the characterisation of other appearance properties such as sparkle (Ferrero et al., 2013).

2.4.3 Multispectral HDR Imaging

A common approach to obtain the spectral reflectance of a surface as well as its spatial characteristics, $R(x, y, \lambda)$, is using spectral imaging, which provides an estimate of the spectral irradiance of the surface, $E_e(x, y, \lambda)$ described by Eq. 2.2. Where a traditional image is a 2D array, where each point represents the amount of light incident on the detector (whether a photosensitive film or a pixel array), a multispectral image has a third dimension which represents the spectral variation. Various imaging solutions are presented to capture these three dimensions: spatial scanners, spectral scanners, and snapshot setups.

Spatial scanners use a 2D detector and a diffraction mechanism to gather both spectral and spatial information at the same time. The spatial dimension is captured by either moving the detector or the object. These are normally called pushbroom devices (Hui, Jianyu and Yongqi, 1998; Lawrence et al., 2003). Spectral scanners also use a 2D detector, but the wavelength dimension is scanned in time, usually done by using spectral filters (Brauers and Aach, 2010; Gat, 2000; Hardeberg, Schmitt and Brettel, 2002).

The most common solution to snapshot setups are based on colour filter arrays (CFA) placed in front of the imaging sensor (Bayer, 1976). By using demosaicing algorithms, the missing pixel intensities are interpolated to obtain a whole image for each spectral filter. This is the principle behind digital cameras, which have a 2 x 2 filter array and give RGB values. In order to obtain accurate colour reproduction, the exact illumination setting and radiometric calibration of the measurement device is required (Green and MacDonald, 2011). This is commonly achieved by measuring the spectral sensitivity function of the digital sensor. The principle behind CFAs can be extended to spectral filter arrays (SFA) with more colour filters which gives a multispectral image of a higher number of bands. This type of multispectral imaging technology is used in the imaging setup presented in **Article C**.

Multi and hyperspectral imaging has been widely used in the field of cultural heritage digitisation and analysis. Pillay (2021), explores calibration, quality, and visualisation of spectral imaging applied to works of art. The spectral and spatial dimensions of multi/hyperspectral images offer the possibility of a wide range of analysis such as pigment mapping of paintings (Deborah, George and Hardeberg, 2019), imaging of stained glass (Babini et al., 2022), to name a few.

Given that the samples studied in this research are goniochromatic, specular surfaces, a high dynamic range (HDR) acquisition approach has to be considered to accurately capture the appearance of the materials. Using a standard dynamic range setup risks either the specular highlights to be overexposed (Martinez et al., 2019), or the diffuse angles to be too dark, close to noise levels. The HDR acquisition requires multiple images of the same scene to be taken at a range of exposure times, to then perform a weighted average to obtain a single HDR image.

In order to obtain spectral reflectance values from a set of multispectral images taken at a range of exposure times the following pipeline, modified from Brauers, Schulte et al. (2008), is developed, and explained in the next sub-section.

Mathematical Model of the Imaging Chain

Given that the radiant power of the i th channel of a detector is given by Eq. 2.2, the radiant energy is computed as

$$Q_{i,j} = \phi_i T_{i,j} \tag{2.12}$$

where $T_{i,j}$ are different exposure times with a total number of J exposure levels. The final camera value is derived by

$$q_{i,j} = f(Q_{i,j}), \quad (2.13)$$

where f is the camera transfer function (CTF), which describes the opto-electronic conversion of radiant energy $Q_{i,j}$ to camera value $q_{i,j}$, and covers the non-linearities of the camera's analog/digital converter.

Transforming Eq. 2.13 into the discrete form, gives

$$\mathbf{q}_i = f(\mathbf{T}_i \phi). \quad (2.14)$$

The spectral radiant power incident on the camera sensor is given by:

$$\phi = k\mathbf{H}\mathbf{S}\beta. \quad (2.15)$$

$k = Aa$ is a camera specific factor, where A is the area of the sensor and a is the aperture of the optics. \mathbf{H} are the spectral characteristics of the sensor filter array, \mathbf{S} is the light source spectral irradiance, and β is the spectral reflectance.

Since H cannot be inverted, Equation 2.15 is re-arranged:

$$\phi = k\mathbf{S}'\mathbf{H}\beta. \quad (2.16)$$

By using the camera response values from the uniform nearly-Lambertian reference white calibration surface, ϕ_{ref} , the discrete spectrum of the light source, \mathbf{S}_{ref} , is approximated, where the reflectance spectrum of the white balance card, β_{ref} , is assumed to be that of a Lambertian surface.

Dividing $\phi \div \phi_{\text{ref}}$ is the equivalent of a multispectral white balance, cancelling out the specific camera factor k , and giving the discrete reflectance factors for each spectral band \mathbf{Q} :

$$\mathbf{Q} = \mathbf{H}\beta. \quad (2.17)$$

Given that \mathbf{H} cannot be inverted, a transformation matrix, \mathbf{T} , is calculated using the known reflectance spectra, β_{cc} , and reflectance factors, \mathbf{Q}_{cc} , of a reference colour chart:

$$\mathbf{T} = \beta_{\text{cc}} \mathbf{Q}'_{\text{cc}} \text{inv}(\mathbf{Q}_{\text{cc}} \mathbf{Q}'_{\text{cc}} + \lambda \mathbf{I}), \quad (2.18)$$

where \mathbf{I} is an identity matrix and $\lambda = 0.0003$ is a regularisation factor which avoids overfitting and guarantees smooth curves.

Thus, the reflectance spectrum, β_{est} , can be estimated using the following equation ⁶:

$$\beta_{\text{est}} = \mathbf{TQ}. \quad (2.19)$$

2.4.4 Perception-Based Evaluation of Appearance Models

The field of soft metrology aims to link measurable properties of materials to responses of the HVS to the same stimulus (Pointer, 2003). This is usually performed through psychophysical experiments. Psychophysical experiments are out of the scope of this thesis, however, it is possible to perceptually evaluate appearance models analytically.

BRDF models can be evaluated analytically by finding the parameters that produce the smallest error between measured and modelled data. However, this does not always mean the best model gives the smallest perceptual difference. Fores, Ferwerda and Gu (2012), evaluate different error metrics to find a perceptual error metric for BRDF modelling. They find that the cube root metric leads to a better perceptual approximation than other root mean square (RMS) based metrics.

Finally, Ferwerda, Pellacini and Greenberg (2001), present perceptually based metrics to evaluate gloss perception, calculated from physical parameters that influence the BRDF. These have been defined from the Ward model, given by Eq. 2.4. The corresponding metrics are contrast gloss, c , defined as

$$c = \sqrt[3]{\rho_s + \rho_d/2} - \sqrt[3]{\rho_d/2} \quad (2.20)$$

and distinctness-of-image gloss, d , defined as

$$d = 1 - \alpha. \quad (2.21)$$

2.5 Surface Microtopography

In the field of metrology, the surface is defined as the feature of a component that interacts with the environment. The surface topography is

⁶There are many methods for estimating the reflectance spectrum from discrete reflectance factors. Here, the pseudo-inverse method is chosen for the processing pipeline used in **Article C**. Other possible, non-exhaustive (Zhang et al., 2022), methods include using neural networks (Ribés, Schmitt and Brettel, 2001; Mansouri, Marzani and Gouton, 2005) and principal component analysis (Agahian, Amirshahi and Amirshahi, 2008).

defined as the overall surface structure of an object, where surface form is the underlying shape of the object, and surface texture are the features that remain once the form has been removed (Leach, 2013).

2.5.1 Topography Measurements

Surface topography measurements can be represented mathematically as a height function, in one or two dimensions, depending on the measurement modality. Topography measurement methods of textured surfaces have been standardised in ISO 25178, which is comprised of various parts. In particular, part 6 subdivides the available methods of surface texture measurement into three classes (ISO, 2010):

- Line profiling: procedures that have an height function $z(x)$ as output. These approaches provide partial data on the structure of the sample.
- Area-integrating: methods that depend on area-integrated properties of the surface texture.
- Areal topography: techniques that produce height functions $z(x, y)$.

Surface measurements are achieved by traversing a stylus across the surface and sampling the height of the object. Non-contact instruments use an optical scanning instrument. In this thesis, the microtopography is measured using an Altimet Altisurf 50 optical profilometer based on chromatic confocal sensing (CCS), hereinafter referred to as microtopography station. The microtopography station is composed of a white light source connected to an optical probe through a fibre optic. The optical probe has a chromatic objective lens that splits the white light into a spectrum. Hence, each wavelength will be incident on the surface at a known height in the z axis.

When measuring an object, a single wavelength will be incident on its surface, reflected to the probe and analysed by a spectrophotometer. Due to the confocal principle, the other wavelengths are filtered. The spectrophotometer measures the peak of the spectrum which is linked to the height of the analysed point. This device has a very good signal-to-noise ratio which makes it possible to measure in a lit environment. The surface is sampled by moving the probe in the desired location and specifying the sampling resolution. The vertical resolution of the probe is theoretically of the order of $0.01 \mu\text{m}$ in the z axis. The spatial resolution in the x and y axes is of $0.999 \mu\text{m}$. The optical probe used has an amplitude of 8 mm.

2.5.2 Typology of Surface Defects

A surface defect can be defined as the sum of deviations of different orders, each order corresponding to a type of defect. At the macroscopic scale, we observe shape and position defects (1st order), then periodic undulation (2nd order). At the microscopic scale, we observe a periodic or pseudoperiodic roughness, formed by streaks or furrows (3rd order) and finally an aperiodic roughness, formed by tears, slits, pits, etc. (4th order).

Waviness and roughness

Roughness refers to all the irregularities and defects that a surface has. In optical metrology, it is more precisely defined as the quantity of defects of a surface which have a small spatial period compared to the characteristic length of the surface.

Filtering

When calculating the roughness, it is necessary to correctly separate the undulation from the roughness. The cut-off wavelength, is defined by the user depending on the case; filtering removes components of wavelength greater than this value. Roughness is composed of low wavelengths (i.e. high spatial frequencies); to remove the ripple and keep only the roughness a low-pass filter is used.

After filtering the initial profile (known as primary), a roughness profile and a waviness profile are obtained. Each is used for the evaluation of its own parameters. The choice of the cut-off crucial: a bad cut-off will give erroneous results because it will not take enough (or on the contrary too much) components into account in the definition of roughness or waviness profiles.

Once the surface microtopography is acquired, it can be analysed by different means. A common parameter used to describe the roughness of the surface is the arithmetic mean height, S_a , defined as the arithmetic mean of the absolute value of the height within a sampling area,

$$S_a = \frac{1}{A} \int \int_A |z(x, y)| dx dy. \quad (2.22)$$

2.6 Applications in Conservation Restoration

Measuring the appearance of an object is a key point when analysing a work of art, in particular before and after restoration. While the measurement of colour is widely known and almost systematically carried out, the measurement of other appearance parameters is less widespread.

Using computer graphic models, Simonot and Elias (2004), apply the Kirchoff approximation to “real” random surfaces, where their surface roughness is of the same order of magnitude as that of a paint, a paper and a textile. The authors find that the rougher the surface becomes, the more its lightness increases. This effect is enhanced when the lightness of the initial surface is low. Thus, a coloured surface which undergoes a change in roughness such as cracks, will tend towards white. Also, they find that the saturation of the colour decreases as the surface becomes rough. This effect is more evident when the lightness of the initial surface is high. Moreover, they find that the colour difference is easily perceivable by observers.

The effect of translucent materials such as varnish has on a painting’s appearance is the reduction of surface roughness, and thus, its apparent gloss and colour saturation (Rie, 1987; Simonot and Elias, 2004; Elias and Simonot, 2004; Elias, Simonot et al., 2004; Elias, Rie et al., 2006; Rie et al., 2010). The spectral absorbance of varnishes is found to be minimal (Elias, Simonot et al., 2004). Glazes which are coloured, have a double impact as they influence surface roughness, and create additional selective spectral absorbance in the sub-surface, changing colour appearance (Harteveld, 2019).

Genty-Vincent et al. (2017), use a four-flux model to simulate the scattering of light in porous varnish layers. The authors find that the pore size changes the colour and opacity of the paint layer, and that the pore concentration and thickness do not affect colour.

Wei, Stangier and De Tagle (2005) and Wei (2011), use a non-contact confocal sensor to measure the roughness of surfaces, and relate the measured roughness to the differences in perceived surface states. This measurement technology is used on specific cases of pre- and post-restoration analysis. Other studies present the same type of analysis before/after restoration, on other surfaces, such as paint on canvas (Stein and Haugen, 2010; Eipper and Frankowski, 2004).

Elkhuizen et al. (2019), use a combination of colour, gloss, and topography

scanning for acquisition and reproduction of the appearance of a painting using 3D printing.

While the mechanisms that influence the appearance and perception of paintings has been investigated and modelled, this is not the case for other cultural heritage materials which present complex appearance properties such as gilding.

Dumazet et al. (2007), used Kubelka-Munk's two flux theory to model the influence of the substrate's colour on the reflected light from the gold leaf, in order to study correlations between gold leaf's imperfections and appearance. Mounier and Daniel (2013), also present colorimetric observations on the appearance of gold leaf on white, red, and black substrates.

Wu et al. (2020), study the influence of substrate colour on the visual appearance of gilding. Gilding mock-ups were fabricated using different methods and the authors used colorimetry and interferometric microscopy to characterise the mock-ups and conclude that the colour of the substrate does not alter the visual appearance of the gilding. However, they report that burnishing the gilding produces a significant change in appearance.

Finally, Sandu, Busani and Sá (2011), study the surface behaviour of water gilding and imitation gilding using liquid gold. The mock-ups were analysed before and after burnishing (for the water gilded samples), and varnishing. They report that the CIE L* value decreases after burnishing. The authors imply that the decrease in lightness means the gloss has decreased, contradicting the hypothesis that burnishing increases gloss. The authors attribute this discrepancy to a faulty burnishing process. However, it must be emphasised that lightness does not equate gloss, and darker objects can be glossier than lighter ones (Hunter, 1937).

The "imitation" gilding samples have been investigated by Sidorov et al. (2020), by performing spectroradiometric measurements at different angles of viewing and illumination. The authors find that the samples exhibit two peaks of specular reflectance, probably due to an initial specular reflection caused by the air/resin interface, and a second peak caused at the resin/silver interface. Harvey, Smithson and Kollandsrud (2018), create physics-based renders of the samples showing that the "imitation" gilding samples exhibit variations in chromaticity and luminance as a function of reflectance angle.

Chapter 3

Summary of Articles

3.1 Introduction

In this chapter, a summary of the main core articles forming this thesis is presented. These include one journal paper, three conference proceedings, and a book chapter. The articles are ordered according to the research objectives they address, defined in Chapter 1. For each article, a summary of motivations, methods, and results is presented. For more details, refer to the respective manuscripts, found in the second part of the thesis.

3.2 Article A: Characterising appearance of gold foils and gilding in conservation and restoration

Arteaga, Y., Sole, A., Hardeberg, J. Y. & Boust, C. "Characterising appearance of gold foils and gilding in conservation and restoration". In *Proceedings of the 11th Colour and Visual Computing Symposium (CVCS)*. CEUR Workshop Proceedings, vol: 3271, num: 11, 2022.

This paper aims to measure and model the appearance of gold leaves commonly used in restoration, and gilding mock-ups using a commercially available handheld multiangle spectrophotometer. The interest in using this device lies in its portability and flexibility as it can be used to measure many surfaces in a rapid way, obtaining twelve reflectance spectra. The reflectance factors obtained are used to render the colour of the samples and to model the [BRDF](#).

The samples measured are 10 gold leaves, including the gold leaf used to fabricate two gilding mock-ups, which are also measured. Different gold leaves have different appearance as their karat composition changes their colour. The multiangle spectrophotometer has two pick-up points at -15° and -45° from the surface normal, and six illumination directions at -60° , -45° , -30° , 0° , 30° , 65° , and -45° , -60° , -30° , -20° , 0° , 30° , and 65° from the surface normal. The reflectance factors are converted to CIE XYZ coordinates using D65 illuminant and CIE 10° observer colour matching functions. (Fig. 3.1.)

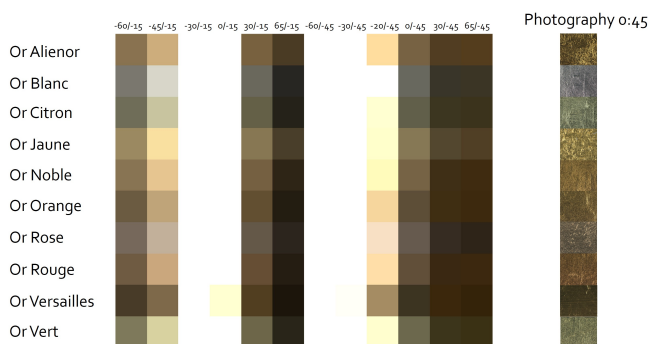


Figure 3.1: sRGB visualisation of the gold foils at all measurement geometries using CIE 10° standard observer colour matching functions and D65 illuminant. The column on the right shows the appearance of the gold foils at illumination geometry 0:45. [Modified from (Arteaga, Sole et al., 2022)]

The model used is an isotropic Cook Torrance BRDF model using the GGX distribution and the Smith G_1 shadowing function (Fig. 3.2). This model is chosen since it is a well established physical model which has been used to model specular materials like gold. The model coefficients are found using a genetic algorithm and the RMS error as the optimisation function.

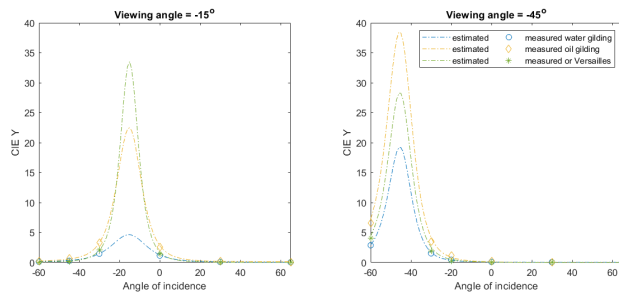


Figure 3.2: Measured CIE Y at viewing angle (*left*) -15° and (*right*) -45° respectively. [Taken from (Arteaga, Sole et al., 2022).]

It is expected that the water gilding sample will have the highest gloss, and the oil gilding the lowest gloss, due to their fabrication method and visual appearance. However, the modelled BRDF shows the contrary. In the case of the viewing angle at -15° the gold leaf has the highest specular peak, and in the case of the viewing angle at -45° the oil gilding sample has the highest specular peak (Fig. 3.2). These results are inconsistent with visual appearance.

It is concluded that the measuring geometry of the handheld multiangle spectrophotometer are not sufficient to model the BRDF of the surface. The points are too sparse and most importantly, the spectrophotometer does not sample the mirror angle, or angles close to it so the model fails at correctly representing the surface.

The dataset gathered in this paper is made publicly available in the CHANGE-ITN repository.¹

¹<https://zenodo.org/record/7543976#.Y-omNnbMK5c>

3.3 Article B: Image-based goniometric appearance characterisation of bronze patinas

Arteaga, Y., Boust, C., Dequier, A. & Hardeberg, J. Y. "Image-based goniometric appearance characterisation of bronze patinas". In *29TH Color and Imaging Conference Proceedings*, pages 294-299. Society for Imaging Science and Technology, 2021.

This paper presents an image-based set up for the appearance characterisation of bronze patinas, based on a method commonly used for sparkle measurement. The bronze patinas investigated in this paper are made by the Coubertin Foundry and have two surface finishes, smooth and rough, in three colours, red, green, and black. The patinas have a goniochromatic appearance which changes at different angles of illumination and observation (Fig. 3.3). The experiment was repeated at two different institutions, with a different set of equipment to test its repeatability and robustness.

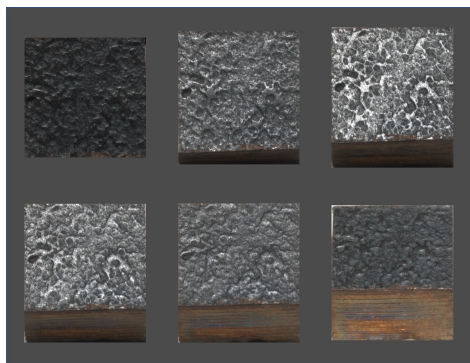


Figure 3.3: Demonstration of black rough patina and its colour change at different angles of tilting. From left to right: 0°, 11°, 22°, 28°, 34° and 45°. The angle of tilting is given from the horizontal axis. [Taken from (Arteaga, Boust, Dequier et al., 2021).]

The interest in finding an imaging-based method for the characterisation of appearance of cultural heritage objects comes from the fact that in most cultural heritage contexts, the availability of specialised equipment such as goniospectrophotometers is limited.

For the purpose of characterising the appearance of the patinas, a method based on a [CCD](#) camera, a light source, and a tilting stage is implemented. The camera and light source are placed at fixed positions, with an

angle of 45° between them. The samples are placed on a tilting stage which has a precision of 1 degree. At each angle of tilting, an image is acquired. Finally, the data is processed by counting the number of pixels which sparkle per angle of tilt, by defining a threshold of sparkle (Fig. 3.4). It is assumed that the points with specular reflections can be considered as flakes in a sparkle model. Table 3.1 shows the parameters used at each institution.

Table 3.1: Parameters used for sparkle measurement

	C2RMF	INP
Acquisition set-up parameters		
Camera	Hasselblad	Nikon D850
Lens	12 mm macro	105 mm macro
Sensor size (pixels)	6708 x 8956	8256 x 5504
Light source	Flash 3000K	LED 5200K
Object distance (cm)	50	40
Illumination distance (cm)	70	80
Pixel size (mm ²)	2.89x10 ⁴	0.50x10 ⁴
Image capture parameters		
f-number	f/14	f/32
Exposure time (s)	1/125	1"30
ISO	50	64

The roughness of the samples is measured using a microtopography station and it is correlated to the maximum value and to the full-width half-maximum of the sparkle. It is found that the full-width half-maxima of the distribution has a linear relationship with the roughness, suggesting rougher samples have a wider specular peak. On the other hand, the maximum of the distribution has a negative exponential relationship. Moreover, it is found that the roughness of the samples poses a limitation on the acquisition system. At roughnesses higher than 35 μm, the sparkle distribution tends to zero because the peaks and valleys on the surface microtopography are too significant and the samples can no longer be assumed to be flat.

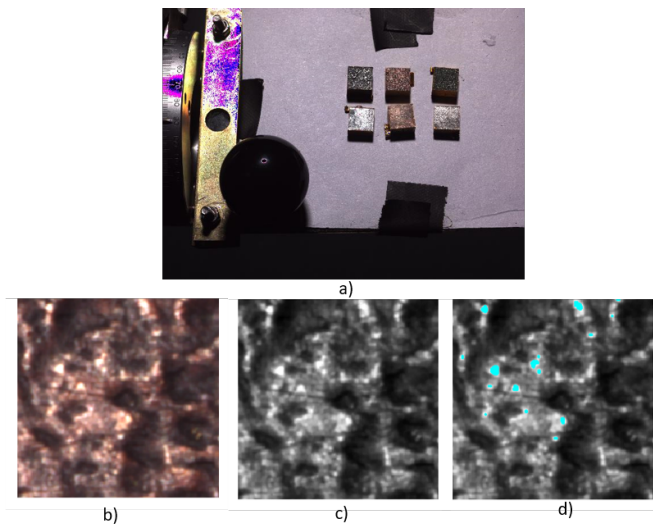


Figure 3.4: Processing steps to obtain sparkle. a): For each patina a patch is extracted from the centre, b): transformed to L*a*b* and a threshold is set in the L* channel. c): The value of sparkle is given by the percentage of pixels over the threshold, highlighted in cyan. [Taken from (Arteaga, Boust, Dequier et al., 2021).]

3.4 Article C: HDR multispectral imaging-based BRDF measurement using flexible robot arm system

Arteaga, Y., Boust, C. & Hardeberg, J. Y. "HDR multispectral imaging-based BRDF measurement using flexible robot arm system". In *30TH Color and Imaging Conference Proceedings*, pages 75-80. Society for Imaging Science and Technology, 2022.

This paper presents an imaging-based method to measure the appearance of cultural heritage objects. The samples used here are the same bronze patinas as in **Article B**. In this case the imaging system is used to acquire bidirectional reflectance measurements at a fixed angle of viewing using a snapshot multispectral camera, a robotic arm used to move the light source, and a tilted stage. Due to the specularities of the patinas, an HDR workflow is developed. The data acquired by the imaging system is evaluated against reflectance factors obtained by a commercially available goniospectrophotometer.

The samples are placed on a tilted stage with an elevation of 22.5° , the camera is placed 30 cm above the sample, and the light illuminates the sample following a half-arc sampling 35° at each side of the mirror angle (Fig. 3.5). The multispectral camera has a SFA, capturing eight narrow bands centred at 440 nm, 473 nm, 511 nm, 549 nm, 623 nm, 665 nm, and 703 nm, and a ninth panchromatic band relatively constant across the visible spectrum. The effective pixel size is of 0.0377 mm. For each angle of illumination, an HDR acquisition is taken at 16 ms, 32 ms, 64 ms, 125 ms, 250 ms, and 499 ms.

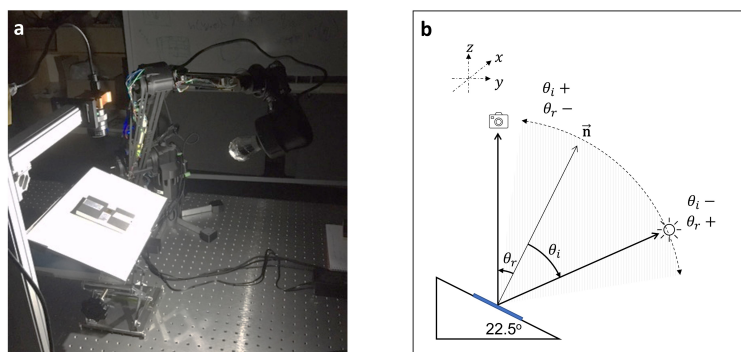


Figure 3.5: Side view schematic of the imaging system. The sample is placed on a tilted stage, the camera is above the sample and the light is held by a robotic arm. **a** Picture of the imaging system. **b** Schematic of the imaging system.

The processing pipeline to obtain the reflectance factors for each angle of illumination is explained in Section 2.4.3 and illustrated in Fig. 3.6. The images are corrected for dark current noise by subtracting the dark current image taken at the same exposure times, with the sensor covered. Then, values proportional with the object radiance are obtained by linearising the images using a look-up table. At this stage the HDR image is created by performing a weighted average across exposure times using a modified Tukey window. A flat-field HDR image of a uniform white reference target is also created following the same steps. Then, the object's HDR image is corrected by multiplying it by the flat-field HDR. Finally, the HDR radiance map is demosaiced using bilinear interpolation and a 8-channel multispectral HDR image and a panchromatic image are obtained. For each sample, an area of pixels from the centre of the sample is averaged across each band, and spectral reconstruction is performed using the pseudo-inverse method, with a regularisation factor. The reflectance factors are interpolated to the range 400-700 nm in steps of 10 nm. The training data for the reconstruction is a 30-patch Color-Gauge Nano Target from Image Science Associates, and measured using the HySpex VNIR-1800 hyperspectral imaging system at 45/0 measurement geometry.

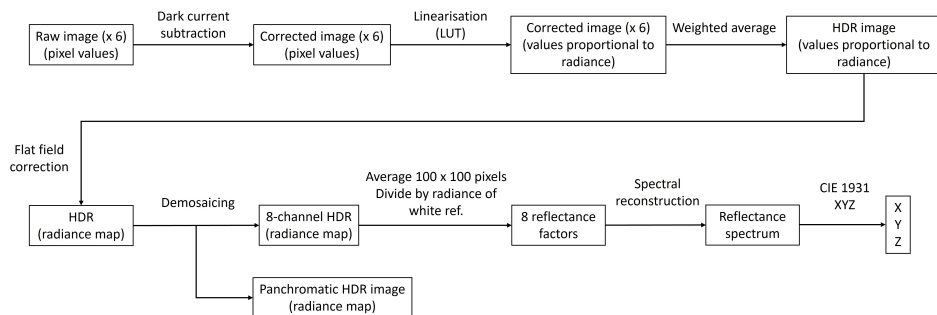


Figure 3.6: A scheme of the processing pipeline followed in **Article B.** to obtain CIE XYZ coordinates from the raw images captured by the imaging system.

The performance of the system is evaluated against a commercially available goniospectrophotometer, GON 360, which is equipped with a CAS 140CT array spectrophotometer. Reflectance factors from the system and from the goniospectrophotometer are converted into CIE 1931 XYZ values and the CIE Y values, representative of the luminance, are compared. The GON 360 provides bidirectional measurements at angles of incidence $\theta_i = -35^\circ, -25^\circ, -15^\circ, -5^\circ, 0^\circ, \text{ and } 5^\circ$, and angles of reflection θ_r in the

range from -45° to 30° in steps of 5° . Since the goniospectrophotometer does not measure the samples at the same angles as the imaging system presented in this article, the values at $\theta_r = -22.5^\circ$ are interpolated using linear interpolation between the measurements at $\theta_r = -25^\circ$ and $\theta_r = -20^\circ$.

The precision of the system is also evaluated by finding the optimal averaging area, by averaging areas of 100×100 , 10×100 , 100×10 , and 10×10 pixels from the centre of the sample. The rationale behind the choice of areas is that a 100×100 pixel window will reduce error from averaging but will also introduce error in the measurement angle. Using a 10×10 pixel window will reduce the error in the measurement angle but will increase the signal-to-noise ratio (SNR). An area of 10×100 pixels is hypothesised to reduce the error on measurement angle and decrease the SNR, whereas an area of 100×10 pixels is considered to increase both the error on measurement angle and the SNR.

It is found that for smooth samples with a roughness lower than $12.48 \mu\text{m}$ the system performs well, matching the data obtained by the goniospectrophotometer. However, for samples with a surface roughness higher than $12.48 \mu\text{m}$, the system has some limitations probably due to the distribution of microfacet normals. Moreover, it is found that for all samples, regardless of the ability of the system to match the goniospectrophotometer, averaging an area of 100×100 pixels significantly reduces the measurement error.

3.5 Article D: Appearance-based evaluation of varnish removal methods in gilded surfaces

Arteaga, Y., Marchioni, D., Courtier, S., Boust, C. & Hardeberg, J. Y. "Appearance-based evaluation of varnish removal methods in gilded surfaces". *Heritage Science*, **11**, 31 (2023)

This paper builds on from **Article A** and **Article C** and is a collaboration with the National Institute of Cultural Heritage. As part of a restoration campaign of a 15th century framed panel painting, gilded wood mock-ups representative of the frame and painting, were fabricated by a professional conservator. Two types of gilding were fabricated, water and oil gilding, techniques widely used since the Middle Ages. These mock-ups were varnished, and four varnish cleaning techniques were tested. (Fig. 3.7). The appearance of the mock-ups was acquired using the imaging system presented in **Article C** and their **BRDF** was modelled, following the indications in **Article A**. By modelling the **BRDF** of the surfaces, perceptual gloss attributes are calculated which are in turn used to cluster the surfaces according to their appearance.

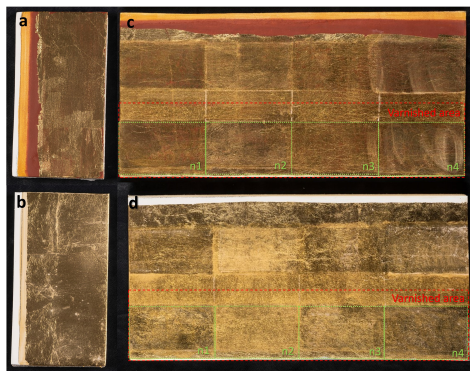


Figure 3.7: Picture of the mock-ups fabricated. **a** Reference unvarnished water gilding. **b** Reference unvarnished oil gilding. **c** Varnished and cleaned water gilding. **d** Varnished and cleaned oil gilding. The red rectangle shows the varnished area with dammar and colophony. The green rectangles show the cleaned area for each method. ©Angéle Dequier/Inp. [Taken from (Arteaga, Marchioni et al., 2023).]

Chemical varnish cleaning is a common restoration technique which has been extensively studied in paintings, however, its effects on gilded wood are not widely documented. The cleaning methods studied in this paper are by solubilisation using a cotton swab, by applying a compress, by

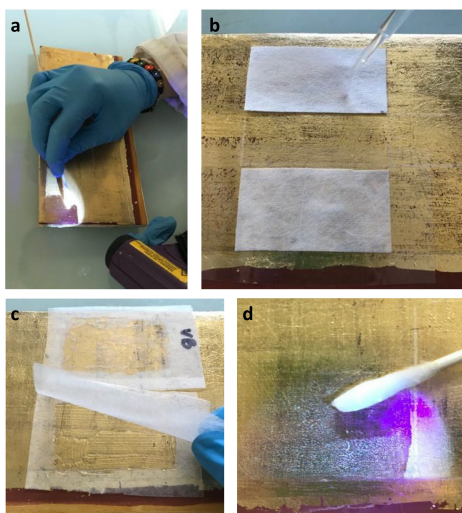


Figure 3.8: Cleaning methods. **a** Solubilisation with a cotton swab under UV light. **b** Solubilisation by applying a compress. A pipette is used to soak the compress with the solvent. **c** Solubilisation by use of a gel. The gel is between two layers of hemp paper. **d** Rinsing the surface using a cotton swab. [Taken from (Arteaga, Marchioni et al., 2023).]

using an aqueous gel, and by using a silicon-based gel (Fig. 3.8). These methods are commonly used, and the focus is given to the effect each method has on the appearance of the gilding.

The samples are measured using conventional colorimetry and gloss measurements, as commonly done in the field of cultural heritage. However, it is found that these measurements are insufficient to characterise and classify the gilding mock-ups in a perceptually accurate manner.

The samples were measured using the imaging system described in **Article C**. The **BRDF** of the surface was modelled using a genetic algorithm and the Cook-Torrance model with the GGX distribution and Smith shadowing function. The **BRDF** of the mock-ups is rendered to provide a visualisation of the appearance of each surface (Fig. 3.9).

Using the coefficients of the **BRDF** model, the contrast gloss and the distinctness-of-image (**DOI**) gloss are calculated. These gloss attributes are correlated to the perception of gloss and are used together with the coefficients of the **BRDF** model in a principal component analysis.

The **PCA** results in two PCs which are correlated with the perceptual at-

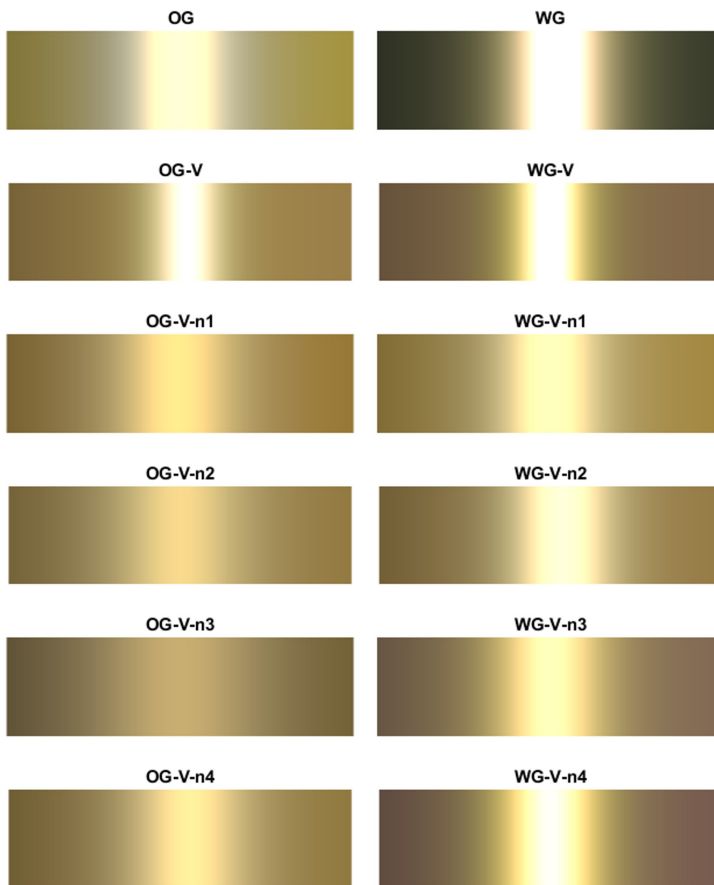


Figure 3.9: Adobe RGB rendered images of the modelled BRDF of each surface at fixed viewing angle, $\theta_r = -22.5^\circ$. Each 10 pixels on the horizontal axis represent a step of one degree in angle of incidence. [Taken from (Arteaga, Marchioni et al., 2023).]

tributes of gloss. (Fig. 3.10). In this component space, the gilded surfaces can be clustered according to the type of gilding, water or oil, and whether they are varnished, or cleaned. It is found that unvarnished water and oil gilding have a very different appearance which is expected from empirical knowledge. When the samples are varnished, their appearance becomes very similar as the contrast gloss and DOI gloss of oil gilding increases, and the DOI gloss of water gilding decreases. This explains the common belief that varnishing a surface saturates its colours and increases its gloss which is not consistent with conventional gloss measurements.

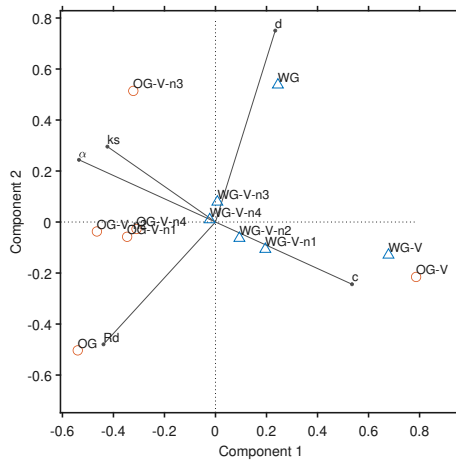


Figure 3.10: Biplot of the PCA for the first two PCs, calculated using the coefficients obtained for the BRDF model in the CIE Y coordinates (α , k_s , and R_d) and gloss attributes (c and d). Oil gilding samples are displayed in orange (round markers), and water gilding samples are displayed in blue (triangle markers). PC1 and PC2 are representative of c and d respectively. Surfaces are clustered depending on their varnish level (reference or no varnish, varnished, and cleaned). [Taken from (Arteaga, Marchioni et al., 2023)]

Moreover, none of the cleaning methods restore the appearance of the gilding either before varnishing or keep the appearance of the varnished gilded wood unchanged.

Finally, the cleaning method which renders an appearance closest to the varnished gilded wood for both water and oil gilding is by applying a compress. These results, combined with other analysis on the mock-ups, guided the restoration campaign of the framed panel painting. It is found that solubilisation by applying a compress is the method that achieves an appearance the closest to the original appearance of the varnished gilded wood, has the most uniform effect, and leaves a thin uniform layer of varnish which helps in protecting the painting from any environmental factors which may damage it.

3.6 Article E: Quantifying the appearance of gilded surfaces

Arteaga, Y., Boust, C. & Hardeberg, J. Y. "Quantifying the appearance of gilded surfaces". To appear in: *Cultural Heritage Analysis for New Generations*, Degriigny, C., George, S., Hardeberg, J. Y. & Østlien, A, editors, Routledge, 2023.

This article presents appearance measurements of three types of gilding, water gilding and oil gilding (unvarnished and varnished), and "imitation" gilding. The samples have been measured using the imaging setup presented in **Article C** and the gloss metrics, contrast and DOI gloss, are calculated.

This paper aims to quantify the perceptual differences between two types of gilding fabricated using gold leaf, and a third type of gilding which is fabricated by covering a burnished silver leaf with a yellow pine resin (Fig. 3.11). This type of gilding, called "imitation" gilding, was popular in the 13th century in Norway. While the gilded surfaces using gold foil have a metallic-like appearance, the "imitation" gilding has a peculiar appearance.

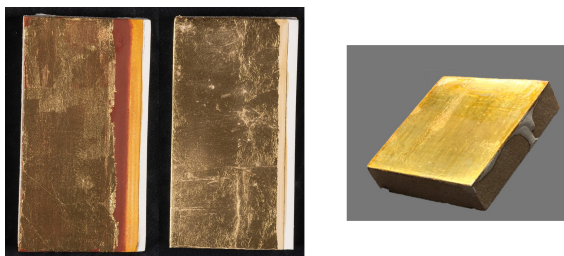


Figure 3.11: Gilding mock-ups. *left:* water gilding and oil gilding. *right:* "imitation" gilding. [Taken from (Arteaga, Boust and Hardeberg, 2023).]

The appearance of metallic materials has been commonly described as a combination of colour and gloss, where polished metals are an extreme case of glossiness. However, this is an incomplete consideration, as metals have a very high extinction index which means their reflection is purely specular and any diffuse-like reflection is caused by scattering at the surface microstructure.

The contrast gloss and DOI gloss of the samples is calculated (Fig. 3.12). It is found that the three types of gilding can be categorised individually.

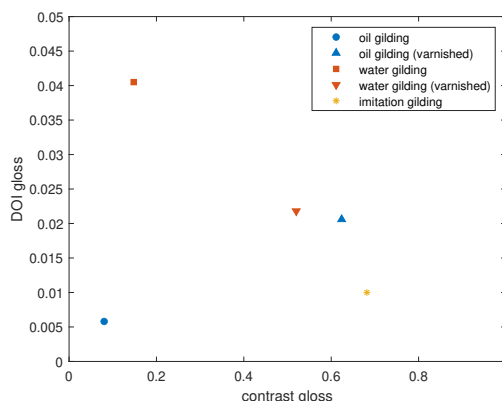


Figure 3.12: Contrast gloss and DOI gloss values obtained from BRDF coefficients for the CIE Y channel modelled for oil gilding and water gilding, varnished and unvarnished, and imitation gilding. [Taken from (Arteaga, Boust and Hardeberg, 2023)]

Water gilding has a high value of DOI gloss because of its metallic nature and its smooth surface. This causes high specular highlights at the mirror angle, resulting in a mirror-like appearance. Its contrast gloss is rather low because metals do not have diffuse-like reflectance, so there is no distinction between highlight and surface colour.

In the case of oil gilding, the DOI gloss is very low because the micro-surface roughness causes scattering which is perceived as diffuse-like reflection and blurring of the reflected environment. Its contrast gloss is similar to that of the water gilded sample. Since both mock-ups are fabricated using the same gold leaf they are expected to have the same colour and no distinction between highlight and surface colour.

The effect of varnishing the mock-ups causes subsurface scattering which increases the contrast gloss for both samples. At the air/varnish interface, a proportion of the light is reflected specularly, governed by Fresnel coefficients, and the spectral characteristics of the light remain unchanged compared to that of the illuminant (Fig. 3.13). Therefore, the contrast between highlight and surface colour increase.

In the case of the water gilding surface, varnishing decreases its DOI gloss because the varnish layer causes distortions in the reflected image. However, in the case of oil gilding the DOI gloss increases because the specular reflection cause by the varnish is higher.

The “imitation” gilding has a low DOI gloss. This is due to the distortion caused by the sub-surface scattering in the volume of the resin layer. However, the contrast gloss of the “imitation” gilding is the highest of the five surfaces. This is due to smooth specular reflection at the mirror angle, which is contrasted with the diffuse reflection caused by the coloured resin.

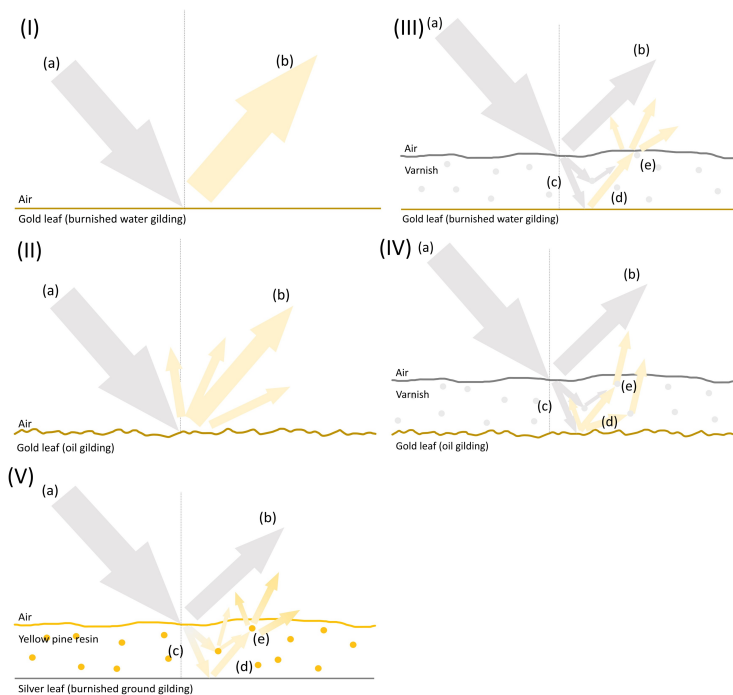


Figure 3.13: Optical model of each sample. (I) Water gilding: the incident light (a) gets reflected specularly (b). (II) Oil gilding: the incident light (a) gets reflected specularly and scattered (b). (III) Varnished water gilding: the incident light (a) gets reflected specularly (b) and refracted into the varnish (c). Then reflected by the gold leaf (d) and scattered and refracted by the varnish (e). (IV) Varnished oil gilding: the incident light (a) gets reflected specularly (b) and refracted into the varnish (c). Then reflected by the gold leaf (d) and scattered and refracted by the varnish (e). (V) “imitation” gilding: the incident light (a) gets reflected specularly (b) and refracted into the resin (c). Then reflected by the silver leaf (d) and scattered and refracted by the resin (e). [Taken from (Arteaga, Boust and Hardeberg, 2023)]

Chapter 4

Discussion

This chapter provides a global evaluation of the research presented by the core papers summarised in Chapter 3. The contribution of material appearance analysis to conservation is discussed in Sec. 4.1 by assessing how this thesis has answered the research questions formulated in Sec. 1.3. Finally, the scope and limits of the research are discussed to contextualise this thesis in Sec. 4.2.

The aim of this thesis is to explore material appearance analysis, focusing on evaluating the appearance of complex cultural heritage materials, to guide conservation and restoration treatments. As a secondary aim, the suitability of an imaging-based method for appearance capture of goniochromatic materials is evaluated.

Materials with complex surface appearance such as gilding, commonly found in cultural heritage objects, require complex measurements to characterise their appearance. Due to the strong angular-dependence of the reflectance characteristics of these materials, individual appearance measurements such as colour and gloss, are insufficient to describe their appearance. Moreover, glossmeter measurements fail to correlate with perceptual cues. Hence the motivation to use more complex acquisition and modelling methods to describe their material appearance, and apply these measurements to the field of conservation and restoration.

This thesis covers two research domains, defined by two research sub-objectives. The first is in the technical domain, and concerns the acquisition and modelling of the appearance of complex cultural heritage materials. The second research domain aims to apply material appearance

analysis to guide conservation. In this context, the appearance of gilded surfaces is investigated and the effect that conservation treatments have, such as varnishing and cleaning.

Within these two sub-objectives, four more specific research questions were defined, which the work in this thesis aims to answer:

- RQ1** What are the challenges and limitations of measuring the appearance of gilding using portable commercially available devices?
- RQ2** Is it possible to perform material appearance measurements of goniochromatic, cultural heritage materials using imaging devices?
- RQ3** How reliable are the measurements obtained from an imaging setup in comparison to a commercially available goniospectrophotometer?
- RQ4** Is it possible to use BRDF models to perceptually evaluate the appearance of cultural heritage materials for conservation purposes?

4.1 Research Contributions

4.1.1 Capture and model the appearance of complex cultural heritage materials

The first sub-objective of this thesis work concerns the technical task of capturing and modelling the appearance of cultural heritage materials. The materials chosen for this are patinated bronze and gilded wood. These materials, as explained in Sec. 1, have peculiar surface appearance. They are glossy, metallic, translucent (when varnished) and with varying surface roughness, which implies traditional appearance measurements are insufficient to characterise their appearance.

To address this sub-objective, three research questions are formulated, and in this subsection, the extent each of them have been answered, through the research in this thesis, will be discussed.

RQ1: What are the challenges and limitations of measuring the appearance of gilding using portable commercially available devices?

Commercial hand-held devices such as spectrophotometers and glossmeters are commonly used to characterise the colour and gloss of many cultural heritage surfaces. These devices are favourable for their practicality, they are non-contact methods and easy to use. However,

given that colorimetric measurements are valid for a fixed combination of illumination and viewing angle, they are unable to characterise goniochromatic materials, such as gilding. Novel devices such as multiangle spectrophotometers have been developed to measure the spectral reflectance of samples at a fixed combination of viewing and illumination directions. These have been used to characterise materials with special effects such as flake paints (Ferrero et al., 2013).

The literature has shown that colorimetry is the main method used for the quantitative characterisation and evaluation of the appearance of gilding (Toque et al., 2010; Wu et al., 2020; Dumazet et al., 2007; Mounier and Daniel, 2013; Sandu, Busani and Sá, 2011). To answer this research question, gilded samples and gold leaves were measured using a multiangle spectrophotometer in **Article A**, and in **Article D**, colour and gloss measurements were used to characterise the appearance of gilded samples before and after varnishing.

The results from **Article A**, show that visualising and modelling the multiangle reflectance of the gold is not sufficient for a proper characterisation. The Adobe RGB visualisation of the reflectance (Fig. 3.1) shows that the "colour" of gold from a purely metrological point of view can be represented by the visualisation of its $L^*a^*b^*$ values using a fixed colour space and standard illumination. However, this is not an accurate perceptual representation of the appearance of these samples. Due to the metallic nature of gold which causes very high specular reflectance, slight changes in viewing and illumination directions cause a large colour change; and thus, in the overall perception of its appearance. Moreover, these measurements are insufficient to model the BRDF of the surface. The BRDF models fail at estimating the reflectance at angles close to the mirror angle, which leads to incorrect models. This stresses the importance of appropriate sampling of reflectance at angles close to the mirror angle to obtain more accurate models.

Using more conventional methods, such as colorimetry and specular gloss measurements, show their inadequacy to characterise the appearance of gilding, as reported in **Article D**. These devices are investigated since they are commonly found in cultural heritage institutions and widely used by conservators. Colorimetry allows for colour differences between samples to be calculated, for example before and after varnishing. However, these colour differences cannot be verified perceptually due to the complex nature of the gilding. Our visual system is incapable of separating the different phenomena that contribute to the total appearance of a sur-

face (Fleming and Bühlhoff, 2005). Since gilding is a complex material, the perception of the total appearance of gilding is very different from individual appearance parameter measurements.

Moreover, as reported by Leloup et al. (2014), glossmeters are not adequate to characterise perceptual gloss differences. These devices are designed to judge gloss differences of surfaces with similar appearances. The resolving power of a specular glossmeter is much inferior to that of the human eye (Hunter and Harold, 1987). Furthermore, the glossmeter provides a relative measurement compared to that of a surface with an index of refraction of 1.567 at 589.3 nm. In the case of unvarnished gilding, the index of refraction of the surface is higher than the standard, leading to values of GU higher than 100.

The inability of colour and gloss measurements to perceptually characterise and evaluate the appearance of gilding has further consequences. They are inadequate to avail conservation treatments, and can lead to misguided conclusions (Sandu, Busani and Sá, 2011). As described in **Article D**, it is expected that varnishing a gilded surface will increase its gloss. However, the glossmeter values show the opposite. The contradiction between empirical knowledge and analytical observation poses the question of whether the empirical knowledge being incorrect, or the analytical observation being unreliable. This question will be addressed in **RQ4**.

RQ2: Is it possible to perform material appearance measurements of goniochromatic cultural heritage materials using imaging devices?

As **RQ1** has shown, traditional measurements such as colour and gloss, as well as commercial multiangle spectrophotometers, are not the most appropriate devices to capture and model the appearance of materials such as gilding. For this reason, more complex bidirectional reflectance measurements and models are necessary to characterise their material appearance. While goniospectrophotometers can provide these measurements, they are expensive and their measurements are time consuming. Moreover, their access is rather limited in a cultural heritage context. Imaging-based methodologies are an alternative to obtain the bidirectional appearance of complex materials (Marschner et al., 1999).

First, **Article B** uses imaging methods and a protocol originally used for sparkle characterisation to measure the specularly of patinas of different colour and roughness. To test the repeatability and robustness of the

method, two sets of equipment, at two different institutions, were compared. The roughness of the samples was correlated to their appearance. The results of this paper show that there is a correlation between the roughness of the samples and the sparkle parameters calculated. Moreover, the two setups obtain results which are relatively similar, but at different scales of magnitude.

There are many limitations to this setup which will be discussed here. First of all, it uses commercial DSLR cameras of which their sensor spectral sensitivities is unknown. This poses the difficulty of the pixel values being camera dependent. For this reason, the results obtained between the two institutions are similar in a relative scale, but not magnitude wise. Moreover, digital cameras do not satisfy the Luther-Ives condition (Sharma, 2017), which requires that the camera sensor sensitivities would be obtainable as a linear combination of the CIE colour matching functions, in order to accurately measure the tristimulus colour coordinate. Another limitation of this setup is its design. By tilting the sample, rather than the illumination or viewing direction, at each angle of tilt, both illumination and viewing direction change. Thus, for each angle of viewing there is one corresponding angle of illumination (rather than a distribution), which would be necessary for appearance models such as the BRDF.

Finally, a limiting aspect of this work is that the angular resolution of the setup is not the same for the devices. The setup at C2RMF has an angular resolution of 0.00015 degrees, and the one at INP of 0.00002. Sparkle is a texture effect which requires an angular resolution comparable to that of the HVS (0.02 degrees), otherwise the effect is perceived as simple scattering on the surface. Since the angular resolution of the devices is not the same, their results are not comparable. These limitations were taken into account into the design of the second imaging setup, presented in **Article C**.

In **Article C**, an existing setup used for various applications (Kitanovski and Hardeberg, 2021), is modified to measure the bidirectional reflectance of the samples. This setup consists of a multispectral camera, a light source held by a robotic arm, and a tilted sample holder. A multi-angle HDR imaging pipeline is developed, and a corresponding processing pipeline to obtain the bidirectional reflectance of the samples. Given that the imaging setup has been defined, the next research question can be addressed.

RQ3: How reliable are the measurements obtained from an imaging setup in comparison to a commercially available goniospectrophotometer?

RQ1 has shown the need for a complex bidirectional measurements for the accurate capture and modelling of the appearance of goniochromatic materials. In **RQ2** two different imaging-based setups were presented. The second imaging-based setup is evaluated in this research question.

The imaging setup presented in **Article C** has various limitations due to measurement errors. In order to evaluate how reliable these measurements are, and the impact of the measurement errors, its accuracy is tested by comparing the results obtained with those of a commercial goniospectrophotometer. For this purpose, the samples investigated are patinated bronze in two colours and varying surface roughness.

It is found that the imaging-system is accurate at measuring the bidirectional reflectance of samples with surface roughness lower than $6 \mu\text{m}$. For surfaces with roughness higher than $12 \mu\text{m}$ the results have a lower accuracy. Also, it is shown that the size and orientation of the averaging area used to calculate the reflectance plays a large role in the precision of the system.

Given that the results obtained by this evaluation are considered satisfactory, this imaging system and its processing pipeline are used in the second sub-objective of the thesis.

Limitations

The work achieved by the first sub-objective has shown the need for complex appearance measurements. An imaging-based setup has been introduced and validated against a commercial goniospectrophotometer. However, there are limitations to this work. First, the surface analysis is limited by the nature of the samples which in this case are flat mock-ups. This limits the type of object and surface that can be analysed. Moreover, as shown in **Article C**, the averaging area plays a large role in the precision of the system which requires that the samples analysed must be homogeneous to guarantee reliable measurements. A final limitation of the setup designed is that it is not portable. This also limits the objects that can be analysed. In a conservation and restoration context, portable devices are favourable so they can analyse objects in situ.

4.1.2 Apply material appearance analysis to guide conservation

RQ4: Is it possible to use BRDF models to perceptually evaluate the appearance of cultural heritage materials for conservation purposes?

The second sub-objective concerns applying material appearance analysis in the context of conservation and restoration. In the context of a collaboration work with the [INP](#) in Paris, gilded wood mock-ups were fabricated. The mock-ups were varnished and different chemical varnish removal methods were evaluated to guide the conservation of a 15th century painted panel. This work is reported in **Article D**. In **Article E**, the appearance of the gilding mock-ups is compared to the appearance of an "imitation" gilding, commonly used in Norway in the 13th century.

The work developed to solve **RQ1**, showed that traditional methods are insufficient to characterise the appearance of gilded surfaces. It was argued that the specular gloss measured by glossmeters is inadequate to characterise perceived gloss differences of gilded surfaces. Thus, to solve these shortcomings, focus is given to [DOI](#) gloss and contrast gloss. As defined in [Sec. 2.4](#), [DOI](#) gloss and contrast gloss are perceptual gloss dimensions which can be calculated from the [BRDF](#) coefficients. These metrics reflect the multidimensional nature of gloss appearance.

In **Article D**, the imaging system presented in **Article C** is used to acquire the appearance of gilded samples. The [BRDF](#) of the surfaces is modelled, and perceptual gloss parameters are calculated. A multidimensional analysis of the [BRDF](#) model coefficients and the gloss parameters leads to the appearance-based comparison of the types of gilding, the effect of varnish on appearance, and the evaluation of varnish removal methods.

Article D also provides a visualisation of the appearance of the samples by rendering the [BRDF](#) model. This offers conservators additional visual information on the appearance of the metal surface as well as a quantified approach to discriminate the gloss of the different types of gilding which is not possible using traditional methods. Moreover, it is found that oil gilding and burnished water gilding, have very distinct gloss parameters. The [DOI](#) gloss of these samples varies due to the burnishing effect which smooths the surface and makes it more mirror-like in the case of water gilding. Varnishing the surface increases both contrast and [DOI](#) gloss of the oil gilding since it saturates its colour and smooths its surface. In the case of water gilding, even though its contrast gloss increases, its [DOI](#) decreases due to the sub-surface scattering of the varnish. The separation

of gloss in its perceptual dimensions, contrast and DOI, can only be calculated from the complex BRDF of the surface. To the authors knowledge, this had not been previously applied in a conservation context.

In **Article E**, an overview of the appearance of gilding is provided. Here, two types of gilding as well as an imitation gilding are examined. The literature and analysis of the gilded samples shows that there is a lack of appropriate vocabulary in the conservation community to describe perceptual aspects of the appearance of gilding. As explained previously, the effect of varnishing a gilded surface is described as saturating the colours and increasing the gloss. However, as shown in the example of oil gilding and water gilding this is not so straightforward. While it is true that the colours saturate, expressed by an increase in contrast gloss, the DOI gloss only increases in the case of oil gilding. Moreover, the gloss metrics allow to describe the perceptual differences between the three types of gilding, separating the metallic surfaces from the non-metallic ones.

The results show that there is a two-fold need in the context of restoration and conservation. On one hand, there is a need for a wider use of appearance models to describe complex materials such as gilding. They provide a much better characterisation of the material's appearance, which can be visualised and is perceptually accurate.

On the other hand, there is a lack of common vocabulary when describing surfaces such as gilding. Gold has a metallic appearance which falls in an ambiguous category of appearance. Thus, gilding can be considered as having an appearance closer to that of a metallic object. However, once the gilding is covered by a translucent layer, in the case of varnished gilding and "imitation" gilding, it is no longer metallic, but glossy.

Gloss is a multidimensional aspect of appearance which is usually described as one dimensional. Judgements such as more/less glossy are misleading and incorrect, as they assume gloss is one dimensional. As shown in **Article D** and **E**, the effect of varnish and the peculiar appearance of "imitation" gilding, can be better described using perceptual gloss parameters as they allow for the discrimination between metallic and non-metallic surfaces. The importance of using a more technical vocabulary when qualitatively describing the appearance of different materials is vital, so these observations can be compared with quantitative analysis. With the common and widespread use of scientific analysis in conservation, these concepts must be well defined to avoid misinterpreting results which can lead to inaccurate conclusions of not only conservation treat-

ments but also an object's use and function.

Moreover, the use of digital models for documentation and digital reconstruction is increasing in the field of conservation with many possible applications and perspectives. Digital restoration can be performed for flat objects such as paintings. However, 3D objects require more complex digital models. The BRDF is the foundation for realistic image synthesis and understanding for computer graphics and digital representation. Thus, it is vital to properly estimate the reflectance properties of different materials. The work presented in **Article D** and **E** is an initial investigation into applying material appearance analysis in a conservation and restoration context.

Limitations

The work presented by **Article D** and **E** show the feasibility and value of using advanced material appearance analysis in conservation, specifically in the case of gilded samples. However, there are limitations to the work carried out. First, the appearance models obtained here are taken from mock-ups of gilded samples. These mock-ups are made following research based methods, after having investigated analytically the composition of the objects and cross-referencing this to multiple historical sources. The mock-ups are intended to be used as replicas of the materials used in real objects. Thus, the appearance models obtained are representative of fabrication techniques and methods but cannot be generalised to the actual surface appearance of real objects. In the case of investigating real objects there are a wide range of implications that must be considered. Ageing and degradation, as well as human intervention such as past restoration change the appearance of the materials. These changes in material appearance are specific to the object's history, and have to be considered when investigating the object. The material appearance obtained for the gilded surfaces studied in this thesis corresponds to that of the gilded mock-ups at the time of fabrication. A possible perspective would be to investigate the effect that ageing and degradation processes have on the appearance of gilded surfaces.

Furthermore, although the appearance models have been evaluated using perceptual gloss parameters and their rendering has been visually examined by professional conservators, there is a need for a more exhaustive psychophysical evaluation of the models. To render this analysis even more complete, a survey of conservators and gilding experts should be made to gather semantic appearance descriptors. This could formalise

the relationship between qualitative and quantitative parameters.

Ethical considerations

As presented in Sec. 2.2, when working with cultural heritage objects there are many ethical considerations which must be taken into account and they will be presented in this subsection.

Possible applications of using BRDF models in conservation and restoration are the creation of digital representations of cultural heritage objects for documentation, digital restoration, or communication purposes. A first point to consider is that the digital representation of the object is a representation. It is based on, and can only be as good as, the knowledge gained from the object in its present condition. The digital model can serve the purpose of documentation to safeguard the appearance of the object at its present time. However, when dealing with appearance, accurate documentation requires not only the physical or chemical properties of the object, but also perceptual characteristics. Thus, material appearance models must be not only realistic, but perceptually accurate.

When reconstructing a cultural heritage object, whether physically or digitally, it must be considered that this reconstruction is only an interpretation of what the object could have originally looked like. There are many examples where the original appearance of the object has drastically changed over time. This appearance change modifies the perception and interpretation of the object. In these cases, reconstructions can help re-interpret and give an object a new meaning based on their original appearance¹. Digital models can be developed as a useful tool for conservators by rendering possible reconstructions of an object without having to manufacture many copies using slightly different materials.

4.2 Scope of the Research

4.2.1 Breadth of the Research

This thesis aims to use material appearance analysis to guide conservation and restoration of goniochromatic materials. Much of the work presented in this thesis focuses on the appearance capture and modelling of the surface appearance of gilded wood and patinated bronze. However,

¹An example of objects with lost polychromy are ancient Greek and Roman sculptures. A recent exhibition at the Metropolitan Museum of Art in New York, *Chroma: Ancient Sculpture in Colour (The Metropolitan Museum of Art, 2023)*, highlights the importance of conveying and communicating new meaning obtained through reconstructions.

several of the papers in this thesis present research that is broader than this field. As defined in Chapter 1, the secondary aim of this thesis is to evaluate suitability of an imaging-based method for appearance capture of goniochromatic materials. For this reason, **Article B** and **C**, focus on appearance capture and modelling. These papers are not specific to the field of cultural heritage and their results can be applied to any material.

Moreover, **Article A, D** and **E** use gilding as an example material but the applicability of the methods and key takeaways can be applied to other glossy and/or metallic cultural heritage surfaces.

4.2.2 Research Impact

In this section the impact of the research will be assessed. Given that this thesis work is multidisciplinary, its impact is two-fold, as technical work in the field of appearance capture and modelling, but also the application of material appearance analysis in the field of conservation and restoration.

First, in **Article A**, the challenges and limitations of using a commercially available hand-held spectrophotometer for the appearance capture and modelling of gold foils and gilding is discussed. This publication highlights the need for sampling the reflectance at the mirror angle in order to obtain accurate BRDF models. Moreover, the spectral reflectance of the ten types of gold foils has been shared in an online repository².

In **Article B** and **C**, imaging techniques are used for the appearance capture of bronze patinas of varying colour and roughness. In **Article C**, the imaging setup, its acquisition parameters, and data processing pipeline are described. Moreover, the results of the system are validated against that of a commercial goniospectrophotometer. The validation of this system allows for it to be used not only as part of this thesis, in **Article D** and **E**, but also for other research purposes by other members of the Colourlab at NTNU.

In terms on conservation and restoration, **Article D**, has evaluated different chemical varnish removal methods on gilded surfaces based on their appearance. This problematic has been widely studied in other fields such as painting conservation but its impact on gilded surfaces was limited. Not only this methodology has proven successful at evaluating the varnish removal methods, but its results have been applied for the res-

²<https://zenodo.org/record/7543976#.Y-oox3bMK5c>

toration of the *Vierge de douleur* [Virgin of Sorrows]. Furthermore, the appearance evaluation of the different types of gilding as well as the effect of varnish and its removal, has elucidated existing misconceptions on the perception of gilding and appearance measurements. This has been further explored in **Article E**, which provides a review on the appearance of gilding and illustrates the limitations when describing the appearance of gilding due to a lack of adequate vocabulary and measurements. These limitations can cause misconceptions, which in turn lead to misinterpretations of the value and purpose of the gilded objects.

Chapter 5

Conclusions and Future Perspectives

5.1 Conclusions

The use of digital imaging technologies has been growing in the field of scientific practice for conservation. These offer a range of analysis and applications which are becoming mainstream. However, a research area which has been little investigated is that of material appearance characterisation for cultural heritage. While it is almost standard practice to perform colour measurements before and after restoration campaigns, other appearance attributes such as gloss, translucency and texture are not widely studied.

Colour measurements as defined by the [CIE](#) are limited to a specific viewing condition, which is only perceptually accurate under these conditions and for a limited set of materials, such as matte, Lambertian surfaces. Most materials present in cultural heritage objects have a complex appearance, whether present as goniochromaticity or due to a combination of appearance attributes such as gloss, metallicity, and translucency. Not to mention non-homogeneous materials with surface texture.

Due to this wide range of materials, it is necessary to obtain more complex reflectance measurements to characterise the appearance of these surfaces. In this thesis, the appearance of complex cultural heritage materials such as gilded surfaces was characterised and evaluated using perceptual models, to guide conservation treatments. The secondary aim of

this thesis was to evaluate the feasibility of using an imaging system for capturing the appearance of these surfaces.

This research has focused on two sub-objectives. The first sub-objective concerned the development and evaluation of an imaging protocol for the acquisition and modelling of the BRDF of complex surfaces. First, conventional methods such as colorimetry, gloss measurements, and multi-angle spectrophotometers were evaluated. It was found that these measurements lack the ability to properly characterise the visual differences between the gilded samples.

An imaging device was presented as an alternative to perform bidirectional reflectance measurements. This device was compared to measurements from a commercial goniospectrophotometer. The accuracy and precision of the imaging setup were found to be appropriate for acquiring the appearance of gilded samples. It was found that the non-uniformity of the samples influences the accuracy of the measurements, while the precision is affected by the physical limitations of the setup.

Finally, the second sub-objective aims to apply material appearance analysis to conservation and restoration. For this purpose, varnish removal methods in gilded surfaces were evaluated. The imaging system described above was used to acquire the bidirectional reflectance of the samples. Their appearance was evaluated using perceptual gloss metrics to describe the differences between the samples. By using perceptual gloss metrics, the varnish removal methods were evaluated to determine the one which causes the smallest change in appearance. This method has been used for the restoration of a 15th century painted panel.

The traditional gilding samples are compared to "imitation" gilding samples. It is found that the perceptual gloss metrics can characterise the different types of gilding based on their appearance. The results are consistent with the various light-matter interactions at the interface of the different materials and can explain the perceptual differences between metallic samples and glossy samples.

In conclusion, the research presented in this PhD thesis has successfully applied material appearance analysis to complex cultural heritage materials. By developing imaging methodologies and processing algorithms, the appearance of gilded samples has been acquired and modelled. The results of the appearance evaluation have been applied to restore a 15th century painted panel and have also been used to explain perceptual dif-

ferences between different types of gilding. This research has highlighted a two-fold need from conservators and restorers. On one hand, it has shown that single appearance attributes are insufficient to characterise the appearance of complex materials. Most cultural heritage materials exhibit a combination of the four appearance attributes, which all interact with each other. Thus, it is necessary to perform more complex bidirectional reflectance measurements to characterise their appearance. And on the other hand, it has shown that by better describing the appearance of surfaces such as gilding, both quantitatively and subjectively, a more accurate understanding of objects and procedures is possible.

5.2 Future Perspectives

As this PhD research has shown, material appearance is field of study which is constantly evolving. While this has not been widely applied to cultural heritage, this thesis opens many perspectives and opportunities of research which will be discussed here.

For material appearance capture, an imaging based setup was presented to obtain bidirectional reflectance measurements of complex surfaces. In order to obtain the reflectance factors, a determined area of pixels is averaged. However, the spatial dimension of the data should be exploited further in order to evaluate the texture and non-uniformity of the samples which is commonly found in many cultural heritage materials.

Moreover, this system is limited to flat samples and there is a limitation on the size of the object. A more important contribution would be to develop a smaller, portable system, which could be used in-situ to measure the appearance of paintings or objects which cannot be transported to a laboratory.

Furthermore, a more thorough investigation should be done on the perceptual qualities of the gilded samples. As part of the second sub-objective, psychophysically based metrics were used to evaluate the appearance models of the gilded surfaces. However, these metrics were developed for ideal glossy surfaces. The appearance of the gilded surfaces is made of a combination of light-matter interactions which are not fully described by an ideal gloss model. Thus, psychophysical experiments should be performed to evaluate how good the models are at reproducing the appearance of the gilding.

Finally, in the case of composite materials such as varnished gilding, or "imitation" gilding, optical models should be evaluated, taking into ac-

count the refractive index of the varnish/resin, and modulating either the roughness of the metal leaf or the roughness of the varnish layer. These models could then be evaluated against the bidirectional reflectance measurements. Moreover, by modelling the optical properties of the samples, effects like weathering and ageing can be investigated.

Bibliography

- Adelson, E. H. (2001). “On seeing stuff: the perception of materials by humans and machines”. In: *Human vision and electronic imaging VI*. Vol. 4299. SPIE, pp. 1–12.
- Agahian, F., Amirshahi, S. A. and Amirshahi, S. H. (2008). “Reconstruction of reflectance spectra using weighted principal component analysis”. In: *Color Research & Application* 33.5, pp. 360–371. ISSN: 0361-2317.
- Althöfer, H. (1981). “Historical and ethical principles of restoration”. In: *Icom committee for conservation. 6th triennial meeting, Ottawa, 21-25 September 1981. Preprints*, pp. 4–4.
- Anderson, B. L. (2011). “Visual perception of materials and surfaces”. In: *Current Biology* 21.24, R978–R983. ISSN: 0960-9822. DOI: [10.1016/j.cub.2011.11.022](https://doi.org/10.1016/j.cub.2011.11.022).
- Arney, J., Heo, H. and Anderson, P. (2004). “A micro-goniophotometer and the measurement of print gloss”. In: *Journal of Imaging Science and Technology* 48.5, pp. 458–463. ISSN: 1062-3701.
- Arteaga, Y., Boust, C., Dequier, A. and Yngve Hardeberg, J. (2021). “Image-based goniometric appearance characterisation of bronze patinas”. In: *Color and Imaging Conference*. Vol. 2021. Society for Imaging Science and Technology, pp. 294–299. ISBN: 2166–9635.
- Arteaga, Y., Boust, C. and Hardeberg, J. Y. (2023). “Quantifying the appearance of gilded surfaces”. In: *Cultural Heritage Analysis for New Generations*. Ed. by C. Degryny, S. George, J. Y. Hardeberg and A. Østlien. to be published. London: Routledge.
- Arteaga, Y., Marchioni, D., Courtier, S., Boust, C. and Hardeberg, J. Y. (2023). “Appearance-based evaluation of varnish removal methods in gilded surfaces”. In: *Heritage Science* 11, p. 31. ISSN: 2050-7445.

- Arteaga, Y., Mélard, N., Boust, C., Hardeberg, J. Y. and Robcis, D. (2022). “Semiautomatic Toolmark Classification in Chased Metals Using Surface Microtopography”. In: *Heritage* 5.4, pp. 2922–2943. ISSN: 2571-9408.
- Arteaga, Y., Sole, A. S., Hardeberg, J. Y. and Boust, C. (2022). “Characterising appearance of gold foils and gilding in conservation and restoration”. In: *Colour and Visual Computing Symposium, Gjovik, Norway*. CEUR. ISBN: 1613–0073.
- ASTM (2008). *ASTM-E2175, Standard practice of specifying the geometry of multiangle spectrophotometers*. Standard.
- ASTM (2012). *ASTM E284 - 17: Standard terminology of appearance*. Standard. URL: www.astm.org.
- Babini, A., Green, P., George, S. and Hardeberg, J. Y. (2022). “Comparison of Hyperspectral Imaging and Fiber-Optic Reflectance Spectroscopy for Reflectance and Transmittance Measurements of Colored Glass”. In: *Heritage* 5.3, pp. 1401–1418. ISSN: 2571-9408.
- Bayer, B. (1976). “Color imaging array”. In: *United States Patent, no. 3971065*.
- Bell, S., Upchurch, P., Snavely, N. and Bala, K. (2015). “Material recognition in the wild with the materials in context database”. In: *Proceedings of the IEEE conference on computer vision and pattern recognition*, pp. 3479–3487.
- Bertholon, R. (2017). “De la pratique à la théorie: une déontologie née dans les ateliers”. In: *Actualités de la conservation* 34, pp. 1–6. ISSN: 1778-4034.
- Billmeyer Jr, F. W. and O’Donnell, F. X. (1987). “Visual gloss scaling and multidimensional scaling analysis of painted specimens”. In: *Color Research & Application* 12.6, pp. 315–326. ISSN: 0361-2317.
- Bradley, S. (1997). *The Interface Between Science and Conservation*. British Museum. ISBN: 9780861591169.
- Brandi, C. (2001). *Théorie de la restauration*. Éditions Allia. ISBN: 9791030414011.
- Brauers, J. and Aach, T. (2010). “Geometric calibration of lens and filter distortions for multispectral filter-wheel cameras”. In: *IEEE Transactions on Image Processing* 20.2, pp. 496–505. ISSN: 1057-7149.
- Brauers, J., Schulte, N., Bell, A. A. and Aach, T. (2008). “Multispectral high dynamic range imaging”. In: *Color Imaging XIII: processing, hardcopy, and applications*. Vol. 6807. SPIE, pp. 26–37.
- Budde, W. (1980). “The Calibration of Gloss Reference Standards”. In: *Metrologia* 16.2, p. 89. DOI: [10.1088/0026-1394/16/2/004](https://doi.org/10.1088/0026-1394/16/2/004).
- Callet, P., Zymła, A. and Mofakhami, A. (2002). “Virtual Metallurgy and Archaeology. Application to the Visual Simulation of a Work of Art”. In: *International Conference on Computer Vision and Graphics*, pp. 25–29.

- Caple, C. (2012). *Conservation skills: judgement, method and decision making*. Routledge. ISBN: 0203086260.
- Chaban, A., Lanterna, G., Gigli, M. C., Becucci, M., Fontana, R. and Striova, J. (2021). "Multi-analytical approach to the study of mecca gilding technique". In: *Microchemical Journal* 168, p. 106415. ISSN: 0026-265X.
- Chadwick, A. C. and Kentridge, R. (2015). "The perception of gloss: A review". In: *Vision research* 109, pp. 221–235. ISSN: 0042-6989.
- Chen, T., Taplin, L. A. and Berns, R. S. (2011). "Munsell color science laboratory artist material database brdf fitting". In: *Munsell Color Science Laboratory Technical Report*, www.art-si.org.
- Choudhury, A. K. R. (2014). *Principles of colour and appearance measurement: Object appearance, colour perception and instrumental measurement*. Elsevier. ISBN: 0857099248.
- CIE (2004). *CIE 15.2 Colorimetry*. Standard.
- Clavir, M. (2012). *Preserving what is valued*. UBC Press. ISBN: 077485250X.
- Conni, M. (2022). "Appearance Characterization of Textiles". PhD Thesis. Norwegian University of Science and Technology. Gjøvik, Norway.
- Cook, R. L. and Torrance, K. E. (1982). "A reflectance model for computer graphics". In: *ACM Transactions on Graphics* 1.1, pp. 7–24.
- Courtier, S. and Dubost, M. (2021). "L'or et la manière : les techniques de la dorure sur bois à travers le temps". In: *Coré* 1.
- Cutajar, J. D., Babini, A., Deborah, H., Hardeberg, J. Y., Joseph, E. and Frøy-saker, T. (2022). "Hyperspectral Imaging Analyses of Cleaning Tests on Edvard Munch's Monumental Aula Paintings". In: *Studies in Conservation* 67.sup1, pp. 59–68. ISSN: 0039-3630.
- Deborah, H., George, S. and Hardeberg, J. Y. (2019). "Spectral-divergence based pigment discrimination and mapping: A case study on The Scream (1893) by Edvard Munch". In: *Journal of the American Institute for Conservation* 58.1-2, pp. 90–107. ISSN: 0197-1360.
- Deborah, H. and Mandal, D. J. (2022). "Evaluation of Text Legibility in Alternative Imaging Approaches to Microfiche Digitization". In: *Archiving Conference*. Vol. 18. Society for Imaging Science and Technology, pp. 96–101.
- Doerschner, K., Boyaci, H. and Maloney, L. T. (2010). "Estimating the glossiness transfer function induced by illumination change and testing its transitivity". In: *Journal of Vision* 10.4, pp. 8–8. ISSN: 1534-7362.
- Dorsey, J., Rushmeier, H. and Sillion, F. (2010). *Digital modeling of material appearance*. Elsevier. ISBN: 008055671X.
- Dumazet, S., Genty, A., Zymla, A., De Contencin, F., Texier, A., Ruscassier, N., Bonnet, B. and Callet, P. (2007). "Influence of the substrate colour on

- the visual appearance of gilded sculptures”. In: *XXI International CIPA Symposium*. Ed. by A. Georgopoulos, pp. 01–06.
- Edelson, J. (2000). “Elaboration d’une méthodologie d’analyse des patines artificielles sur les bronzes du patrimoine artistique”. Master Thesis. École des Mines de Paris. Paris, France.
- Eipper, P.-B. and Frankowski, G. (2004). “Examination of cleaned oil paint surfaces by 3D-measurement technology”. In: *The picture restorer* 26, pp. 5–13. ISSN: 0964-9662.
- Elias, M. and Simonot, L. (2004). “Bi-directional reflectance of a varnished painting Part 1: Influence of the refractive indices without using the approximations of Saunderson correction–exact computation”. In: *Optics communications* 231.1-6, pp. 17–24. ISSN: 0030-4018.
- Elias, M., Rie, E. R. de la, Delaney, J. K., Charron, E. and Morales, K. M. (2006). “Modification of the surface state of rough substrates by two different varnishes and influence on the reflected light”. In: *Optics communications* 266.2, pp. 586–591. ISSN: 0030-4018.
- Elias, M., Simonot, L., Thoury, M. and Frigerio, J. M. (2004). “Bi-directional reflectance of a varnished painting: Part 2: Comparison between the effects of the refractive indices, of the surface states and of the absorption of the varnish–experiments and simulations”. In: *Optics communications* 231.1-6, pp. 25–33. ISSN: 0030-4018.
- Elkhuizen, W., Essers, T., Song, Y., Geraedts, J., Weijkamp, C., Dik, J. and Pont, S. (2019). “Gloss, Color, and Topography Scanning for Reproducing a Painting’s Appearance Using 3D Printing”. In: *Journal on Computing and Cultural Heritage* 12.4. ISSN: 1556-4673. DOI: [10.1145/3317949](https://doi.org/10.1145/3317949).
- Eugène, C. (2008). “Measurement of “total visual appearance”: a CIE challenge of soft metrology”. In: *12th IMEKO TC1 & TC7 Joint Symposium on Man, Science & Measurement*, pp. 61–65.
- Fairchild, M. D. (2013). *Color appearance models*. John Wiley & Sons. ISBN: 1118653106.
- Ferrero, A., Rabal, A., Campos, J., Martínez-Verdú, F., Chorro, E., Perales, E., Pons, A. and Hernanz, M. L. (2013). “Spectral BRDF-based determination of proper measurement geometries to characterize color shift of special effect coatings”. In: *Journal of the Optical Society of America A* 30.2, pp. 206–214. DOI: [10.1364/JOSAA.30.000206](https://doi.org/10.1364/JOSAA.30.000206).
- Ferwerda, J. A., Pellacini, F. and Greenberg, D. P. (2001). “Psychophysically based model of surface gloss perception”. In: *SPIE 4299, Human Vision and Electronic Imaging VI*. Vol. 4299. SPIE, pp. 291–301. DOI: <https://doi.org/10.1117/12.429501>.

- Fleming, R. W. (2014). “Visual perception of materials and their properties”. In: *Vision research* 94, pp. 62–75. ISSN: 0042-6989.
- Fleming, R. W. and Bühlhoff, H. H. (2005). “Low-level image cues in the perception of translucent materials”. In: *ACM Transactions on Applied Perception (TAP)* 2.3, pp. 346–382. ISSN: 1544-3558.
- Fleming, R. W., Dror, R. O. and Adelson, E. H. (2003). “Real-world illumination and the perception of surface reflectance properties”. In: *Journal of vision* 3.5, pp. 3–3. ISSN: 1534-7362.
- Fleming, R. W., Jäkel, F. and Maloney, L. T. (2011). “Visual perception of thick transparent materials”. In: *Psychological science* 22.6, pp. 812–820. ISSN: 0956-7976.
- Fleming, R. W., Wiebel, C. and Gegenfurtner, K. (2013). “Perceptual qualities and material classes”. In: *Journal of vision* 13.8, pp. 9–9. ISSN: 1534-7362.
- Fores, A., Ferwerda, J. and Gu, J. (2012). “Toward a perceptually based metric for BRDF modeling”. In: *Color and Imaging Conference*. Vol. 2012. Society for Imaging Science and Technology, pp. 142–148. ISBN: 2166-9635.
- Gat, N. (2000). “Imaging spectroscopy using tunable filters: a review”. In: *Wavelet Applications VII* 4056, pp. 50–64.
- Genty-Vincent, A., Van Song, T. P., Andraud, C. and Menu, M. (2017). “Four-flux model of the light scattering in porous varnish and paint layers: towards understanding the visual appearance of altered blanched easel oil paintings”. In: *Applied Physics A* 123, pp. 1–9. ISSN: 0947-8396.
- Gigilashvili, D., Shi, W., Wang, Z., Pedersen, M., Hardeberg, J. Y. and Rushmeier, H. (2021). “The role of subsurface scattering in glossiness perception”. In: *ACM Transactions on Applied Perception (TAP)* 18.3, pp. 1–26. ISSN: 1544-3558.
- Gigilashvili, D., Thomas, J.-B., Hardeberg, J. Y. and Pedersen, M. (2021). “Translucency perception: A review”. In: *Journal of Vision* 21.8, pp. 4–4. ISSN: 1534-7362.
- Green, P. and MacDonald, L. (2011). *Colour engineering: achieving device independent colour*. John Wiley & Sons. ISBN: 0470854138.
- Guarnera, D., Guarnera, G. C., Ghosh, A., Denk, C. and Glencross, M. (2016). “BRDF representation and acquisition”. In: *Computer Graphics Forum* 35.2, pp. 625–650. ISSN: 0167-7055.
- Hardeberg, J. Y., Schmitt, F. and Brettel, H. (2002). “Multispectral color image capture using a liquid crystal tunable filter”. In: *Optical engineering* 41.10, pp. 2532–2548. ISSN: 0091-3286.

- Harteveld, G. (2019). "Investigation of the Effect of the Green Glaze Layer in the Background of Girl with a Pearl Earring by Johannes Vermeer: An Approach using Optical Properties of Paints and Rendering Technique". PhD Thesis. Delft University of Technology. Delft, The Netherlands.
- Harvey, J., Smithson, H. E. and Kollandsrud, K. (2018). "Not All That Glitters: Probing Material Perception With a Physical Imitation Gold Stimulus". In: *Perception*. Vol. 47. Sage Publications, pp. 572–572. ISBN: 0301-0066.
- Harvey, J. S. and Smithson, H. E. (2021). "Low level visual features support robust material perception in the judgement of metallicity". In: *Scientific Reports* 11.1, p. 16396. ISSN: 2045-2322.
- Hecht, E. (2012). *Optics*. Pearson Education India. ISBN: 8131718077.
- Heitz, E. (2014). "Understanding the masking-shadowing function in microfacet-based BRDFs". In: *Journal of Computer Graphics Techniques* 3.2, pp. 32–91.
- Ho, Y.-X., Landy, M. S. and Maloney, L. T. (2008). "Conjoint measurement of gloss and surface texture". In: *Psychological science* 19.2, pp. 196–204. ISSN: 0956-7976.
- Hui, S., Jianyu, W. and Yongqi, X. (1998). "Key technology of pushbroom hyperspectral imager (PHI)". In: *Journal of Remote Sensing* 2.4, pp. 251–254.
- Hunt, R. W. G. and Pointer, M. R. (2011). *Measuring colour*. John Wiley & Sons. ISBN: 1119975379.
- Hunt, R. W. G. (1995). *The reproduction of colour*. Vol. 4. Wiley Online Library.
- Hunter, R. S. (1937). "Methods of determining gloss". In: *Journal of Research of the National Bureau of Standards* 18.
- Hunter, R. S. and Harold, R. W. (1987). *The measurement of appearance*. John Wiley & sons.
- Hutchings, J. (1995). "The continuity of colour, design, art, and science. I. The philosophy of the total appearance concept and image measurement". In: *Color Research & Application* 20.5, pp. 296–306. ISSN: 0361-2317.
- ISO (2010). *Geometrical product specifications (gps) - surface texture: Areal - part 6: Classification of methods for measuring surface texture*. Standard. URL: www.iso.org.
- Ji, W., Pointer, M. R., Luo, R. M. and Dakin, J. (2006). "Gloss as an aspect of the measurement of appearance". In: *Journal of the Optical Society of America A* 23.1, pp. 22–33. ISSN: 1520-8532.

- Kitanovski, V. and Hardeberg, J. Y. (2021). “Objective evaluation of relighting models on translucent materials from multispectral RTI images”. In: *Electronic Imaging* 2021.5, pp. 133-1-133-8. ISSN: 2470-1173.
- Kollandsrud, K. (2017). “Polychrome Light in Medieval Norwegian Church Art (12th–13th Centuries)”. In: *From Conservation to Interpretation*. Ed. by J. Kroesen, E. Nyborg and M. Sauerberg. Peeters.
- Kollandsrud, K. and Plahter, U. (2019). “Twelfth and early thirteenth century polychromy at the northernmost edge of Europe: past analyses and future research”. In: *Medievalista [online]* 26. ISSN: 1646-740X. DOI: [10.4000/medievalista.2303](https://doi.org/10.4000/medievalista.2303).
- Komatsu, H., Nishio, A., Okazawa, G. and Goda, N. (2013). “‘Yellow’ or ‘gold’?: Neural processing of gloss information”. In: *Computational Color Imaging: 4th International Workshop, CCIW 2013, Chiba, Japan, March 3-5, 2013. Proceedings*. Springer, pp. 1–12. ISBN: 3642366996.
- Lapray, P.-J., Thomas, J.-B., Gouton, P. and Ruichek, Y. (2017). “Energy balance in Spectral Filter Array camera design”. In: *Journal of the European Optical Society-Rapid Publications* 13, pp. 1–13.
- Lawrence, K. C., Park, B., Windham, W. R. and Mao, C. (2003). “Calibration of a pushbroom hyperspectral imaging system for agricultural inspection”. In: *Transactions of the ASAE* 46.2, p. 513.
- Leach, R. (2013). *Characterisation of Areal Surface Texture*. Springer.
- Learner, T. J., Smithen, P., Krueger, J. W. and Schilling, M. R. (2007). *Modern Paints Uncovered: Proceedings from the Modern Paints Uncovered Symposium*. Los Angeles: The Getty Conservation Institute.
- Leloup, F. B., Obein, G., Pointer, M. R. and Hanselaer, P. (2014). “Toward the soft metrology of surface gloss: A review”. In: *Color Research & Application* 39.6, pp. 559–570. ISSN: 0361-2317.
- Liu, C., Sharan, L., Adelson, E. H. and Rosenholtz, R. (2010). “Exploring features in a bayesian framework for material recognition”. In: *2010 IEEE Computer Society Conference on computer vision and pattern recognition*. IEEE, pp. 239–246. ISBN: 1424469856.
- Lu, R., Koenderink, J. J. and Kappers, A. M. (1998). “Optical properties (bi-directional reflection distribution functions) of velvet”. In: *Applied Optics* 37.25, pp. 5974–5984. ISSN: 2155-3165.
- MacDonald, L., Vitorino, T., Picollo, M., Pillay, R., Obarzanowski, M., Sobczyk, J., Nascimento, S. and Linhares, J. (2017). “Assessment of multispectral and hyperspectral imaging systems for digitisation of a Russian icon”. In: *Heritage Science* 5.1. ISSN: 2050-7445. DOI: [10.1186/s40494-017-0154-1](https://doi.org/10.1186/s40494-017-0154-1).

- Mandal, D. J., George, S., Pedersen, M. and Boust, C. (2021). "Influence of acquisition parameters on pigment classification using hyperspectral imaging". In: *Journal of Imaging Science and Technology* 65 (5), pp. 050406-1–050406-13.
- Mansouri, A., Marzani, F. S. and Gouton, P. (2005). "Neural networks in two cascade algorithms for spectral reflectance reconstruction". In: *IEEE International Conference on Image Processing 2005*. Vol. 2. IEEE, pp. II–718. ISBN: 0780391349.
- Marchioni, D. (2021). "Conservation-restauration d'une vierge de douleur, panneau peint et doré de la fin du XVeme siecle, et de son cadre doré et polychromé (Musée Jacquemart-André, Paris). Recherche de provenance et datation de l'oeuvre. Étude comparative de différentes méthodes de nettoyage d'une dorure sur bois vernie." Master thesis. National Heritage Institute, Conservation Department. Paris, France.
- Marschner, S. R., Westin, S. H., Lafortune, E. P., Torrance, K. E. and Greenberg, D. P. (1999). "Image-based BRDF measurement including human skin". In: *Rendering Techniques'99: Proceedings of the Eurographics Workshop in Granada, Spain, June 21–23*. Springer, pp. 131–144. ISBN: 321183382X.
- Martinez, M. A., Valero, E. M., Nieves, J. L., Blanc, R., Manzano, E. and Vilchez, J. L. (2019). "Multifocus HDR VIS/NIR hyperspectral imaging and its application to works of art". In: *Optics Express* 27.8, pp. 11323–11338. DOI: [10.1364/OE.27.011323](https://doi.org/10.1364/OE.27.011323).
- Martínez Domingo, M., Valero, E., Huertas, R., Durbán, M., Espejo, T. and Blanc, R. (2019). "Spectral information to get beyond color in the analysis of water-soluble varnish degradation". In: *Heritage Science* 7, pp. 1–16.
- Mecklenburg, M. F., Charola, A. E. and Koestler, R. J. (2013). *New insights into the cleaning of paintings: proceedings from the cleaning 2010 international conference, Universidad Politécnica de Valencia and Museum Conservation Institute*. Washington DC: Smithsonian Institution Scholarly Press.
- Mounier, A. and Daniel, F. (2013). "The role of the under-layer in the coloured perception of gildings in medieval mural paintings". In: *Open Journal of Archaeometry* 1.1, e16. ISSN: 2038-1956 2038-1948. DOI: [10.4081/arc.2013.e16](https://doi.org/10.4081/arc.2013.e16).
- Muñoz-Viñas, S. (2002). "Contemporary theory of conservation". In: *Reviews in Conservation* 3, pp. 25–34.
- Muñoz-Viñas, S. (2012). *Contemporary theory of conservation*. Routledge. ISBN: 008047683X.

- Neven, S. (2016). *The Strasbourg Manuscript: A Mediaeval Tradition of Artists' Recipe Collections (1400-1570)*. London: Archetype Publication.
- Nicodemus, F. E. and Richmond, J. C. (1977). *Geometrical considerations and nomenclature for reflectance*. Standard. National Bureau of Standards.
- O'Donnell, F. X. and Billmeyer Jr, F. W. (1986). "Psychometric scaling of gloss". In: *Review and evaluation of appearance: Methods and techniques. ASTM STP 914*, pp. 14–32.
- Obein, G., Leroux, T. and Vienot, F. (2001). "Bidirectional reflectance distribution factor and gloss scales". In: *Photonics West 2001 - Electronic Imaging*. Vol. 4299. SPIE.
- Obein, G., Knoblauch, K. and Viénot, F. (2004). "Difference scaling of gloss: Nonlinearity, binocularity, and constancy". In: *Journal of vision* 4.9, pp. 4–4. ISSN: 1534-7362.
- Olkkonen, M. and Brainard, D. H. (2010). "Perceived glossiness and lightness under real-world illumination". In: *Journal of vision* 10.9, pp. 5–5. ISSN: 1534-7362.
- Olkkonen, M. and Brainard, D. H. (2011). "Joint effects of illumination geometry and object shape in the perception of surface reflectance". In: *i-Perception* 2.9, pp. 1014–1034. ISSN: 2041-6695.
- Papanikolaou, A., Dzik-Kruszelnicka, D. and Kujawinska, M. (2022). "Spatio-temporal monitoring of humidity induced 3D displacements and strains in mounted and unmounted parchments". In: *Heritage Science* 10.1, pp. 1–25. ISSN: 2050-7445.
- Pedrotti, F. L., Pedrotti, L. M. and Pedrotti, L. S. (2017). *Introduction to optics*. Cambridge University Press. ISBN: 1108597548.
- Petzet, M. (1999). "Principles of Monument Conservation. Principes de la Conservation des Monuments Historiques". In: *ICOMOS–Hefte des Deutschen Nationalkomitees* 30. ISSN: 2365-5631.
- Philippe, E. (2008). "Innover, connaître et transmettre. L'art de la restauration selon François-Toussaint Hacquin (1756-1832)". In: *Techné* 27–28, pp. 53–59.
- Pillay, R. (2021). "Multispectral and Hyperspectral Imaging of Art: Quality, Calibration and Visualization". PhD Thesis. Norwegian University of Science and Technology. Gjøvik, Norway.
- Pointer, M. R. (2003). *Measuring visual appearance—a framework of the future. Project 2.3 measurement of appearance*. NPL Report.
- Qi, L., Chantler, M. J., Siebert, J. P. and Dong, J. (2012). "How mesoscale and microscale roughness affect perceived gloss". In: *Proceedings of the*

- 3rd International Conference on Appearance (Edinburgh, UK)*, pp. 48–51.
- Ribés, A., Schmitt, F. and Brettel, H. (2001). “Reconstructing Spectral Reflectances of Oil Pigments with Neural Networks”. In: *Restoration* 6, p. 14.
- Rie, E. R. de la (1987). “The influence of varnishes on the appearance of paintings”. In: *Studies in conservation* 32.1, pp. 1–13. ISSN: 0039-3630.
- Rie, E. R. de la, Delaney, J. K., Morales, K. M., Maines, C. A. and Sung, L.-P. (2010). “Modification of surface roughness by various varnishes and effect on light reflection”. In: *Studies in conservation* 55.2, pp. 134–143. ISSN: 0039-3630.
- Ruskin, J. (2008). *The lamp of memory*. Vol. 48. Penguin UK. ISBN: 0141036672.
- Sandu, I., Busani, T. and Sá, M. H. de (2011). “The surface behavior of gilding layer imitations on polychrome artefacts of cultural heritage”. In: *Surface and Interface Analysis* 43.8, pp. 1171–1181. ISSN: 0142-2421.
- Sharan, L., Rosenholtz, R. and Adelson, E. H. (2014). “Accuracy and speed of material categorization in real-world images”. In: *Journal of vision* 14.9, pp. 12–12. ISSN: 1534-7362.
- Sharma, G. (2017). “Color fundamentals for digital imaging”. In: *Digital color imaging handbook*. CRC press, pp. 1–114. ISBN: 1315220083.
- Sidorov, O., Hardeberg, J. Y., George, S., Harvey, J. S. and Smithson, H. E. (2020). “Changes in the Visual Appearance of Polychrome Wood Caused by (Accelerated) Aging”. In: *Electronic Imaging*. Ed. by M. Hebert. Society for Imaging Science and Technology, pp. 060-1–060-7. DOI: doi.org/10.2352/ISSN.2470-1173.2020.5.MAAP-060.
- Simonot, L. and Elias, M. (2004). “Color change due to a varnish layer”. In: *Color Research & Application* 29.3, pp. 196–204. ISSN: 0361-2317.
- Simonot, L., Elias, M. and Charron, E. (2004). “Special visual effect of art glazes explained by the radiative transfer equation”. In: *Applied optics* 43.12, pp. 2580–2587. ISSN: 2155-3165.
- Smith, T. and Guild, J. (1931). “The CIE colorimetric standards and their use”. In: *Transactions of the optical society* 33.3, p. 73. ISSN: 1475-4878.
- Sole, A., Farup, I., Nussbaum, P. and Tominaga, S. (2018). “Evaluating an image-based bidirectional reflectance distribution function measurement setup”. In: *Applied Optics* 57.8, pp. 1918–1928. ISSN: 2155-3165.
- Sole, A., Guarnera, G., Farup, I. and Nussbaum, P. (2021). “Measurement and rendering of complex non-diffuse and goniochromatic packaging materials”. In: *The Visual Computer* 37.8, pp. 2207–2220. ISSN: 0178-2789.

- Sole, A. S. (2019). “Image-Based Bidirectional Reflectance Measurement of Non-Diffuse and Gonio-Chromatic Materials”. PhD Thesis. Norwegian University of Science and Technology. Gjøvik, Norway.
- Stein, M. and Haugen, A. (2010). “Topographic registration of surfaces on canvas paintings: investigations with a mobile non-contact profilometer”. In: *Restauro: Forum für Restauratoren, Konservatoren und Denkmalspfleger, 2010*. Vol. 116, pp. 396–401. ISBN: 0933-4017.
- Tamura, H., Higashi, H. and Nakauchi, S. (2018). “Dynamic visual cues for differentiating mirror and glass”. In: *Scientific reports* 8.1, p. 8403. ISSN: 2045-2322.
- Te Pas, S. E. and Pont, S. C. (2005). “A comparison of material and illumination discrimination performance for real rough, real smooth and computer generated smooth spheres”. In: *Proceedings of the 2nd Symposium on Applied Perception in Graphics and Visualization*, pp. 75–81.
- The Metropolitan Museum of Art (2023). *Chroma: Ancient Sculpture in Color*. Website. (Accessed: April, 2023.) URL: <https://www.metmuseum.org/exhibitions/chroma>.
- Todd, J. T. and Norman, J. E. (2018). “The visual perception of metal”. In: *Journal of Vision* 18.3, p. 9. ISSN: 1534-7362. DOI: [10.1167/18.3.9](https://doi.org/10.1167/18.3.9).
- Toque, J., Komori, M., Murayama, Y. and Ide-Ektessabi, A. (2010). “Analytical Imaging of Traditional Japanese Paintings Using Multispectral Images”. In: *VISIGRAPP: International Joint Conference on Computer Vision, Imaging and Computer Graphics Theory and Applications*. Ed. by A. Ranchordas. Springer, pp. 119–132.
- Torrance, K. E. and Sparrow, E. M. (1967). “Theory for off-specular reflection from roughened surfaces”. In: *Journal of the Optical Society of America* 57.9, pp. 1105–1112.
- Toscani, M., Guarnera, D., Guarnera, G. C., Hardeberg, J. Y. and Gegenfurtner, K. R. (2020). “Three perceptual dimensions for specular and diffuse reflection”. In: *ACM Transactions on Applied Perception (TAP)* 17.2, pp. 1–26. ISSN: 1544-3558.
- UNESCO World Heritage Committee (1994). *Nara Document on Authenticity*. Chart.
- Urban, P., Tanksale, T. M., Brunton, A., Vu, B. M. and Nakauchi, S. (2019). “Redefining A in RGBA: Towards a standard for graphical 3D printing”. In: *ACM Transactions on Graphics (TOG)* 38.3, pp. 1–14. ISSN: 0730-0301.
- Vangorp, P., Barla, P. and Fleming, R. W. (2017). “The perception of hazy gloss”. In: *Journal of vision* 17.5, pp. 19–19. ISSN: 1534-7362.

- Vangorp, P., Laurijssen, J. and Dutré, P. (2007). “The influence of shape on the perception of material reflectance”. In: *ACM SIGGRAPH 2007 papers*, 77–es.
- Viollet-le-Duc, E. (1875). *Dictionnaire raisonné de l'architecture française*. Morel Paris.
- Walter, B., Marschner, S. R., Li, H. and Torrance, K. E. (2007). “Microfacet models for refraction through rough surfaces”. In: *Eurographics conference on Rendering Techniques*. Eurographics Association, pp. 195–206.
- Ward, G. J. (1992). “Measuring and modeling anisotropic reflection”. In: *Proceedings of the 19th annual conference on Computer graphics and interactive techniques*, pp. 265–272.
- Wei, W. (2011). “Surface micro-roughness, cleaning, and perception”. In: *ICOM-CC 16th triennial conference. Almada (Portugal): Criteiro, 2011*.
- Wei, W., Stangier, S. and De Tagle, A. (2005). “In situ characterisation of the surface of paintings before and after cleaning using white light confocal profilometry”. In: *Proceedings of Art 5*.
- Wijntjes, M. W. and Pont, S. C. (2010). “Illusory gloss on Lambertian surfaces”. In: *Journal of Vision* 10.9, pp. 13–13. ISSN: 1534-7362.
- Wills, J., Agarwal, S., Kriegman, D. and Belongie, S. (2009). “Toward a perceptual space for gloss”. In: *ACM Transactions on graphics (TOG)* 28.4, pp. 1–15. ISSN: 0730-0301.
- Wolbers, R. C., Stavroudis, C. and Cushman, M. (2020). “Aqueous methods for the cleaning of paintings”. In: *Conservation of Easel paintings*. Ed. by J. H. Stoner and R. Rushfield. 2nd. London: Routledge, pp. 526–548.
- Wu, Q., Hauldenschild, M., Rösner, B., Lombardo, T., Schmidt-Ott, K., Watts, B., Nolting, F. and Ganz, D. (2020). “Does substrate colour affect the visual appearance of gilded medieval sculptures? Part I: colorimetry and interferometric microscopy of gilded models”. In: *Heritage Science* 8.118. ISSN: 2050-7445. DOI: [10.1186/s40494-020-00463-3](https://doi.org/10.1186/s40494-020-00463-3).
- Xiao, B., Walter, B., Gkioulekas, I., Zickler, T., Adelson, E. and Bala, K. (2014). “Looking against the light: How perception of translucency depends on lighting direction”. In: *Journal of vision* 14.3, pp. 17–17. ISSN: 1534-7362.
- Zhang, J., Su, R., Fu, Q., Ren, W., Heide, F. and Nie, Y. (2022). “A survey on computational spectral reconstruction methods from RGB to hyper-spectral imaging”. In: *Scientific reports* 12.1, p. 11905. ISSN: 2045-2322.

Part II

Original Papers

Article A

Yoko Arteaga, Aditya Sole, Jon Y. Hardeberg, and Clotilde Boust. Characterising appearance of gold foils and gilding in conservation and restoration. In *2022 Colour and Visual Computing Symposium (CVCS)*, vol: 3271, num: 11. CEUR workshop, 2022

Characterising appearance of gold foils and gilding in conservation and restoration

Yoko Arteaga^{1,2,*}, Aditya Sole², Jon Yngve Hardeberg² and Clotilde Boust^{1,3}

¹Centre for Research and Restoration of the Museums of France, Palais du Louvre, Porte des Lions, 14 quai François Mitterrand, 75001 Paris, France

²Colourlab, Norwegian University of Science and Technology, Teknologivegen 22, 2815 Gjøvik, Norway

³PSL-PCMTH UMR8247, CNRS, 11 Rue Pierre et Marie Curie, 75005 Paris, France

Abstract

Materials with complex optical properties like gold foils are commonly used for gilding in the field of conservation and restoration to render the visual appearance of the restoration object. Characterising the appearance of these materials is important to render an accurate visual appearance that can be obtained with different gilding techniques. In this paper, the bidirectional reflectance of gold foils commonly used for gilding is characterised and as well as gilding mock-ups. The dataset of gold foils is publicly available.

Keywords

BRDF measurement, gold, material appearance

1. Introduction

Gold material is commonly found in artworks in the form of gilding. In the past, artists used gold not only because of its cultural and religious importance but also because of its interesting appearance properties. Gilding is a form of polychromy found in medieval paintings and altarpieces [1]. It consists of a ground layer where a gold foil is attached to by different means. Different gilding techniques render different appearances. For example, oil gilding is known to have a matte and rough appearance whereas water gilding is smooth and glossy due to the final burnishing process using an agate stone [2].

In the field of conservation, it is important to have a deep understanding of the properties of different materials and how they contribute to the original appearance of surfaces. Gilding is a composite material in which its elements are arranged in layers, gold being one of them. It is thus, vital to characterise the appearance of the gold layer in the gilding to carry out better conservation campaigns which can render a more faithful appearance of the gilded object.

Gold material shows complex reflectance properties as its appearance changes with the change in the illumination direction [3]. Characterising the appearance of such materials is therefore difficult using the reflectance measurement geometries (like 0:diffuse, and 0:45) defined by the

The 11th Colour and Visual Computing Symposium, September 08–09, 2022, Gjøvik, Norway


*Corresponding author.

✉ yoko.arteaga@culture.gouv.fr (Y. Arteaga); aditya.sole@ntnu.no (A. Sole); jon.hardeberg@ntnu.no (J. Y. Hardeberg); clotilde.boust@culture.gouv.fr (C. Boust)

🆔 0000-0002-6787-789X (Y. Arteaga); 0000-0002-7916-5363 (A. Sole); 0000-0003-1150-2498 (J. Y. Hardeberg); 0000-0001-6019-1118 (C. Boust)



© 2022 Copyright for this paper by its authors. Use permitted under Creative Commons License Attribution 4.0 International (CC BY 4.0).

 CEUR Workshop Proceedings (CEUR-WS.org)

standardising bodies like ASTM and ISO. Bidirectional reflectance measurements are therefore necessary to characterise these materials appearance. Bidirectional reflectance measurements are performed using multi-angle spectrophotometers and goniospectrophotometers. Moreover, various types of gold foils are used in gilding that vary in karat, composition, and provenance which affects the gilding appearance visually. Famous examples besides traditional gold are white gold and rose gold [1].

In this paper, ten different gold foils commonly used for restoration, and two gilding mock-ups made by professional restorers have been bidirectionally measured and characterised using a bidirectional reflectance measurement device and a well established reflectance model. The gilding mock-ups are produced using one of the gold foils presented in this paper.

The structure of the paper is as follows: the next section of this paper presents a brief literature review of appearance modelling of gold and gilding. The third section presents the gold foils used and describes the fabrication method of the gilding mock-ups, the setup used for the bidirectional measurements, and the reflectance model fitting. Finally, the results and discussion are presented followed by the conclusion and final remarks.

2. Background

2.1. Appearance modelling of gold and gilding in restoration

Several attempts have been made to model and render the appearance of gold surfaces in cultural heritage objects. Callet et al. [4] proposed an empirical model based on the metallic structure of gold and used Kubelka Munk's two flux theory to render the gilding of polychrome statues.

The influence of the colour of the substrate on the appearance of gilding is actively studied within the field of cultural heritage and has been tested empirically by Dumazet et al. [5] by changing the colour of the substrate in their model and thus rendering different appearances of gilded surface. A similar study has been carried out by Mounier et al. [6] on medieval mural paintings. Mounier et al. [6] observed that the final appearance of the gilding is affected by the substrate colour.

Wu et al. [7] studied the influence of the substrate colour on the gild appearance by fabricating gilding mock-ups using different methods such as oil gilding, water gilding and ground gilding. Colorimetric and interferometric microscopic measurements were made to characterise the mock-ups. They concluded that the colour of the substrate does not alter the visual appearance of gilding. However, it was observed that burnishing the gild shows a significant visual change in its appearance.

MacDonald et al. [8] conducted a round-robin test to evaluate the quality of different multi- and hyper-spectral imaging devices both in terms of spectral and spatial quality. They studied objects with metal like finish and golden appearance. It was observed that the specularity of the surface and the golden appearance of the object increase the difficulty of accurately reproducing both colour and spectral characteristics of the object.

In [9] an HDR hyperspectral imaging methodology was proposed to accurately capture the reflectance spectra of an illuminated image with gold areas. The diffuse reflectance was then rendered within an uniform dynamic range.

A different type of gilding is found in medieval sculptures in Norway where instead of using a gold foil, a silver foil is used and then a yellow resin is applied to it, which gives the appearance of gold. In [10], bidirectional reflectance measurements of these samples are performed. It was observed that the samples showed two specular peaks due to its composite structure. One being from the interface air-resin and one from the interface resin-silver.

2.2. Bidirectional reflectance modelling

Bidirectional reflectance of a material can be modelled using a distribution function called bidirectional reflectance distribution function (BRDF) defined by Nicodemus in [11]. A BRDF describes how light is reflected off a surface. It is defined by the ratio between the differential irradiance along \mathbf{l} at point x and the differential outgoing radiance along \mathbf{v} :

$$f(x, \mathbf{l}, \mathbf{v}) = \frac{dL_r(x, \mathbf{v})}{dE(x, \mathbf{l})} \quad (1)$$

For a BRDF model to be physically valid it must obey two properties: be energy conserving and reciprocal. Due to the law of conservation of energy, the radiant energy reflected at a surface must not be greater than the energy incident on the surface. The second property is known as Helmholtz reciprocity, which dictates that the BRDF must be symmetrical. This means that reversing incoming and outgoing light does not change the BRDF outcome.

BRDF of a material can be further divided into isotropic and anisotropic. Regular surfaces with a rotational symmetry are called isotropic and the BRDF is expressed as $f(x, \theta_i, \theta_r)$, following the notation in Figure 4. Anisotropic surfaces exhibit a change in BRDF when rotated around the surface normal, giving $f(x, \theta_i, \phi_i, \theta_r, \phi_r)$.

A number of empirical and physical reflectance models have been defined till now to model different types of materials and for applications [12]. Cook-Torrance (CT) is a well established physical model and is used extensively to model specular materials like gold [3, 13, 14].

2.2.1. Cook-Torrance BRDF:

Cook-Torrance (CT) is a physical model based on the micro-facet theory [13]. CT model consists of specular and diffuse reflection components and mathematically is defined as follows:

$$f = k_d R_d + k_s R_s, \quad (2)$$

In Eq. 2, k_d and k_s are weighting parameters and $k_d + k_s = 1$. The specular term is based on micro-facet theory, which dictates that only the micro-facets on the surface with orientations in between the viewing vector and the incident vector, called half-vector $\mathbf{h} = \mathbf{l}, \mathbf{v}$, will contribute to the reflected light.

The general form of the CT specular term is:

$$R_s = \frac{1}{\pi} \frac{FDG}{(\mathbf{n}, \mathbf{l})(\mathbf{n}, \mathbf{v})}, \quad (3)$$

where F is the Fresnel term [15], G is the geometrical attenuation factor accounting for shadowing and masking of micro-facets, and D is the distribution of normals facing \mathbf{h} .

GGX distribution Walter et al. [16] propose a Bidirectional Scattering Distribution Function (BSDF) called GGX. This GGX BRDF is inspired by the micro-facet model proposed by Cook and Torrance. The general form of the GGX is given by:

$$R_s = \frac{1}{4} \frac{FDG}{(\mathbf{n} \cdot \mathbf{l})(\mathbf{n} \cdot \mathbf{v})}, \quad (4)$$

which is the same as the general form of the Cook-Torrance in Eq. 3, except that the normalisation factor for the Fresnel term is changed to 4. The Fresnel term in the GGX distribution is the same as the one proposed by Cook and Torrance. The GGX normal distribution function of micro-facets is given by:

$$D = \frac{\alpha_g^2 \chi^+(\mathbf{h} \cdot \mathbf{n})}{\pi \cos^4 \theta_h (\alpha_g^2 + \tan^2 \alpha_h)^2}, \quad (5)$$

where α_g is a width parameter for the specular lobe, θ_h is the angle between the half-vector, \mathbf{h} , and the surface normal, \mathbf{n} , and χ^+ is a positive characteristic function which equals to one if its parameter is greater than zero and zero if its parameter is lesser or equal to zero.

The geometrical attenuation factor which describes the shadowing and masking effects in the GGX is derived from D. This is given by the monodirectional shadowing term defined as

$$G_1(\mathbf{v}) = \chi^+ \left(\frac{\mathbf{v} \cdot \mathbf{h}}{\mathbf{v} \cdot \mathbf{n}} \right) \frac{2}{1 + \sqrt{1 + \alpha_g^2 \tan^2 \theta_v}}, \quad (6)$$

where θ_v is the angle between the viewing vector \mathbf{v} and the surface normal \mathbf{n} .

2.3. BRDF metrics

When optimising a BRDF model, different metrics can be used to find the best approximation to the surface reflectance. There is no consensus in the literature as to which metric should be used. A common metric to use is the Root Mean Square error (RMSE). In [17], the BRDF of a set of materials is estimated using different error metrics. The estimated BRDFs are then tested in a psychophysical experiment to correlate the choice of error metric and perceived appearance. The authors find that while metrics such as RMSE can provide a good optimisation when evaluating the BRDF plot, this does not always correlate to a faithful appearance reproduction if the rendered images are compared.

3. Method

3.1. Measurement samples: Gold foils

Ten gold foils that are commonly used in restoration were measured bidirectionally using a multiangle spectrophotometer. Table 1 gives the name and specification of these 10 gold foils. Since an extremely thin layer (approximately 0.2 microns in thickness) of the gold foils is used for gilding, the foil samples were prepared by a professional restorer to allow for production

Table 1

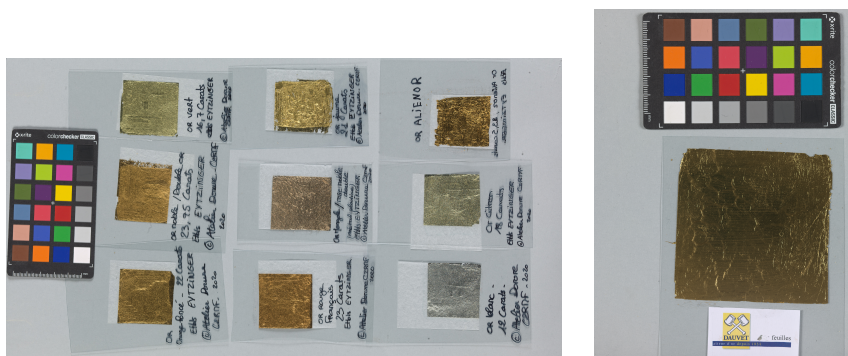
Specifications of the gold foils used. ©C2RMF/Stéphanie Courtier.

Name	Colour	Karat	Manufacturer
Or Alienor	Deep yellow/orange	23.5	Dauvet (FR)
Or Blanc	Light grey	12	Eytzinger (DE)
Or Citron	Light yellow	18	Eytzinger (DE)
Or Jaune	Deep yellow	21	Eytzinger (DE)
Or Noble	Deep yellow/orange	23.75	Eytzinger (DE)
Or Orange	Deep orange	22	Eytzinger (DE)
Or Rose	Rose	22	Eytzinger (DE)
Or Rouge	Deep orange/red	23	Eytzinger (DE)
Or Versailles	Deep yellow	22	Dauvet (FR)
Or Vert	Light yellow/green	16.7	Eytzinger (DE)

accuracy, layer uniformity, sample transportation, and measurement possibility. The gold foils have been prepared following the steps of oil gilding as follows:

- A ground layer of glue is applied to an acrylic sheet,
- When the glue is sticky, the gold foil is placed on top of the glue with the aid of a trowel and a gilder's tip, illustrated in Figure 2a,
- A gilder's duster is used to tap on any air bubbles which may have formed between the gold sheet and the acrylic.

Figure 1 shows the 10 gold foils used in this study.



(a) or Orange, or Noble, or Vert, or Rouge, or Rose, or Jaune, or Blanc, or Citron, or Alienor. (b) or Versailles used for the gilding mock-ups

Figure 1: Gold foil samples

3.1.1. Gilding samples:

Gilding using the gold foils can be carried out using 2 well established techniques called water gilding, and oil gilding. In both the techniques, a wood piece surface is first prepared using a ground layer made of chalk diluted with rabbit skin glue. In the water gilding technique, a substrate layer of red coloured clay, called bole, is applied to the surface and is made wet using ethanol and water before the gold foil is applied to it. In the next step, excess water (if any) is removed using a gilder's duster. The gold foil is then burnished manually with an agate stone in a single direction of the surface plane. This process gives the surface a very high gloss. The water gilding technique is therefore also known as "glossy gilding" technique.

In the oil gilding technique, a layer of oil-based adhesive called 'gold-size' is used as both, the substrate and adhesive. When the gold-size is tacky but not completely dry, the gold foil is applied to it using a gilder's tip. Due to the nature of the gold size it is not possible to burnish this surface, giving it a matte finish.



(a) Gold foil on a gilders cushion, cut with a trowel before being placed on the substrate using the gilder's tip (pink)
©C2RMF/Stéphanie Courtier



(b) Gilding mock-ups.
Oil gilding on the left and water gilding on the right. ©Inp/Angèle Dequier

3.2. Bidirectional reflectance measurements

Bidirectional reflectance from the gold foil sample surface was measured using an X-Rite MA-T12 multi-angle spectrophotometer. The MA-T12 instrument measures at six illumination sources and two pick-up points according to the specifications of industry standards for metallic colours [18, 19, 20]. It measures surface reflectance in the ranges of 400 - 700nm at 10nm

intervals. The illumination source is a polychromatic white LED with blue enhancement and its spot size is of 9 mm by 12 mm. Figure 3 illustrates the combination of illumination and viewing directions obtained by the MA-T12.

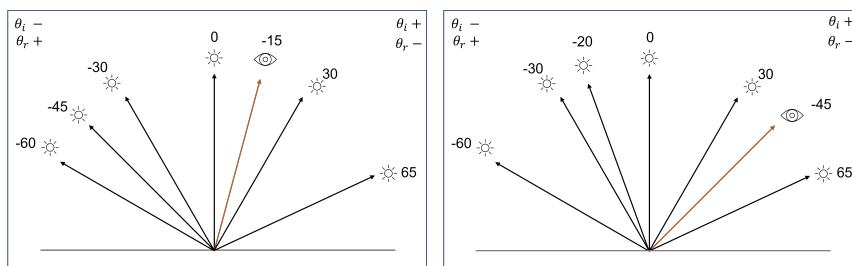


Figure 3: Measurement geometry of the MA-T12. **Left:** Illumination directions for viewing at -15° . **Right:** Illumination directions for viewing at -45° .

For each gold foil the measurements were repeated at five different locations, illustrated in Figure 4. For each location, the MA-T12 was rotated clockwise around the normal, four times. Since each measurement of the MA-T12 gives 12 spectra, 48 reflectance spectra were measured per area at five different locations, giving a total of 240 reflectance spectra per sample. Table 2 shows all the combinations of incidence and viewing directions. The convention for the angles is illustrated in Figure 4. The elevation angle (θ) ranges from -90° to 90° and is measured from the normal of the surface and the azimuth angle (ϕ) ranges from 0° to 360° and is measured clockwise from the x-axis. Illumination directions are positive clockwise from the normal and viewing directions are positive anti-clockwise from the normal.

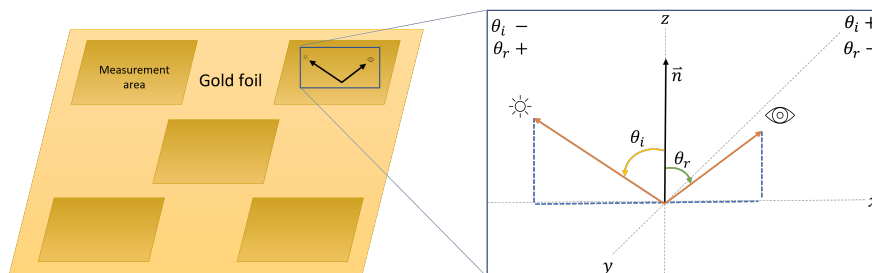


Figure 4: **Left:** Diagram representing five areas measured for each gold foil: the four corners and the centre. **Right:** Proposed parametrisation of the BRDF as a function of (θ_i) and (θ_r) . For each area in the gold foil 48 reflectance spectra are taken.

The gilding mock-ups were measured in the same way as the gold foils with the exception that the measurement was not repeated at different areas due to limited sample surface size.

Table 2

Elevation and azimuth angles for incident and viewing positions. The elevation angles are given from the normal of the surface and the azimuth angles are given clockwise from the x-axis. All angles are in degrees.

Illumination direction (θ_i)	Viewing direction (θ_r)
-15°	-60° -45° -30° 0° 30° 65°
-45°	-60° -30° -20° 0° 30° 65°
Illumination azimuth (ϕ_i)	Viewing azimuth (ϕ_r)
0° 90° 180° 270°	180° 270° 0° 90°

3.3. BRDF fitting

Spectral reflectance measurements obtained from the MA-T12 were used to train the isotropic CT model with the GGX distribution. The model was trained in the CIEXYZ colorimetric space. CIEXYZ values were calculated using Equation (7). In Equation (7), $r(\lambda)$ is the measured spectral reflectance at the sample surface, $S(\lambda)$ is the spectral power distribution of the D65 illuminant, and $\bar{x}(\lambda)$, $\bar{y}(\lambda)$, $\bar{z}(\lambda)$ are the CIE 1964 colour matching functions,

$$\begin{bmatrix} X \\ Y \\ Z \end{bmatrix} = \frac{1}{N} \int_{\lambda} S(\lambda) r(\lambda) \begin{bmatrix} \bar{x}(\lambda) \\ \bar{y}(\lambda) \\ \bar{z}(\lambda) \end{bmatrix} d\lambda, \quad (7)$$

where

$$N = \int_{\lambda} r(\lambda) \bar{y}(\lambda) d\lambda. \quad (8)$$

The diffuse reflection component coefficient (R_d) in the CT model was optimised individually (R_{dX} , R_{dY} , and R_{dZ}) in the CIEXYZ colour space while a single coefficient for the specular reflection (R_s) and roughness (m) component was optimised across CIEXYZ as shown in Equation (9).

$$I_P = s \begin{bmatrix} I_{Px} \\ I_{Py} \\ I_{Pz} \end{bmatrix} = I_a R_a + I_i \cos \theta_i \left(k_s R_s + (1 - k_s) \begin{bmatrix} R_{dX} \\ R_{dY} \\ R_{dZ} \end{bmatrix} \right) \quad (9)$$

In Equation (9), I_P is the CIE tristimulus value at point P with illumination direction θ_i and viewing direction θ_r . $I_a R_a$ is the ambient light term which is assumed to be zero as the experiment is performed in a dark environment. I_i is the incident light intensity, R_{dXYZ} are the diffuse reflectance components to be optimised. The specular components R_s are given by Equation 4 following the GGX distribution of micro-facets normals.

An extra parameter s is optimised as a scaling factor due to the fact the CIE Y values go well above one. This is because the domain is limited to that of a white Lambertian surface and in this case the samples have reflectance values above one. The scaling parameter violates the conservation of energy constraint of the BRDF model but it is necessary to add it in order to fit the model. To simplify the optimisation problem, the diffuse component R_d is not estimated

and the value at 0/45 measurement geometry is used. Using a genetic algorithm, the RMSE formula is used as an objective function and only the CIE Y value is estimated. The RMSE is given by

$$RMSE = \sqrt{\frac{\sum((M(\theta_i, \theta_r) - E(\theta_i, \theta_r, p))^2)}{n}}, \quad (10)$$

where M are the measured CIE XYZ values (Eq. 7) and E are the estimated BRDF values obtained using the Cook-Torrance GGX BRDF model (Eq. 9), with the parameters p , calculated for the n pairs of incident and reflected directions.

4. Results and Discussion

The gold foils and gilding mock-ups were measured to obtain their bi-directional reflectance according to the geometries previously described. CIE $L^*a^*b^*$ values are calculated and to evaluate the luminance of the samples, the L^* values are analysed as a function of angle of incidence. A BRDF model is estimated for the gilding mock-ups and the gold foil used for their fabrication, namely Or Versailles.

All the gold foils have a different appearance due to their karat composition, which gives them a different colour. However, due to the metallic properties of gold and the fact that the gold foils have been produced in a similar way, they should have a similar shine. On the contrary, the gilding mock-ups have been manufactured using techniques which alter the surface of the gold foil and thus, the shape of their BRDF is expected to be different even if their diffuse colour is similar to that of the original gold leaf.

4.1. Gold foils: colour and reflectance spectra

The reflectance spectra of the gold foils is plotted as a function of wavelength in the visible spectrum range from 400 to 700 nm in Figure 5 and Figure 6. The measurement geometries are specified in Table 2. All the measurements have been averaged, regardless of their location in the gold foil and the orientation of measurement, assuming the samples are isotropic. The curves are smooth and for all samples at both viewing angles the reflectance factors go above one at illumination directions -30° and 0° (yellow and purple curves), and -60° and -45° (blue and orange curves) respectively. This is because the white reference used is a Lambertian white reference which assumes a value of one for all directions and wavelengths. The different gold foils reflectance curves have more or less contribution on the longer end of the spectrum depending on their colour.

Figure 7, shows the sRGB visualisation of the gold foils at all measurement geometries. The rendering was done using CIE standard observer 10° colour matching functions and D65 illuminant. As described previously, each gold foil has a different hue due to its different karat composition. The colour is rendered as white in the case of all gold foils except Or Versailles at angles of incidence -30° and 0° for viewing direction -15° , and -60° and -30° for viewing direction -45° . This is because the reflectance factors exceed one for these measurement geometries and thus the luminance of the samples cannot be rendered in a standard dynamic range display.

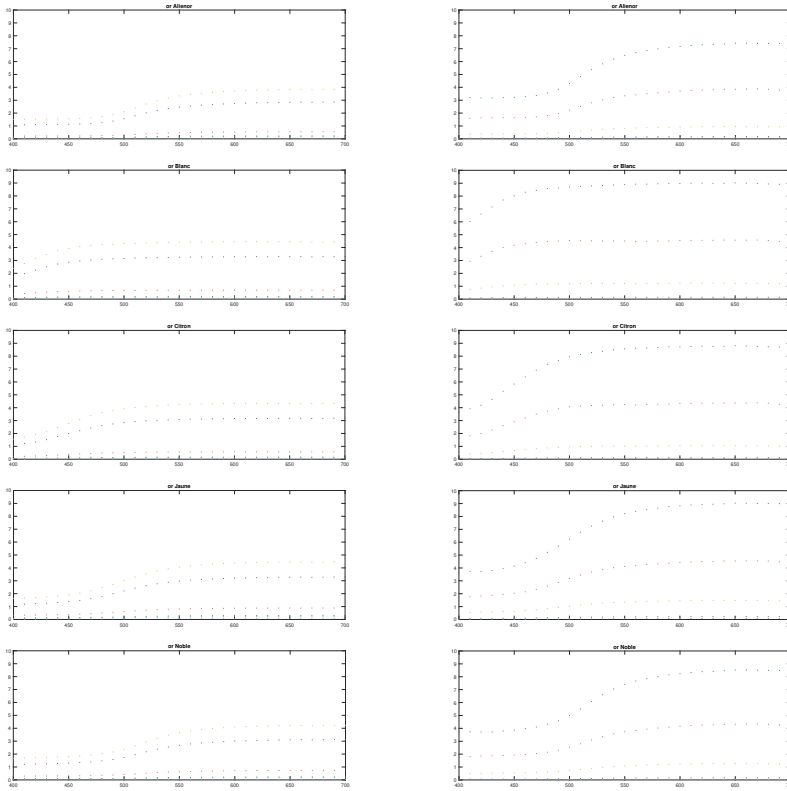


Figure 5: Reflectance curve of gold foils (1/2). The viewing angles are -15° and -45° . For each viewing direction the illumination directions are defined in Table 2.

Figure 8 shows the mean CIE L^* value for all gold foils as a function of the illumination direction. The error bars represent two standard deviations. For all gold foils the value of L^* greatly increases as the illumination angle approaches the mirror angle. The values of L^* go much higher than 100 because the spectrophotometer is taking the reference white to be a Lambertian white surface.

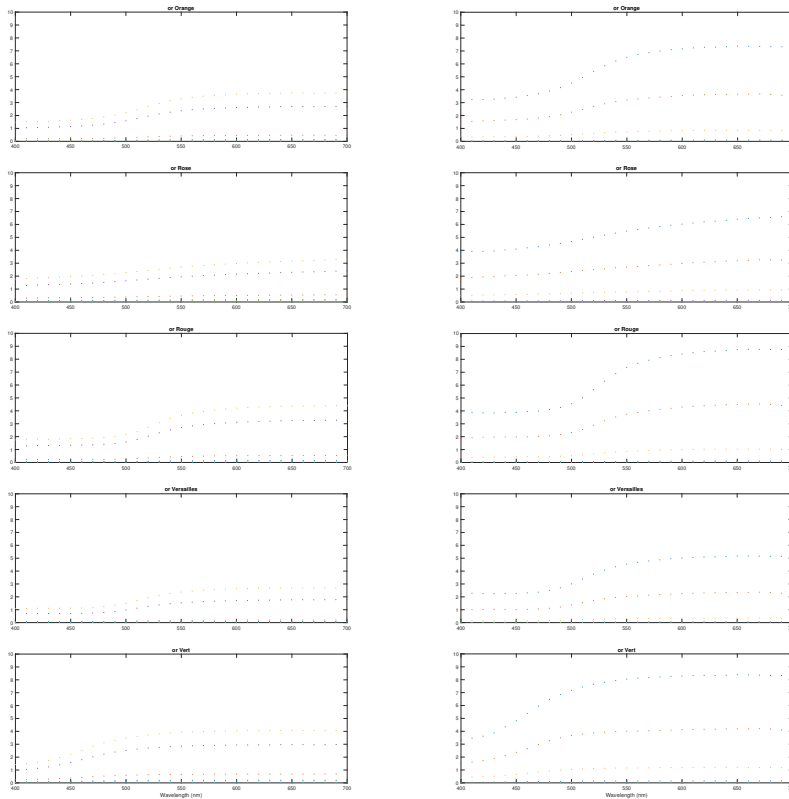


Figure 6: Reflectance curve of gold foils (2/2). The viewing angles are -15° and -45° . For each viewing direction the illumination directions are defined in Table 2.

4.2. Gold foils: bidirectional measurements

4.3. Comparing gold foil, water gilding, and oil gilding

Different manual processes and techniques are expected to alter the surface of the gold foil and change its appearance when used for gilding. While oil gilding is known to have a more matte appearance, water gilding has a higher gloss due to the final burnishing step which is not performed in the former.

Figure 9, shows the CIE Y values as a function of the illumination direction for the oil gilding mock-up, water gilding mock-up and Or Versailles gold foil at viewing directions -15° and -45° . These samples have also been used to train a BRDF model using the GGX distribution and a genetic algorithm to optimise the RMSE as objective function. The BRDF model was trained for

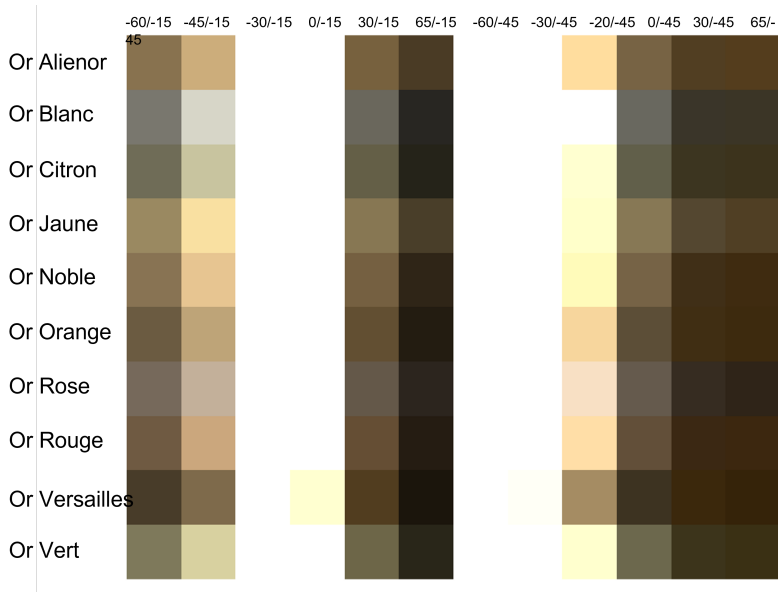


Figure 7: sRGB visualisation of the gold foils at all measurement geometries using CIE standard observer 10° colour matching functions and illuminant D65.

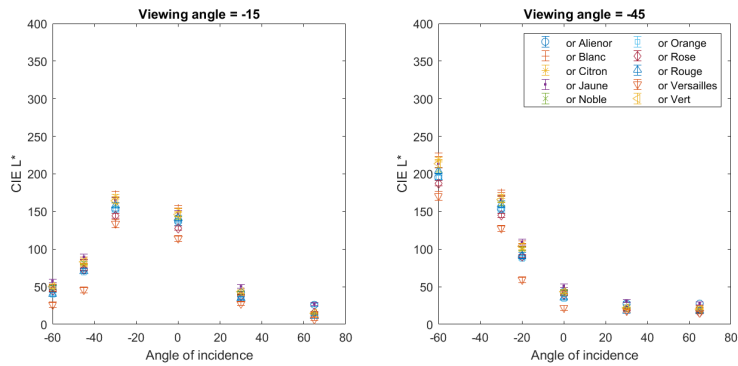


Figure 8: Measured CIE L^* of gold foils at viewing directions -15° (left) and -45° (right).

each viewing direction rather than training a single model with both viewing directions. This is because the data is sparsely sampled and an acceptable model that satisfied both viewing directions was not achieved.

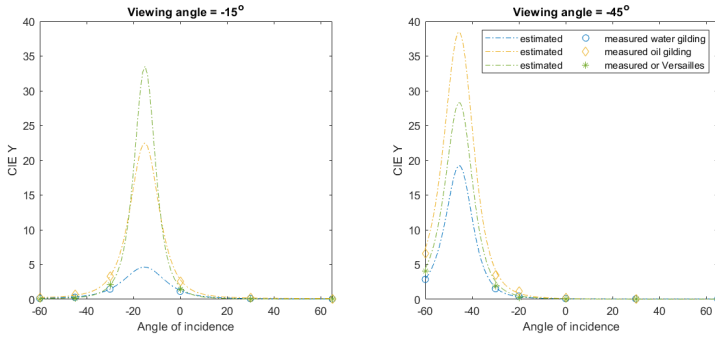


Figure 9: Measured CIE Y at viewing angle -15° (left) and -45° (right) respectively. BRDF model with estimated parameters in Table 3

Table 3

BRDF model estimated parameters using GGX distribution and genetic algorithm to optimise RMSE.

	Water gilding		Oil gilding		Or Versailles	
	-15°	-45°	-15°	-45°	-15°	-45°
Scaling factor	1.506	2.086	3.092	3.379	2.951	3.156
k_s	0.694	0.667	0.819	0.988	0.706	0.672
α	0.137	0.090	0.096	0.099	0.071	0.092

The BRDF parameters estimated and used to plot the values in Figure 9 are shown in Table 3. The scaling factor was limited to the range $[0, 5]$ and both k_s and α defined in the range $[0, 1]$.

The three samples show a similar behaviour at both viewing directions. At viewing direction -15° , oil gilding shows the higher values of CIE Y for all angles of illumination. The gold foil has lower values of CIE Y for angles further from the mirror angle, but for angles of illumination -30° and 0° , the water gilding has the lowest values of CIE Y. The same trend is seen at viewing direction -45° . However, the BRDF models show a different relative difference between the samples. At viewing direction -15° , water gilding has a much lower peak than oil gilding and the gold foil has the highest peak. On the other hand, for -45° viewing direction, oil gilding has the highest peak. The shape of the curves is more similar at this viewing direction as well.

The gloss of the water gilding and oil gilding mock-ups was measured using a Rhopoint IQ glossmeter. Table 4 shows the gloss values obtained at 20° , 60° and 85° geometry. It can be seen that water gilding has a much higher gloss than oil gilding.

4.4. Discussion and future work

Complex materials such as gold foils and gilding present particular appearance properties which cannot be simply described by colorimetry. Moreover, the metallic nature of the samples requires the specular peak to be sampled with a fine resolution to properly characterise these

Table 4

Gloss measurements of water and oil gilding. The measurements were done using a Rhopoint IQ glossmeter.

	Gloss 20	Gloss 60	Gloss 85
Water gilding	315	360	77
Oil gilding	25	85	22

surfaces.

In the field of heritage science, gilded or golden surfaces are frequently characterised by colour measurements performed at single measurement geometries. Normally, measurements are done in a diffuse domain for example $0/45$, which is insufficient to properly describe the appearance of gold. In Figure 7, the sRGB render of the reflectances at different measurement geometries shows that the colour of gold is very different from the visual perception that observers have of these materials. For example at $0/-45$, column ten in Figure 7, the colour of the gold foils is very dark.

Evidently, pure colour measurements are not sufficient to properly characterise the appearance of golden surfaces. As demonstrated, a BRDF model certainly can help to render the appearance of gold and gilding in more realistic way which is related to visual perception. An attempt to estimate the BRDF model of the gilding mock ups and its gold foil was presented in Figure 9.

The BRDF models obtained fail to properly characterise the differences in appearance of the gold foil, water gilding, and oil gilding. This is probably due to the fact the BRDF model is a data hungry model which requires more number of measurements to train coefficients that can accurately represent the surface at many combinations of angles of incidence and viewing. In this paper, the models are trained with six measurements for each viewing direction and moreover, the reflectances are not sampled at angles close to the specular peak. The fact that the BRDF model is trained on each individual viewing direction independently rather than just having a single model does not allow for the models to then be directly comparable. This is because the specular peak is unknown and thus the model cannot be properly trained.

Finally, a remark must be made on the fact that the gilding mock-ups have been made with the same gold foil. The only difference between the pure gold foil (Or Versailles), the oil gilding mock-up, and the water gilding mock-up is the orientation of the micro-facets of each surface. The Fresnel coefficient of the three surfaces will be the same since the chemical composition of the gold foil is unchanged by either gilding techniques. The amount of radiance being absorbed by the three surfaces is the same. Thus, the distribution of the scattered rays can be normalised over all incident directions to a constant that will be the same for the three surfaces.

Future work should include improvement in the fitting of the BRDF model. Although the Cook-Torrance BRDF model using a GGX distribution seems to be the appropriate model for the samples, some limitations have to be overcome to obtain more faithful models. First of all, the high specularity of the surfaces must be accounted in the BRDF model so the scaling factor is not violating any rule such as conservation of energy. Additionally, the lack of data close to the specular peak requires that some assumptions are to be made to characterise these. For example, the fact that the Fresnel coefficient of the surfaces is the same should be exploited.

Moreover, once the BRDF models are obtained, they will have to be evaluated. It would be valuable to perform a psychophysical experiment to evaluate how good the models are at rendering the subtleties in appearance difference between these surfaces. Also, the models can be tested for their ability to characterise the surfaces with respect to each other by performing a classification task based on the coefficients.

In the field of conservation science, it would be valuable to understand how the different gilding techniques change the BRDF model and thus the appearance of the surfaces. This could give insights into restoration techniques and procedures that render an appearance closest to that of the original gilding. Another interesting possibility would be to characterise the effects of ageing on gilded surfaces in order to create a model linking the original appearance of the gilding and its aged appearance for virtual restoration purposes.

5. Conclusion

In this paper, ten different gold foils commonly used for restoration have been measured and characterised using a bidirectional reflectance measurement device and an well established reflectance model. Two types of gilding mock-ups, water gilding and oil gilding, fabricated with one of the gold foils studied, have also been measured. It is found that the gold foils and gilded mock-ups are very specular and present reflectance factors higher than one at angles as close as 15° from the mirror angle.

It is found that these measurement angles are not enough to fit a BRDF model that accurately describes the appearance of the surfaces. It is suggested that the model is modified so the high specularity of the surface is better described. Also, given the surfaces should have the same transmittance and absorption, the BRDF models can be normalised to have the same value over all angles of incidence.

Acknowledgments

This work has received funding from the European Union's Horizon 2020 research and innovation program under grant agreement No. 813789, through the the MSCA ITN project CHANGE (<https://change-itn.eu/>).

We would like to thank Stéphanie Courtier from the Centre of Research and Restoration of the Museums of France, for her help in the preparation of samples.

References

- [1] K. Kollandsrud, U. Plahter, Twelfth and early thirteenth century polychromy at the northernmost edge of europe: past analyses and future research, *Medievalista online* (2019). URL: <https://dx.doi.org/10.4000/medievalista.2303>. doi:10.4000/medievalista.2303.
- [2] G. P. Mastrotheodoros, K. G. Beltsios, Y. Bassiakos, V. Papadopoulou, On the metal-leaf decorations of post-byzantine greek icons, *Archaeometry* 60 (2018) 269–289. URL: <https://onlinelibrary.wiley.com/doi/abs/10.1111/arcm.12287>. doi:<https://doi.org/10.1111/arcm.12287>.

- [3] A. Sole, G. C. Guarnera, I. Farup, P. Nussbaum, Measurement and rendering of complex non-diffuse and goniochromatic packaging materials, *The Visual Computer* 37 (2021) 2207–2220.
- [4] P. Callet, A. Zymła, A. Mofakhami, Virtual metallurgy and archaeology. application to the visual simulation of a work of art, in: ICCVG, 2002, pp. 25–29.
- [5] S. Dumazet, A. Genty, A. Zymła, F. De Contencin, A. Texier, N. Ruscassier, B. Bonnet, P. Callet, Influence of the substrate colour on the visual appearance of gilded sculptures, in: XXI International CIPA Symposium, 2007, pp. 01–06.
- [6] A. Mounier, F. Daniel, The role of the under-layer in the coloured perception of gildings in mediaeval mural paintings, *Open Journal of Archaeometry* 1 (2013). doi:10.4081/arc.2013.e16.
- [7] Q. Wu, M. Hauldenschield, B. Rösner, T. Lombardo, K. Schmidt-Ott, B. Watts, F. Nolting, D. Ganz, Does substrate colour affect the visual appearance of gilded medieval sculptures? part I: colorimetry and interferometric microscopy of gilded models, *Heritage Science* 8 (2020). doi:10.1186/s40494-020-00463-3.
- [8] L. W. MacDonald, T. Vitorino, M. Picollo, R. Pillay, M. Obarzanowski, J. Sobczyk, S. Nascimento, J. Linhares, Assessment of multispectral and hyperspectral imaging systems for digitisation of a Russian icon, *Heritage Science* 5 (2017). doi:10.1186/s40494-017-0154-1.
- [9] M. A. Martinez, E. M. Valero, J. L. Nieves, R. Blanc, E. Manzano, J. L. Vilchez, Multifocus hdr vis/nir hyperspectral imaging and its application to works of art, *Opt Express* 27 (2019) 11323–11338. doi:10.1364/OE.27.011323.
- [10] O. Sidorov, J. Y. Hardeberg, S. George, J. S. Harvey, H. E. Smithson, Changes in the visual appearance of polychrome wood caused by (accelerated) aging, in: *Electronic Imaging, Society for Imaging Science and Technology*, 2020, pp. 060–1–060–7. doi:doi.org/10.2352/ISSN.2470-1173.2020.5.MAAP-060.
- [11] F. E. Nicodemus, R. JC, et al., Geometrical considerations and nomenclature for reflectance. (1977).
- [12] D. Guarnera, G. C. Guarnera, A. Ghosh, C. Denk, M. Glencross, Brdf representation and acquisition, in: *Computer Graphics Forum*, volume 35, 2016, pp. 625–650.
- [13] R. L. Cook, K. E. Torrance, A reflectance model for computer graphics, *ACM Transactions on Graphics* 1 (1982) 7–24.
- [14] A. Sole, I. Farup, P. Nussbaum, S. Tominaga, Bidirectional reflectance measurement and reflection model fitting of complex materials using an image-based measurement setup, *Journal of Imaging* 4 (2018). URL: <https://www.mdpi.com/2313-433X/4/11/136>. doi:10.3390/jimaging4110136.
- [15] K. E. Torrance, E. M. Sparrow, Theory for off-specular reflection from roughened surfaces, *Journal of the Optical Society of America* 57 (1967) 1105–1112.
- [16] B. Walter, S. R. Marschner, H. Li, K. E. Torrance, Microfacet models for refraction through rough surfaces, in: *Eurographics conference on Rendering Techniques*, Eurographics Association, 2007, pp. 195–206.
- [17] A. Fores, J. Ferwerda, J. Gu, Toward a perceptually based metric for brdf modeling, in: *Color and imaging conference*, Society for Imaging Science and Technology, 2012, pp. 142–148.
- [18] *Standard Practice for Specifying the Geometry of Multiangle Spectrophotometers*, ASTM

- E2175-01, Standard, American Society for Testing and Materials, Pennsylvania, USA, 2001.
- [19] *Standard Practice for Multiangle Color Measurement of Metal Flake Pigmented Materials*, ASTM E2194-12, Standard, American Society for Testing and Materials, Pennsylvania, USA, 2012.
- [20] *Tolerances for Automotive Paint—Part 2: Goniochromatic Paints*, DIN 6175-2, Standard, Deutsches Institut für Normung, e.V, Berlin, DE, 2001.

6. Online Resources

The dataset of gold foils reflectances is available in the CHANGE-ITN repository (<https://zenodo.org/communities/change/?page=1&size=20>).

Article B

Yoko Arteaga, Clotilde Boust, Angèle Déquier, and Jon Y. Hardeberg. Image-based goniometric appearance characterisation of bronze patinas. In *Color and Imaging Conference (CIC)*, volume 2021, pages 294 – 299. Society for Imaging Science and Technology, 2021

Image-based goniometric appearance characterisation of bronze patinas

Yoko Arteaga^{1,2}, Clotilde Boust¹, Angèle Dequier³, Jon Yngve Hardeberg²

¹ Centre of Research and Restoration of the Museums of France; Paris, France

² Norwegian University of Science and Technology; Gjøvik, Norway

³ National Institute of Cultural Heritage; Paris, France

Abstract

Patinas are a form of metal polychromy used to decorate metallic artworks. Due to the nature of the metallic surface, their colour and gloss is perceived differently when the illumination and viewing directions vary. Sparkle effect on surfaces is a physical phenomenon caused by micro-facets on the surface coating which are also perceived with changing viewing and illumination geometry.

In this paper, a method designed for the measurement of sparkle is applied for the goniometric characterisation of bronze patinas. Using a set of six different patinas, in three colours and two surface finishes, it is found that these surfaces exhibit different appearance when illuminated and viewed at different angles. Moreover, the roughness of the patinas is measured and as expected, as the roughness increases the specular reflection peak decreases. The experiment is repeated at two different institutions with different sets of equipment to test its repeatability and robustness.

The sparkle is presented as a function of the angle of tilting, and it is characterised by its maximum value and full-width half-maximum. It is found that the maximum and the roughness have a negative exponential relationship whereas the full-width half-maximum and the roughness have a linear relationship.

Introduction

Studying the visual appearance of cultural heritage objects is of great importance not only for aesthetic purposes but also because it provides information about the objects' provenance, manufacturing technique, storage conditions, and ageing processes amongst other attributes. Correctly measuring, characterising, and identifying these properties is extremely valuable for conservators but also the ease, availability, and practicality of the technologies used must be considered.

Patinas are a form of metal polychromy widely used to decorate metallic artworks. They allow craftsmen to obtain various coloured surfaces on copper-based alloys by applying chemical treatments which build a compound layer on the surface [1]. In this work, the patinas used were made by the Coubertin foundry, located in the outskirts of Paris. The patinas are present in three different colours, red, green, and black and they have been made with two surface finishes, smooth and rough. Examples of works fabricated using these techniques are the famous bronze sculptures by Rodin.

Sparkle is a visual effect in which, when viewed and illuminated from different angles, the surface exhibits points of high specular reflection [2]. This is caused by micro-facets added to

the surface coating which are placed randomly at different orientations. Gloss, on the other hand, is an optical property which describes how an object reflects light in a specular direction. Gloss, similar to sparkle, is also perceived when viewed and illuminated from different directions however, the physical properties of the materials responsible of creating said effects are completely different. Despite being inherently different phenomena, the dynamics in which both effects are observed are similar and thus, it is interesting to evaluate the applicability of a method used to measure sparkle to measure gloss of bronze patinas.

Several commercial instruments are available to perform multi-angle planar measurements such as gloss-meters or the BYK-Mac specifically designed for sparkle measurements. However, these instruments are expensive and measure fixed illumination and reflection angles. Gonio-spectro-photometers used in research institutions provide a more accurate goniometric measurement, yet they are expensive and slow. Thus, there is an interest to develop an accurate but also fast and inexpensive method.

In this work, a method initially developed for the measurement of sparkle is tested and validated for the goniometric characterisation of bronze patinas used in cultural heritage statues. The benefit of using this method is the availability of the equipment necessary, which can be found in any cultural heritage research or documentation facility. Based on only a directional light source, a CCD camera and a tilting stage, these measurements can be done in museums, restoration workshops and laboratories. In order to test the robustness of the method, the experiment has been repeated in two different laboratories, the Centre for Research and Restoration of the Museums of France (C2RMF) and the National Institute of Cultural Heritage (INP), using the equipment available in each institution.

The patinas are also characterised in terms of their roughness, to evaluate the feasibility of applying this method to samples belonging to a range of different roughness. Since the bronze patinas do not strictly present sparkle by definition, whenever the author refers to *sparkle* in italic font, they mean the specular reflections from the patinas which have been calculated using the proposed method for sparkle measurements.

Related works

Sparkle

Sparkle is a sensation produced by different materials, where many luminous points are observed. These mini reflections are caused by the various orientations of many micro-facets on the surface which cause specular reflections. Some materials which can cause sparkle are inclusions of mica or sand in a paint. Given

that each of these micro-facets has a different and random orientation, the sparkle effect is observed when either the illumination source or the viewing angle is modified. This is a non-permanent effect where the sparkle changes constantly as the observer or illumination changes.

To date there is still not a methodology defined by the CIE to measure sparkle, as this is a very current problem area. The CIE JTC 12 has as an objective to provide a standardised way to measure and evaluate sparkle [3].

Ferrero *et al.*, has defined sparkle as a non-uniform texture which is observed under a directional illumination, at a metre or less from the surface [2]. Sparkle, as previously defined, is given by a low density of highly reflective points over a darker background. In the case of a diffuse illumination, the perceived texture is no longer sparkly, and the effect becomes graininess. Thus, the illumination conditions are very important when studying sparkle or graininess. Under directional light the observed effect will be sparkle and under diffuse light, graininess.

A physical model is defined to simulate both sparkle and graininess [2]. Given the orientation of each micro-facet, the reflection flux can be simulated. In this model, sparkle and graininess are two extremes in the same reflection phenomenon. The contrast between the reflective points and the darker background will determine if the texture (sparkle or graininess) is observable or not. The density of lighter points defines the effect. For a high contrast and low density there is sparkle and for a low contrast and high density, graininess. Both characteristics, contrast and density are dependent on the source of illumination, the illumination and observation geometries, and the orientation of the micro-facets.

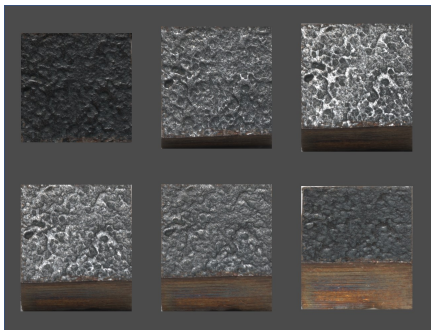


Figure 1: Demonstration of *black rough* patina mock-up and its colour change at different angles of tilting. From left to right: 0°, 11°, 22°, 28°, 34° and 45°. The angle of tilting is given from the horizontal axis.

Sparkle measurements

Ferrero *et al.* [4], proposes a protocol for the measurement of sparkle. The authors use the GEFE (Gonioespectrofotometro Español) for bidirectional measurements where the illumination and observation directions are modified. This device allows the absolute measurement of the bidirectional reflectance distribution function (BRDF). In the GEFE configuration, the sample is placed on a fixed platform relative to the illumination beam and the detector revolves around the sample [5].

The authors obtain grey level images, where the sparkle points are visible. From these images, three values are calculated relative to four parameters. Firstly, the contrast of a single sparkling point, C_S , given by the ratio of the flux of the point to the flux of the almost Lambertian background. It represents the ratio between the fluxes specularly reflected by the flake and diffusely reflected by the background. This ratio varies with the geometry of the surface coating because of the angular dependence of the Fresnel reflection and the non-perfect Lambertianity of the background.

To determine at which geometries the sparkle is visible, the whole contrast is necessary. The contrast of the set of sparkling points, C_{SP} , is defined as the mean of contrasts C_S higher than a threshold defined by Ferrero *et al.* as $C_{th} = 0.5$.

Finally, the density of the sparkle points, d_{SP} , is defined as the number of sparkle points per area with $C_S > C_{th}$. This is related to the number of flakes per area whose specularly reflected fluxes are partially or totally collected. It depends on the distribution of the inclination of the flakes, and in consequence, also on the illumination/viewing geometry. This distribution is usually peaked at inclinations where the flakes are parallel to the coating surface. Additionally, the wider the distribution, the more constant is the observed sparkle density at different geometries.

Due to the complexity of the sparkle effect, its measure cannot be reduced to a single number. Thus, four visual attributes related to sparkle are defined. The maximum sparkle visibility, defined as the capacity of the human visual system to discriminate sparkle events, correlated to C_S . The maximum density of sparkle points, correlated to d_{SP} . The visibility inconstancy, which is the variation of sparkle visibility as a function of illumination/viewing geometry, correlated to the total variation of C_S relative to its maximum. Finally, the anisotropy refers to the variation of the density of sparkle points with respect to the illumination/viewing geometry, which is correlated to the total variation of d_{SP} relative to its maximum.

Visual appearance in cultural heritage

Although bronze patinas are widely found in cultural heritage objects, they are normally characterised based on their chemical composition, using analytical methods such as X-ray diffraction, particle induced X-ray emission [1], Raman microscopy [6], scanning electron microscopy [7] and others [8]. To the authors knowledge, there have not been extensive works on the characterisation of the visual appearance of bronze patinas using imaging techniques.

Other cultural heritage materials that have been studied in terms of their visual appearance by performing goniometric measurements are polychrome wood [9] and paint and varnish [10]. Although surface characterisation is strategic for studies in conservation [8], this is not frequently done as most goniometric investigations of optical properties of surfaces are mostly performed considering industrial materials.

Materials and Methods

Sample patinas

The samples used for this work are bronze patinas from the Coubertin art foundry [11]. Six patinas are available, in three colours: red, green and black and two surface finishes: smooth and rough. Due to the polychrome alteration of the surface of the

metal, a significant change in appearance dependent on viewing angle is produced, illustrated in Figure 1.

Goniometric sparkle measurements



Figure 2: Snapshot of sparkle set-up used at INP.

The sparkle measurements have been adapted from work done by Ferrero *et al.* [4] and Page [12]. This is illustrated in Figure 2 and Figure 3 shows a schematic of the set-up. The samples are placed on a tilting support, where the angle of inclination can be controlled with a micrometric turning stage. The camera is placed vertically above the samples and the illumination is set at a zenithal angle of 45° degrees. The specular configuration corresponds to a 22.5° rotation around the horizontal axis and the exposure is adjusted at this configuration. At every 1 degree, a capture is made. Table 1 shows the image acquisition parameters and experimental set-up used at each institution.

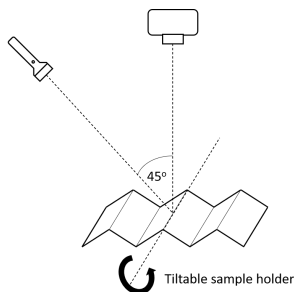


Figure 3: Set-up used for sparkle measurements.

The images are taken in raw format. To process the images and calculate the sparkle, an area of 200×200 pixels from the centre of each patina square is taken. This image is converted into the CIE 1976 $L^*a^*b^*$ colour space assuming the original images are in the sRGB colour space, using D65 illuminant as the white point, and only the L^* channel is used. The images are calibrated by using a Lambertian white surface as a reference and setting its L^* value to 95. The sparkle is defined as the percentage of pixels in the image over a threshold. Given that sparkle is defined by micro mirror-like facets, the threshold should be representative of specular reflections on the surface. In this case, the threshold is defined as $L^* = 96$, since the Lambertian white has a value of 95. Finally, the percentage of pixels over the threshold is plotted for each patina, as a function of angle of rotation. This is illustrated

Table 1: Parameters used for sparkle measurements

	C2RMF	INP
Acquisition set-up parameters		
Camera	Hasselblad	Nikon D850
Lens	120 mm macro	105mm macro
Sensor size (pixels)	6708 x 8956	8256 x 5504
Light source	Flash 3000K	LED 5200K
Object distance (cm)	50	40
Illumination distance (cm)	70	80
Pixel size (mm^2)	2.89×10^4	0.50×10^4
Image capture parameters		
f-number	f/14	f/32
Exposure time (s)	1/125	1*30
ISO	50	64

in Figure 4.

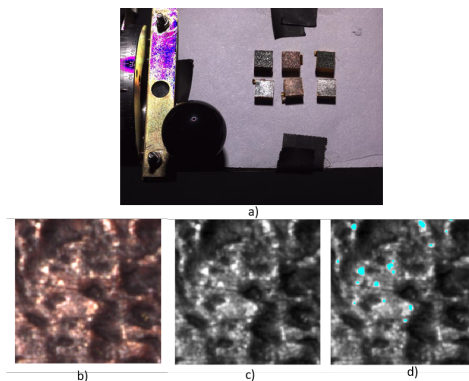


Figure 4: Processing steps to obtain sparkle. a): For each patina a patch is extracted from the centre, b): transformed to $L^*a^*b^*$ and a threshold is set in the L^* channel. c): The value of sparkle is given by the percentage of pixels over the threshold, highlighted in cyan.

Roughness

The roughness of the patinas is measured under a white-light profilometer with chromatic coding (Altisurf 50 by AltimetTM). A 8 mm probe is used with a $2 \mu\text{m}$ step in x and y directions; resolution in z is of 50 nm. The surface roughness is calculated using the arithmetical mean height (S_a), according to ISO25178, given by

$$S_a = \frac{1}{A_A} |Z(x,y)|, \quad (1)$$

where A is the area of the surface and Z is the height of each point from the arithmetical mean of the surface [13].

Results and discussion

Sparkle

Following the protocol introduced in the previous section, the *sparkle* is presented as a function of the difference between the angle of incidence and the angle of observation. Figure 5 shows the *sparkle* obtained using the equipment at C2RMF and Figure

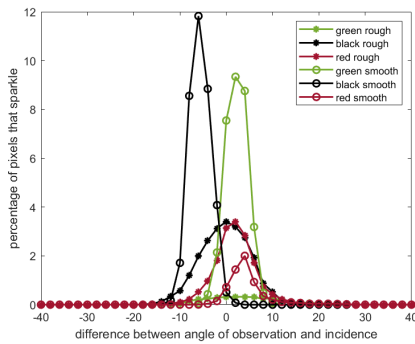


Figure 5: *Sparkle* as a function of the difference between the angle of incidence and reflection for images taken at C2RMF. Smooth samples are presented with a round marker, and rough samples are presented with a star marker.

6 shows the *sparkle* obtained at INP. The patinas can be grouped into two different types of curves: smooth samples have a narrow curve with a high peak and rough samples have a wider curve with a less pronounced peak.

It is expected that the peak in the *sparkle* curve occurs when the angle of incidence is the same as the angle of observation, at the specular configuration. This is not the case for all the patinas since they present a small difference in height. Thus, when the samples are placed at a rotation of 0° on the horizontal, the angle of incidence is not 45° for all of them.

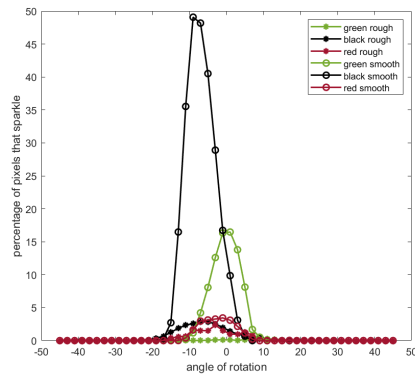


Figure 6: *Sparkle* as a function of the difference between the angle of incidence and reflection for images taken at INP. Smooth samples are presented with a round marker, and rough samples are presented with a star marker.

The *sparkle* curves can be described by their maximum point (percentage of pixels that sparkle) and spread, given by the full-width half-maximum (FWHM) in degrees. The values obtained from Figure 5 and Figure 6 are presented in Table 2. Except for the black and green smooth samples, there is a general agreement

between the maximum values obtained. In terms of the FWHM, the relative difference between each patina is not so different with the exception of the red smooth sample.

Sparkle and roughness

The roughness of the patinas is calculated given Equation 1. The results are presented in Table 3. The roughest sample is the *green rough* patina and the smoothest is the *black smooth* patina. Although the patinas are grouped in two categories, smooth and rough, the variation in roughness of the smooth group is much lower than the variation in roughness of the rough group.

Figure 8 shows the FWHM taken from Figure 5 and Figure 6 as a function of surface roughness, Sa, given by Equation 1. A linear equation has been fit to both sets of data.

Table 2: Maximum and full-width half-maximum

Patina	max (%)		FWHM (°)	
	C2RMF	INP	C2RMF	INP
Green rough	0.3	0.3	20.57	16.04
Black rough	3.4	2.8	13.15	15.48
Red rough	3.4	2.4	8.32	10.32
Green smooth	9.3	16.5	6.53	9.88
Black smooth	11.8	49.1	6.00	9.87
Red smooth	2.0	3.4	5.07	12.73

The results show that there is a linear relationship between the roughness and the FWHM. As the roughness increases so does the FWHM and the spread of the *sparkle* curve gets wider. Considering a theoretical surface with a roughness equal to 0 would imply a perfect mirror-like surface. Said surface would present a very narrow distribution with a FWHM close to the y-intercept since most of the light would be reflected at the angle of specular reflection. On the other hand, a very rough surface where many facets are oriented at all possible orientations implies that at all angles of tilting a fraction of the light would be reflected at the same angle as the observation. Thus, the curve would be spread over a large range of angles.

Figure 7 shows the maximum taken from Figure 5 and Figure 6 as a function of surface roughness, Sa, calculated according to Equation 1. A two-term exponential model of the form $Ae^{Bx} + Ce^{Dx}$ has been fitted to both sets of data, where A, B, C and D are constants.

Table 3: Arithmetical mean height (µm) for each patina calculated according to ISO25178 standards. Scanning resolution of 2 µm, using an 8 mm probe.

Green rough	Red rough	Black rough
31.51	12.48	21.91
Green smooth	Red smooth	Black smooth
5.33	6.19	3.45

As the roughness increases, the *sparkle* decreases. Moreover, as the roughness approaches 0, the *sparkle* tends to infinity. Considering the same theoretical surfaces as above, it is expected that a surface with a roughness equal to 0 would have a maximum

of *sparkle* tending to infinity as all the light incident on the surface would be reflected at the angle of specular reflection. On the other hand, surfaces with very high roughness would reflect only a partial amount of the radiant incident flux and thus the *sparkle* would be lower.

Although this method has been applied to goniometrically characterise the *sparkle* of bronze patinas, there are limitations on the range of samples that can be analysed with it. This method can only be applied to surfaces that are flat at a macro-scale. As commonly found in material appearance experiments, the surface topography and shape of the object play an important role in the light-matter interactions. Thus, at a macro-scale, when the interface between the light and the object is no longer a plane, computing the difference between the angle of observation and the angle of incidence is not sufficient.

However, at a micro-scale the surface topography poses another limitation. As seen on Figure 7, as the roughness increases, the maximum of the sparkle distribution tends towards 0. Thus, samples with a roughness higher than $35\ \mu\text{m}$ cannot be characterised following this method.

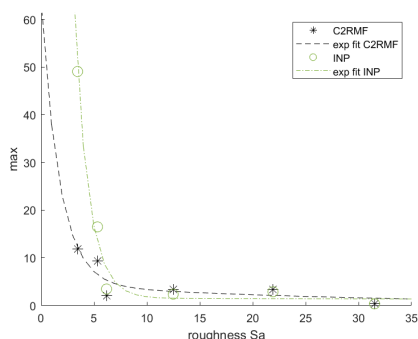


Figure 7: Maximum as a function of $S_a\ (\mu\text{m})$. Star markers are given for data taken at C2RMF and round markers for data taken at INP. The fit used is a two-term exponential model.

Robustness and repeatability

The robustness and repeatability of this experiment has been tested by repeating the experiment at two different institutions. The results obtained are presented in Figure 7 and Figure 8. There are slight differences in the distributions of maximum and FWHM as a function of roughness. Although both sets of results follow similar distributions, the constants used to fit the exponential model in the case of Figure 7 and the gradients on Figure 8 differ. However, it must be noted that the relative difference between each individual sample is relatively similar. The aim of this method is not to give an absolute result as a measure of *sparkle*, but to provide a simple protocol which compares the appearance of different surfaces. Since the results come from different equipment (camera and light source) it is evident that a calibration step is necessary to obtain more robust and comparable results.

However, there is potential for this method to be widely used in the cultural heritage field. This protocol is very accessible since the necessary materials can be found in any cultural heritage in-

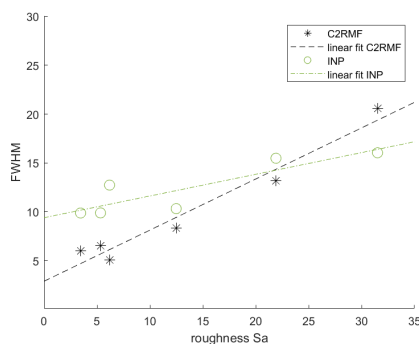


Figure 8: Full-width half-maximum as a function of $S_a\ (\mu\text{m})$. Star markers are given for data taken at C2RMF and round markers for data taken at INP. The fit used is a linear model.

stitution such as museums, laboratories and conservation workshops. The presented method is quick and inexpensive, and can be performed by non technical experts using only a CCD camera, a light source and a tilting stage.

Discussion

As mentioned previously, this method provides a relative characterisation of samples in terms of their roughness and appearance. However, in order to make these results more robust and accurate, a calibration step is needed. This could be done by calibrating the light source so the same amount of light is incident on the samples. Another possibility would be to make calibration targets with known roughness and gloss. This would allow a calibration step to be introduced in the processing pipeline to obtain repeatable results.

To produce such calibration targets, a possibility would be to analyse a set of samples ranging over a larger scale of roughness. In the case of the patinas used for this investigation, they have been labelled as smooth and rough. However, from the roughness measurements, it is clear that the samples cannot be just discriminated by smooth/rough. Moreover, they do not represent an equally distributed range of roughnesses either. Since the smooth samples do not vary very much in roughness, they can be considered almost as one set of similar samples. By having a wider range of roughnesses, the relationship between *sparkle* and roughness could be better understood. Moreover, the morphological characteristics of the surface such as the orientation and size of its micro-facets could be further related to the sparkle, as it is done by Ferrero *et al.* [2], where these parameters are fitted into a model to predict the sparkle.

Additionally, this method is limited by the scale of analysis. While this investigation has been done at a micro-scale, it is important to also evaluate if this method can be applied to the larger, macro-scale. Ferrero *et al.* defines sparkle as a texture observed at a distance of a meter or less. This limits the study of sparkle to smaller surfaces. From a cultural heritage point of view, it would be valuable to use this protocol as a means of monitoring samples before and after restoration processes such as cleaning and waxing in the case of patinas. Waxing is a common proce-

ture which increases the saturation of the patinas and makes the surface glossier. This monitoring process could help conservators choose the most appropriate methods for conservation and restoration of cultural heritage objects.

Conclusion

In this work, a method initially proposed for sparkle measurements has been applied to goniometrically characterise the appearance of bronze patinas. Although there is an inherent difference between sparkly surfaces and the patinated bronze samples, it is possible to obtain information on the appearance of the bronze patinas.

A clear dependence between *sparkle* and angle of rotation has been found. As expected, the surfaces considered smooth have a narrow curve with a higher peak than the surfaces considered rough, which have a much wider curve and lower peak. Moreover, it has been found that there is linear relationship between the roughness of the samples and the FWHM of the *sparkle* distribution curve for each sample. Additionally, a negative exponential relationship has been found between the maximum of the *sparkle* curve and the roughness of the surfaces. Further, the experiment has been repeated at two institutions using the available equipment, giving similar results for the same set of samples.

Future work includes adding a calibration step in the processing of the data to make protocol more robust and repeatable. This could be done by exploring further the relationship between surface micro-topography and sparkle. By characterising the size and orientation of surface facets, a better understanding of the light-matter interactions at the surface can be achieved. Moreover, it is suggested to use the protocol as a monitoring tool for conservation methods.

Acknowledgements

This research was funded with the support of CHANGE Cultural Heritage Analysis for New Generations European Union's Horizon 2020 research and innovation programme under the Marie Skłodowska-Curie grant agreement No. 813789.

The authors would like to thank Anne Maigret for her help with the image acquisition and Dominique Robcis for access to the bronze patinas used in this experiment.

References

- [1] F. Mathis, S. Descamps, D. Robcis and M. Aucouturier, "Original surface treatment of copper alloy in ancient Roman Empire: chemical patination on a Roman strigil", *Surface Engineering*, 21, p. 346-351 (2005).
- [2] A. Ferrero, J. Campos, A.M. Rabal and A. Pons, "A single analytical model for sparkle and graininess patterns in texture of effect coatings", *Optics Express*, 21, p. 26812-26819 (2013).
- [3] JTC 12 (D2/D1/D8): The measurement of sparkle and graininess. [url=http://cie.co.at/technicalcommittees/measurement-sparkle-and-graininess](http://cie.co.at/technicalcommittees/measurement-sparkle-and-graininess) (Accessed 01/06/2021)
- [4] A. Ferrero and S. Bayón, "The measurement of sparkle", *Metrologia*, 52:2, p. 317-323 (2015).
- [5] A. M. Rabal, A. Ferrero, J. Campos, J. L. Fontecha, A. Pons, A. M. Rubiño and A. Corróns, "Automatic gonio-spectrophotometer for the absolute measurement of the spectral BRDF at in- and out-of-plane and retroreflection geometries", *Metrologia*, 49, p. 213-223 (2012).
- [6] E. Joseph, A. Simon, S. Prati, M. Worle, D. Job and R. Mazzeo, "Development of an analytical procedure for evaluation of the protective behaviour of innovative fungal patinas on archaeological and artistic metal artefacts", *Analytical and Bioanalytical Chemistry*, 9 (2011).
- [7] V. Hayez, T. Segato, A. Hubin and H. Terryn, "Study of copper nitrate-based patinas", *Journal of Raman Spectroscopy*, 37:10, p. 1211-1220 (2006).
- [8] A. Giunilia-Mair, C. Albertson, G. Boschian, G. Giachi, P. Iacomussi, P. Pallecchi, G. Rossi, A. N. Shugar and S. Stock, "Surface characterisation techniques in the study and conservation of art and archaeological artefacts: a review", *Materials Technology*, 25:5, p. 245-261 (2010).
- [9] O. Sidorov, J. Y. Hardeberg, S. George, J. S. Harvey and H. E. Smithson, "Changes in the Visual Appearance of Polychrome Wood Caused by (Accelerated) Aging", *Proc. EI, Material Appearance Conference Proceedings*, pp. 60-1-60-8(8) (2020).
- [10] P. Iacomussi, M. Radis and G. Rossi, "Goniometric and colorimetric properties of paints and varnish", *Proc. SPIE, Measuring, Modeling, and Reproducing Material Appearance*, p.201 1 214 (2015).
- [11] J. Edelson, "Elaboration d'une méthodologie d'analyse des patines artificielles sur les bronzes du patrimoine artistique", Master's thesis - École des Mines de Paris (2000).
- [12] M. Page, "Création d'objets mats: optimisation d'un procédé d'impression en relief en termes d'apparence", PhD diss. Conservatoire national des arts et métiers - CNAM (2018).
- [13] ISO25178-2:2012 Geometrical product specifications (GPS) - Surface texture: Areal - Part. 2: Terms, definitions and surface texture parameters.

Author Biography

Yoko Arteaga is a Marie Skłodowska-Curie early stage research fellow at the Centre of Research and Restoration of the Museums of France and part of the Colourlab at the Norwegian University of Science and Technology. She has a background in Physics and Colour Science. For her PhD she is working in the development of techniques to characterise surface topography and appearance for cultural heritage objects.

Clotilde Boust received her engineering degree in photography from the Ecole Nationale Supérieure Louis Lumière, France in 1998. After working for two years as a colour consultant in the press industry and one year as researcher in the Vision laboratory of the National Museum of Natural History, she began a Ph.D. in image quality with Océ Print Logic Technologies and Paris VI University. She is now the head of the Imaging Group at the Centre for Research and Restoration of the Museums of France (C2RMF).

Angèle Dequier is a scientific documentalist for the French Ministry of Culture and a photographer-radiologist. She has worked at the Louvre Museum and at the National Institute of Cultural Heritage (INP) on 3D projects and applications of imaging in conservation and restoration of cultural objects. She is currently head of imaging sector at the Arc'Antique underwater archaeology laboratory in Nantes, France.

Jon Y. Hardeberg is Professor of Colour Imaging at NTNU, Department of Computer Science, The Norwegian Colour and Visual Computing Laboratory, Gjøvik, Norway. His current research interests include spectral imaging, image quality, colour management, material appearance, cultural heritage imaging, and medical imaging, and he has co-authored more than 300 publications within the field. He has led several research projects funded by the Research Council of Norway, been NTNU's representative in two Erasmus Mundus Joint Master Degrees (CIMET and COSI), and the coordinator of three Marie Skłodowska Curie ITN projects (CP7.0, ApPEARS, CHANGE).

Article C

Yoko Arteaga, Clotilde Boust, and Jon Y. Hardeberg. HDR multispectral imaging-based BRDF measurement using flexible robot arm system. In *Color and Imaging Conference (CIC)*, volume 2022, pages 75 – 80. Society for Imaging Science and Technology, 2022

HDR multispectral imaging-based BRDF measurement using flexible robot arm system

Yoko Arteaga^{1,2}, Clotilde Boust^{1,3}, Jon Yngve Hardeberg²

¹ Centre of Research and Restoration of the Museums of France; Paris, France

² Norwegian University of Science and Technology; Gjøvik, Norway

³ PSL-PCMTH UMR8247 CNRS; Paris, France

Abstract

Materials with special appearance properties such as goniochromatic materials require complex bidirectional measurements to properly characterise their colour and gloss. Normally, these measurements are performed by goniospectrophotometers which are expensive and not commonly available. In this paper a flexible imaging system composed of a snapshot multispectral camera and a light source attached to a robotic arm, is used to obtain HDR BRDF measurements of patinas commonly used in cultural heritage objects. The system is evaluated by comparing the results to those of a commercially available goniospectrophotometer. It is found that with a known uncertainty, the system is capable of producing accurate measurements of samples with a roughness equal or lower than $6.19 \mu\text{m}$. For roughnesses higher than $12.48 \mu\text{m}$, the accuracy of the system decreases. Moreover, it is found that the size and orientation of the region of interest plays a great influence on the precision of the imaging system.

Introduction

Materials with special appearance properties such as patinas can be called goniochromatic, as their appearance changes at different angles of viewing and illumination. In order to characterise said materials, traditional colour measurements are insufficient [1]. Thus, it is recommended to use devices which perform bidirectional measurements such as goniospectrophotometers. These devices are normally expensive, or the measurements are very time consuming [2].

Patinas are a form of metal polychromy used to decorate metallic artworks in which the colour of the metal is changed. In the field of restoration and conservation, it is important to characterise the appearance of artistic materials and understand how different processes modify it, to carry out better restoration and conservation treatments [3] [4]. Moreover, the proper characterisation of the appearance of said materials is crucial and should be thoroughly studied. Commonly, in museums and conservation workshops, colour and gloss measurements are performed but, these alone are insufficient to provide a complete characterisation of the appearance of complex materials. However, most goniospectrophotometers are not easily available, are expensive and mostly used for the absolute appearance characterisation of materials. Thus the interest in a flexible, cheap, multipurpose system which allows cultural heritage actors to characterise a wide range of materials. Moreover, the accurate capture and modelling of specularities present in materials such as patinas require HDR capture.

In this paper, a flexible HDR multispectral imaging system

is used to perform BRDF measurements of bronze patinas commonly found in cultural heritage objects. To evaluate the performance of this system, these measurements are compared to measurements from a commercially available goniospectrophotometer. The flexible HDR multispectral imaging system presented here is composed of a multispectral snapshot camera, and a light source attached to a robotic arm. Due to the flexibility of the robotic-arm, many angles of illumination can be obtained with a very high resolution.

The structure of this paper is as follows: the next section describes the set-up of the imaging system used, the processing pipeline, and the samples studied. The accuracy of this system is evaluated against data obtained from a commercially available goniospectrophotometer and the results are presented in section three, as well as future work. Finally, the conclusion is presented in the fourth section.

Materials and methods

Flexible HDR multispectral-imaging BRDF system

The system presented in this paper is composed of three main elements: a five-joint Dexter robotic arm from Haddington Dynamics [5], a Spectral Filter Array (SFA) multispectral snapshot camera Silius CMS-C [6], and a tilted stage made in-house. This is a modified version of the set-up used in [7].

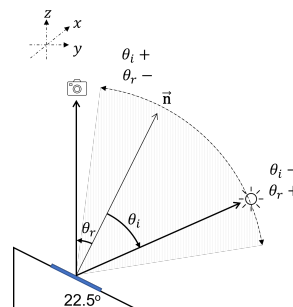


Figure 1: Side view schematic of the system. The camera is looking down on the surface which is on a tilted stage with an elevation of 22.5° . The light is attached to the robotic arm (not illustrated here) and it moves in a 70° arch on the y - z plane.

The robotic arm is used to hold the light source which in this case is a commercially available LED light bulb with a CCT of

6500 K. The robotic arm has the capability of covering a half-hemisphere around the object with an elevation from 10° to 80° . The distance between the light source and the sample is 34 cm. The space available for the movement of the robotic arm is limited due to the shadow cast by the camera at angles close to the viewing angle, and at angles further away from the viewing angle (close to the x-y plane) the light source hits the table. For the purposes of this paper, the sample is illuminated at a fixed angle of observation, $\theta_r = -22.5^\circ$, covering an arch of 35° from both sides of the mirror angle, as illustrated in Figure 1. The angles of illumination range from $\theta_i = -57.5^\circ$ to $\theta_i = 12.5^\circ$, with a total of 63 angles. The illumination sampling is of 3° , 2° , 1° , and 0.5° , increasing as θ_i comes closer to the mirror angle at $\theta_i = -22.5^\circ$. The sampling of the illumination angles is uneven in order to have higher resolution at angles close to the specular peak, and lower at angles further away from it to save processing time and storage.

The multispectral camera used has a 3x3 SFA and it captures eight narrow bands centred at 440nm, 473 nm, 511 nm, 549 nm, 585 nm, 623 nm, 665 nm, and 703 nm. It also has a ninth panchromatic band relatively constant across the visible spectrum. The camera spectral sensitivities are presented in Figure 2. The camera is positioned vertically over the sample at 30 cm, and its optical axis passes through the centre of the arch covered by the robotic arm. The images are acquired at maximum zoom of 3x and maximum aperture size. The effective pixel size is of 0.0377 mm. The samples are placed on an in-house built stage with an angle of elevation of 22.5° . This is chosen so the incident light at the sample ranges equidistantly from the mirror angle. Thus, the angle of observation is of -22.5° . All components of the system are on top of a Thorlabs optical table [8] which removes ambient vibrations.

The robotic arm has five joints which are all controlled from a programming environment. For the given measurement positions, the angles of the joints are calculated using an iterative inverse-kinematic solver. The robotic arm is manually calibrated to its reference position to align it to the virtual 3D kinematic model.

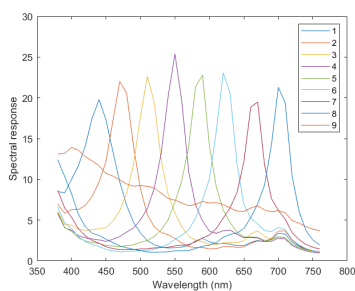


Figure 2: Spectral characteristics of SFA multispectral snapshot camera.

HDR acquisition pipeline

Due to the specularity of the samples, an HDR acquisition pipeline is developed. For each angle of illumination, six images are taken at exposure times 16 ms, 32 ms, 64 ms, 125 ms, 250 ms,

and 499 ms. Thus, for 63 angles of illumination, a total of 378 images are taken with an average time of 20 minutes per sample. A cropped area of 660×660 pixels ($1'' \times 1''$) from the centre of the image is stored to reduce the data processing time.

For each acquisition, a dark-current set of images is obtained at the same exposure times to account for dark current in the sensor. The non-uniformity of the light source is also corrected for by performing a flat-field correction. This is done by acquiring a set of images of a uniform white reference target [9].

Data processing pipeline

The data captured by the system is processed to obtain an HDR BRDF of the sample at the chosen viewing angle. The HDR multispectral image is created following the method proposed by Bravers et al. For each sample, at each angle of illumination, six raw images with 10-bit depth are taken with different exposure times. The dark current is subtracted for each exposure time. Each image is linearised using a look-up-table, to obtain values proportional with the object radiance. At this stage, the HDR image is created by performing a weighted average across exposure times, using a modified Tukey window. Due to quantisation effects, camera noise, and saturation noise can be introduced in the image. The weight function thus, favours values in the centre range over those at borders. The weights presented in this paper have been modified from those proposed by Brauers et al. [10] For all exposure times except the shortest (16 ms) and longest (499 ms), values proportional to radiance smaller than 100 and greater than 923 are completely discarded. For the shortest exposure time, the lowest valued pixels are weighted by the Tukey-window. Likewise, for the longest exposure time and highest valued pixels the values are weighted. This is done to keep all relevant information and discard all noise from artefacts such as blooming effect.

A flat-field HDR image of a uniform nearly-Lambertian reference white calibration surface is generated following the same steps to correct for non-uniformity in the illumination. The flat-field correction is performed by multiplying the flat-field image from the HDR image. Then, this HDR radiance map is demosaiced using bilinear interpolation where a multispectral image of 8 bands is obtained as well as a panchromatic image as the ninth channel.

An area of pixels is averaged and spectral reconstruction is performed using the pseudo-inverse method with a regularisation factor, $\lambda=0.0003$, to guarantee smooth curves and avoid overfitting. The training data for the reconstruction is a 30 patch colour chart which was measured using the HySpex VNIR-1800 hyperspectral imaging system at 45/0 measurement geometry. Reflectance factors values are interpolated to the range 400 nm - 700 nm in steps of 10 nm.

Evaluation of the system's performance

The BRDF measurement obtained by the system is evaluated against the BRDF of the samples obtained by a commercially available goniospectrophotometer, GON 360, equipped with a CAS 140CT array spectrophotometer [11]. This device provides bidirectional measurements at angles of incidence $\theta_i = -35^\circ, -25^\circ, -15^\circ, -5^\circ, 0^\circ, \text{ and } 5^\circ$, and angles of reflection θ_r in the range from -45° to 30° in steps of 5° . The measurement spot has a 10 mm diameter. Figure 3 shows the angles measured by the goniospectrophotometer compared to the angles measured by

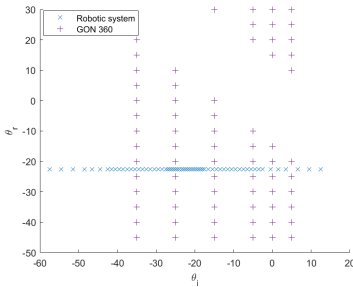


Figure 3: Comparison of both systems' measurement range. Blue x markers: robotic arm system. Purple + markers: goniospectrophotometer.

the system as described above.

To evaluate the reflectance factors given by the flexible imaging-based system to the reflectance factors from the goniospectrophotometer, both datasets, $S(\lambda)$ are taken to an independent colour space i.e. CIE 1931 XYZ colour space (Eq. 1) using standard illuminant D65, $I(\lambda)$, and colour matching functions, $\bar{x}(\lambda)$, $\bar{y}(\lambda)$, $\bar{z}(\lambda)$.

$$\begin{bmatrix} X \\ Y \\ Z \end{bmatrix} = \frac{1}{N} \int_{\lambda} S(\lambda) I(\lambda) \begin{bmatrix} \bar{x}(\lambda) \\ \bar{y}(\lambda) \\ \bar{z}(\lambda) \end{bmatrix} d\lambda, \quad (1)$$

where

$$N = \int_{\lambda} I(\lambda) \bar{y}(\lambda) d\lambda. \quad (2)$$

Since the goniospectrophotometer does not measure the samples at the same angles as the system presented in this paper, the values at $\theta_r = -22.5^\circ$ are interpolated using linear interpolation between the measurements at $\theta_r = -20^\circ$ and $\theta_r = -25^\circ$.

Since the system evaluated gives an image-based BRDF, the area and quantity of pixels averaged greatly influences the results. As seen in Figure 1, at the measurement area edges, θ_i and θ_r are changed with respect to those at the middle of the measurement area. Thus, the larger the distance, higher the uncertainty in the measuring angle. Since the distance of the points to the camera changes both θ_i and θ_r , the influence of using different sized averaging windows is studied. The chosen sizes are 100 x 100 pixels, 10 x 10 pixels, 100 x 10 pixels, and 10 x 100 pixels. The averaged areas are presented in Figure 4 and are selected at the centre of the sample.

The rationale behind the choice of windows is that a 100 x 100 pixel averaging window introduces error in the measurement angle, but also it reduces error from averaging the pixel values. Any error introduced from registration issues, problems between acquisitions, or non-uniformity on the sample will be averaged out. Using a 10 x 10 pixel averaging window reduces the error on the angles but consequently, increases the SNR. Also, if the sample is non-uniform, this reduces repeatability, as the results will be highly dependent on the location chosen. A window of 10 x 100 pixels decreases the error induced by the angle, but also maximises the area averaged so the non-uniformity and registration

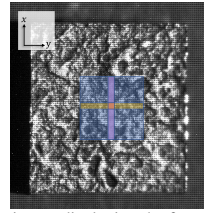


Figure 4: Example image displaying the four averaging windows. In blue 100 x 100, orange 10 x 10, yellow 100 x 10, purple 10 x 100.

errors can be discarded. An area of the same size but in different orientation, 100 x 10 pixels, would increase the error due to the angle uncertainty, but also maximise the area being averaged.

Sample patinas

The samples used for this experiment are bronze patinas from the Coubertin art foundry [12]. Four patinas are available, in two colours: red, and black and two surface finishes: smooth and rough. Hereafter the samples will be referred to as RS, RR, BS, and BR, the first letter being the colour and second their surface finish (smooth or rough). The roughness of the samples, represented by the arithmetical mean height and calculated according to ISO25178 standards [13], is presented in Table 1 [14].

Table 1: Arithmetical mean height (μm) for each patina calculated according to ISO25178 standards. Scanning resolution of 2 μm , using an 8 mm probe.

	Black	Red
Smooth	3.45	6.19
Rough	21.95	12.48

Results and discussion

The calculated luminance, CIE Y, values obtained by the system are plotted as a function of the angle of incidence, θ_i , for the fixed angle of observation, $\theta_r = -22.5^\circ$. For each sample there are four curves corresponding to the four different areas averaged to obtain the CIE Y values. These are displayed as dot markers with error bars. The interpolated values obtained from the goniospectrophotometer are plotted only at the angles of incidence available from the measurements, displayed as black star markers. For the available angles refer to Figure 3.

The standard error of means (SEM) for each point is calculated and displayed as error bars according to:

$$SEM = \frac{\sigma}{\sqrt{N}}, \quad (3)$$

where σ is the standard deviation, and N is the number of observations. The graphs display two standard errors of the mean. Figure 9 shows the mean SEM for each sample and each averaging window.

Smooth samples

Figures 5 and 6, show the curves obtained for the smooth samples. The shape of the curve is smooth and the samples have a peak between $\theta_i = -20^\circ$ and $\theta_i = -25$, close to the theoretical mirror angle at $\theta_i = -22.5^\circ$.

In general, averaging 100 x 100 and 100 x 10 pixels gives a similar response. Averaging 10 x 100 pixels give lower luminance values and a lower specular peak.

BS and RS present similar behaviour. In both cases, the system is precise as the values obtained with the imaging system are quite similar to those from the goniospectrophotometer. The point measured at $\theta_i = -35^\circ$ with the goniospectrophotometer has a slightly higher luminance value than those measured with the imaging system but the shape of the specular peak is well sampled.

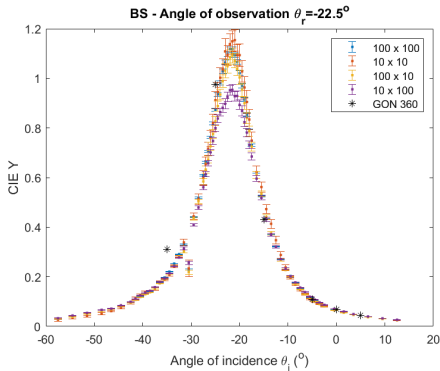


Figure 5: Luminance (CIE Y) as a function of angle of incidence (θ_i) at angle of viewing $\theta_r = -22.5^\circ$. Sample BS.

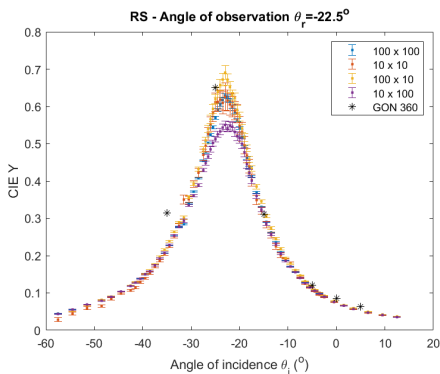


Figure 6: Luminance (CIE Y) as a function of angle of incidence (θ_i) at angle of viewing $\theta_r = -22.5^\circ$. Sample RS.

Rough samples

The rough samples are presented in Figures 7, and 8. These samples present quite a different behaviour than that of the smooth

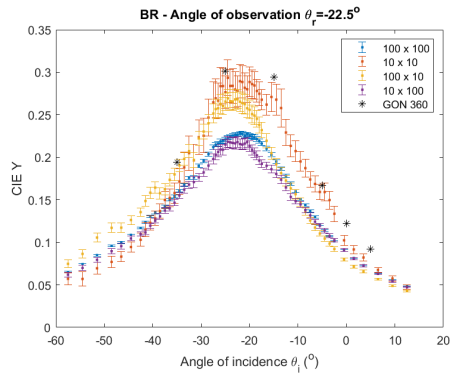


Figure 7: Luminance (CIE Y) as a function of angle of incidence (θ_i) at angle of viewing $\theta_r = -22.5^\circ$. Sample BR.

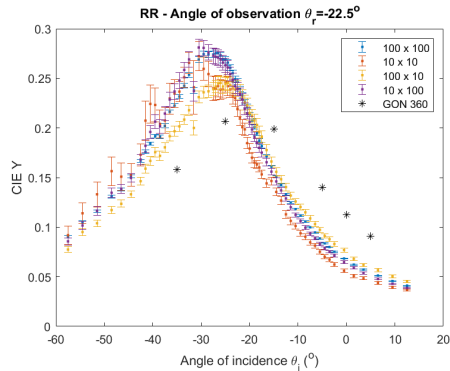


Figure 8: Luminance (CIE Y) as a function of angle of incidence (θ_i) at angle of viewing $\theta_r = -22.5^\circ$. Sample RR.

samples. For BR, the best results are obtained using the 10 x 10 averaging window as they are quite consistent with those from the goniospectrophotometer. However, the 10 x 10 curve is much noisier than the other three. Curves at 100 x 100 and 10 x 100 averaging window have the poorest precision but higher accuracy. The effect of the averaging window is different for RR, presented in Figure 8. All averaging windows give a rather similar curve, with the exception that using 100 x 10 gives a lower specular peak. The main difference between these curves and the ones from the other samples is that the specular peak seems to be shifted to the left, lying between $\theta_i = -25^\circ$ and $\theta_i = -30^\circ$. This could be explained due to the fact the samples are very rough and thus the distribution of microfacets normals could be quite different from the surface normal. Moreover, for sample RR, the curves are quite noisy, particularly 10 x 10, at angles of incidence lower than $\theta_i = -25^\circ$. This could be due to the roughness of the sample and irregularity of the surface. It is possible that many microfacets in the 10 x 10 area are facing the light source at angles smaller than $\theta_i = -25^\circ$, since larger averaging areas have smaller error bars for the same angles.

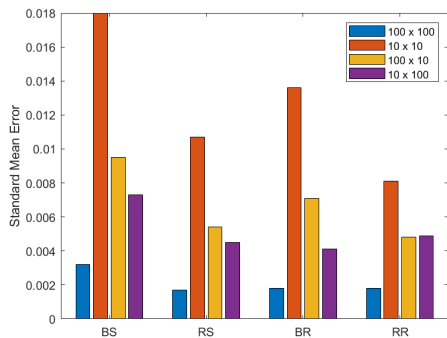


Figure 9: Mean SEM for all samples at different averaged areas.

Precision evaluation

Figure 9 shows the mean of the SEM for all the samples acquired by the custom system, at the four different averaging windows which are presented in Figure 4. Regardless of whether the BRDF curve is accurate or not, the precision of the measurement greatly increases when averaging 100 x 100 pixels. Likewise, averaging 10 x 10 pixels increases the error by almost a full order of magnitude in the case of BS and BR.

In the case of areas 100 x 10 and 10 x 100 which have the same size but different orientation, averaging 10 x 100 pixels minimises the error in both angle of incidence and viewing. Contrary to averaging 100 x 10 pixels which increases the error.

For sample RR, averaging 100 x 10 or 10 x 100 pixels does not change the mean SEM. This could be because this sample is very rough and thus the effect of the non-uniformity of the surface is more significant than the error on the angle.

Discussion and future work

For smooth samples in Figures 5 and 6, it can be seen that the imaging system is as accurate as the goniospectrophotometer. In both cases there is a small difference between the curves obtained by the system presented here and the commercially available goniospectrophotometer. Moreover, the size and orientation does not influence too much the shape of the curves. This suggests the samples are quite uniform as their microfacets normals are oriented evenly which is confirmed by their roughness presented in Table 1. In the case of rough samples, presented in Figures 7 and 8, the system has a lower accuracy at characterising their BRDF than the goniospectrophotometer. In the case of BR, Figure 7, the curve averaging 10 x 10 pixels is accurate as the points measured by the goniospectrophotometer have similar values and the shape of the curves is similar. However the precision at 10 x 10 is rather low. Since both devices work by averaging a small area of the sample, the match in BR could just be a coincidence. If the system was appropriate for this sample, averaging more pixels would increase its accuracy, not decrease it as is the case here. Since this sample has a rough surface, in this case averaging more pixels is equivalent to having a more uneven distribution of microfacets normals. Hence the specular peak at 100 x 100 and 10

x 100 pixels is lower than that at 10 x 10 pixels. In the case of sample RR in Figure 8, the curves do not match the values obtained by the goniospectrophotometer. As it is seen in the graph, the specular peak is at around $\theta_r = -30^\circ$. Moreover, the curves become very noisy at angles lower than the specular peak. This could be also explained by an averaging effect. This sample is also rough, and it is possible that the area being averaged here has a distribution of microfacets normals which is strongly tilted compared to the area measured by the goniospectrophotometer. Moreover, it can be seen that the curve obtained by averaging 100 x 10 pixels has a less prominent shift which could indicate the microfacets with a normal shift are lying along the y-axis rather than the x-axis. It must also be noted that the values obtained by the goniospectrophotometer also come from averaging a small area on the sample and that this device is not optimised for samples with this level of roughness.

As mentioned previously, the size and orientation of the averaging area plays a large role in the precision of the system as presented in Figure 9. Regardless of the accuracy of the system and whether the values obtained are confirmed or not by the goniospectrophotometer, averaging a large area decreases the error of the measurement compared to a smaller area. Even if the small area decreases the uncertainty introduced by the viewing and incident angles, the overall error increases. Moreover, equally sized areas at different orientations do not introduce equivalent errors. As mentioned before, averaging 10 x 100 pixels reduces the error because it decreases the uncertainty introduced by the angles of incidence and viewing. The uncertainty in the angle has a strong contribution in the overall precision of the system. However, for sample RR, the error from 100 x 10 is equal to that of 10 x 100. This could be caused by the uncertainty introduced by the non-uniformity of the sample being larger than the contribution from the angle uncertainty.

Given that different points on the sample image give different combinations of incident and viewing angles, this could be used as an advantage. By doing simple trigonometry, it is possible to find the exact angles of incidence and viewing at different points of the sample along the y-axis. Thus, by averaging different equally sized areas along the y-axis, more BRDF measurements can be obtained from a single acquisition, without the need of moving either the camera or the sample. Moreover, since the light source is held by the robotic arm, this provides a lot of flexibility to chose different angles of illumination which can be changed depending on the material being measured. Also, the system presented here has the samples on an in-house built tilted stage. If this stage was replaced by a very accurate, tiltable stage, a further degree of freedom would be introduced which consequently would provide a higher combination of viewing and illumination angles. Finally, it must be noted that this experiment can be repeated with more simple equipment, by replacing the robotic arm by an arch with fixed light sources or a dome type of illumination system which is commonly used in the cultural heritage field for RTI acquisition.

Conclusion

In this paper, a flexible multispectral imaging system and the processing pipeline required to obtain HDR BRDF measurements with it have been presented. The imaging system is used to measure four patina samples commonly used in artistic workshops. The results obtained by the imaging system are compared

to measurements from a commercially available goniospectrophotometer. It is found that for smooth samples with roughness equal or lower than $6.19 \mu\text{m}$, the results are reliable as they have a known uncertainty and are consistent with those from the goniospectrophotometer. However, for rough samples with a roughness equal or higher than $12.48 \mu\text{m}$, the results present a higher error and the accuracy of the system decreases compare to that of the goniospectrophotometer. For both cases, it is also found that the size and orientation of the averaging window used greatly influences the precision of the imaging system and it should be preferable to use larger areas. Moreover, it is found that the error introduced by the angle uncertainty is higher than that of the non-uniformity of the sample. Finally, it is noteworthy that the illumination system presented here can be easily replaced by simpler and more accessible set-ups such as RTI domes to illuminate the surface at different angles of incidence.

Acknowledgements

This research was funded with the support of CHANGE Cultural Heritage Analysis for New Generations European Union's Horizon 2020 research and innovation programme under the Marie Skłodowska-Curie grant agreement No. 813789.

The authors would like to thank Dominique Robcis for access to the bronze patinas used in this experiment. Many thanks to Tanzima Habib and Donatela Saric for their help measuring the patinas at FOGRA and Vlado Kitanovski for invaluable help with the data acquisition using the robot system.

References

- [1] C. McCamy, "Observation and measurement of the appearance of metallic materials. part i. macro appearance", *Color Research & Application*, 32, p. 378-387, (2007).
- [2] A. Sole, I. Farup and P. Nussbaum, "Evaluating an image-based bidirectional reflectance distribution function measurement setup", *Applied Optics*, 57, p. 1918-1928, (2018).
- [3] F. Mathis, S. Descamps, D. Robcis and M. Aucouturier, "Original surface treatment of copper alloy in ancient Roman Empire: chemical patination on a Roman strigil", *Surface Engineering*, 21, p. 346-351, (2005).
- [4] E. Joseph, A. Simon, S. Prati, M. Worle, D. Job and R. Mazzeo, "Development of an analytical procedure for evaluation of the protective behaviour of innovative fungal patinas on archaeological and artistic metal artefacts", *Analytical and Bioanalytical Chemistry*, 9, (2011).
- [5] Haddington Dynamics, online. <https://www.hdrobotic.com>
- [6] Silios multispectral cameras, online. <https://silios.com/cms-series>
- [7] V. Kitanovski and J. Y. Hardeberg, "Objective evaluation of relighting models on translucent materials from multispectral RTI images", *IS&T International Symposium on Electronic Imaging, Material Appearance Conference Proceedings*, p. 133-1-133-7, (2021).
- [8] Optical breadboards, online. https://www.thorlabs.com/newgrouppage9.cfm?objectgroup_id=7159
- [9] ColorChecker white balance, online. <https://www.xrite.com/en/categories/calibration-profiling/colorchecker-white-balance>
- [10] J. Brauers, N. Schulte, A. A. Bell and T. Aach, "Multispectral High Dynamic Range Imaging", *IS&T/SPIE Electronic Imaging, Conference Proceedings*, p. 33-42, (2008).
- [11] CAS 140CT Array Spectrometer, Instrument Systems. Konica Minolta, online. https://www.instrumentsystems.com/fileadmin/Downloads/Brochures_Datasheets/CAS140CT_EN.pdf
- [12] J. Edelson, "Elaboration d'une méthodologie d'analyse des patines artificielles sur les bronzes du patrimoine artistique", Master's thesis - École des Mines de Paris (2000).
- [13] ISO25178-2:2012 Geometrical product specifications (GPS) - Surface texture: Areal - Part, 2: Terms, definitions and surface texture parameters.
- [14] Y. Arteaga, C. Boust, A. Dequier and J. Y. Hardeberg, "Image-based goniometric appearance characterisation of bronze patinas", *IS&T Color and Imaging Conference Proceedings*, p. 294-299, (2021).

Author Biography

Yoko Arteaga is a Marie Skłodowska-Curie early stage research fellow at the Centre of Research and Restoration of the Museums of France and part of the Colourlab at the Norwegian University of Science and Technology. She has a background in Physics and Colour Science. For her PhD she is working in the development of techniques to characterise surface topography and appearance for cultural heritage objects.

Clotilde Boust is the head of the Imaging Group at the Centre for Research and Restoration of the Museums of France (C2RMF). She is developing spectral, 3D, and XR imaging in order to measure and understand artworks before restoration.

Jon Y. Hardeberg is Professor of Colour Imaging at NTNU, Department of Computer Science, The Norwegian Colour and Visual Computing Laboratory, Gjøvik, Norway. His current research interests include spectral imaging, image quality, colour management, material appearance, cultural heritage imaging, and medical imaging, and he has co-authored more than 300 publications within the field. He has led several research projects funded by the Research Council of Norway, been NTNU's representative in two Erasmus Mundus Joint Master Degrees (CIMET and COSI), and the coordinator of three Marie Skłodowska Curie ITN projects (CP7.0, ApPEARS, CHANGE).

Article D

Yoko Arteaga, Diane Marchioni, Stéphanie Courtier, Clotilde Boust, and Jon Y. Hardeberg. Appearance-based evaluation of varnish removal methods in gilded surfaces. *Heritage Science*, **11**, 31, 2023

RESEARCH

Open Access



Appearance-based evaluation of varnish removal methods in gilded surfaces

Yoko Arteaga^{1,2*}, Diane Marchioni³, Stéphanie Courtier¹, Clotilde Boust^{1,4} and Jon Y. Hardeberg²

Abstract

This paper outlines the use of bidirectional reflectance measurements for the characterisation and evaluation of appearance changes in gilded surfaces caused by varnishing and cleaning. Oil and water gilding mock-ups representative of a 15th-century panel painting were varnished, and a selection of four varnish removal methods was applied. By measuring the bidirectional reflectance of the samples, their appearance was modelled and evaluated according to perceptual gloss attributes. Three main perceptual groups were found for each gilding type: unvarnished, varnished and cleaned surfaces. Finally, for the studied samples, the most appropriate method for removing dammar and colophony varnish from a gilded surface, in terms of appearance change, is solubilisation by applying an Evolon CR compress.

Keywords Gilding, Material appearance, BRDF measurement, Varnish removal, Gloss

Introduction

Gilding is a form of polychromy where a gold leaf is attached to a substrate by different means. Commonly used in the Middle Ages, gilding gives a golden appearance to a surface dependent on its fabrication method. While oil gilding is believed to have a cooler appearance due to its matte and rough surface, water gilding is described as warmer and glossier due to burnishing which smooths the surface and gives it a metallic appearance [1].

It is common to find gilded surfaces that have been varnished for various reasons: to protect the surface from abrasions and mechanical damages [2, 3], to change its appearance [4], and to imitate another metal [5, 6]. Varnish can change the appearance of a gilded surface by

modulating its gloss, or depending on the varnish, change its hue [3].

However, varnish is an organic material which changes appearance over time. Common restoration techniques involve cleaning the superficial layer, leaving the varnish intact, or removing the varnish without damaging the surface underneath it. Due to the fragility of the gold leaf, it is important to understand the mechanisms at play when removing the varnish to avoid any damage or modification to the gilded surface. Empirical knowledge on the appearance of gilding is vast amongst conservators and restorers; appearance differences between distinct types of gilding as well as conservation treatment effects such as varnishing are well understood in this community. However, these appearance changes have not been thoroughly studied in a quantifiable manner which correlates to perception.

Gilded surfaces have a metallic appearance which cannot be described solely with traditional colorimetry since many elements influence how it is perceived. While the appearance of diffuse materials such as mineral pigments can be described by colour measurements, the appearance of metallic surfaces is mainly described by their colour and gloss [7]. Materials which present colour changes

*Correspondence:

Yoko Arteaga
yoko.arteaga@culture.gouv.fr

¹ Centre of Research and Restoration of the Museums of France, Paris, France

² Department of Computer Science, Norwegian University of Science and Technology, Gjøvik, Norway

³ National Heritage Institute, Paris, France

⁴ PSL-PCMTM UMR8247, CNRS, Paris, France



© The Author(s) 2023. **Open Access** This article is licensed under a Creative Commons Attribution 4.0 International License, which permits use, sharing, adaptation, distribution and reproduction in any medium or format, as long as you give appropriate credit to the original author(s) and the source, provide a link to the Creative Commons licence, and indicate if changes were made. The images or other third party material in this article are included in the article's Creative Commons licence, unless indicated otherwise in a credit line to the material. If material is not included in the article's Creative Commons licence and your intended use is not permitted by statutory regulation or exceeds the permitted use, you will need to obtain permission directly from the copyright holder. To view a copy of this licence, visit <http://creativecommons.org/licenses/by/4.0/>. The Creative Commons Public Domain Dedication waiver (<http://creativecommons.org/publicdomain/zero/1.0/>) applies to the data made available in this article, unless otherwise stated in a credit line to the data.

under different illumination-viewing conditions, such as gilding, are called goniochromatic [8]. Three viewing geometries have been defined suitable to describe metallic paints: near-specular, face, and flop angles [9]. Vast research has been done to characterise goniochromatic films and paints [10, 11]. However, this has not been applied to gilding.

In the case of gilding, colour differences calculated for a fixed angle of incidence and reflection may be unrepresentative of perceptual differences. Gloss measurements provide angular information, as they are performed at three different angles; and thus, its perception is highly dependent on illumination and viewing directions. However, the correlation between gloss units and human perception is not clearly defined [12]. It is found gloss perception has a nonlinear relationship with instrumental gloss values and many factors such as binocular vision influence gloss sensitivity [13]. Recommendations by experts and industry are to perform psychophysical experiments to define gloss tolerances for a batch of samples [14]. In the case of gilded surfaces, many factors can affect their visual perception such as the illumination type, geometry and intensity, the viewing conditions, the material composition of the gilding, and the presence of surface coatings, to name a few [15].

For many applications, complex surface appearance can be characterised by the bidirectional reflectance distribution function (BRDF) which is the physical quantity for gloss measurement [16]. The BRDF describes how light is reflected off a surface and depends on illumination and viewing directions. Multidirectional reflectometry is an approach in which one directly measures the ratio of reflected over incident light at each combination of angles to model the BRDF of a given surface. This method allows obtaining a full model of the BRDF which can describe the appearance of the surface at different combinations of viewing and illumination directions.

It is thus, of great interest to measure the BRDF of gilded surfaces to characterise their appearance. By obtaining a more accurate appearance measurement, the effect that conservation treatments such as varnishing, and its eventual removal, have on the perception of gilded surfaces can be evaluated. Varnish is believed to increase the saturation of colours and the gloss of surfaces, altering the appearance and perception of the artwork. While this is well documented in the case of pigments, its effect on gilding has not been studied. Finally, varnish removal methods can be evaluated to find which will, amongst other desirable qualities, return the gilded object the closest to its original appearance.

This work has been developed in conjunction with the National Heritage Institute in Paris, France, as part of a final-year conservation studies project dedicated to a

15th century framed panel painting, named after its iconography, the *Vierge de douleur/Virgin of Sorrows* and belonging to the Jacquemart-André Museum in Paris. (Fig. 1).

The technological study of the artwork revealed that the gilding present on the *Vierge de douleur/Virgin of sorrows* was covered with a thick layer of coloured varnish. The analysis showed that this layer was constituted of different types of varnish, including an original varnish which constituted the original decor of the painting. Therefore, the aim of removing the varnish by using chemical methods is not to completely remove the varnish from the gilded surface but to remove superficial layers of the soiled varnish by controlling the surface appearance. In addition, the adhesive of the gold leaf on the original gilding could have been soluble in the same solvents as the varnish, demanding a very controlled protocol. The main results of the technological study of the painted panel are presented in the Appendix.

Research aims

The primary aim of this paper is to propose a framework to measure, quantify, and evaluate the appearance of gilded surfaces. The second aim is to apply the presented framework to evaluate appearance changes induced by different chemical varnish removal methods on varnished, gilded wood. Finally, these findings can be used to potentially guide the restoration of the painting. An imaging-based method is presented to measure the BRDF of two types of gilding mock-ups. These have been varnished and four chemical varnish removal methods have been tested. The BRDF of the surface is modelled and the BRDF parameters are used to classify the gilding in terms of its appearance.



Fig. 1 Unknown. *Vierge de douleur/Virgin of sorrows*. 15th century. Painted panel. 36.8 x 34.0 cm (62.3 x 43.0 cm with frame). Jacquemart-André Museum, Paris. **a** Before restoration. **b** After restoration. ©Angèle Dequier/Inp

Background

Gilding fabrication techniques

The samples designed for this study are intended to be representative of the gilding present on the studied artwork. Thus, the findings can potentially be used directly for restoration. Two types of gilding were produced, water gilding, representative of the frame, and oil gilding. Although the gilding of the painted panel was not identified with certainty when the samples were produced, it seemed more likely that it was oil gilding. Even if this is ultimately not the case, it is still valuable to compare the behaviour of these two types of gilding when faced with cleaning. Indeed, these are the two major traditional gilding techniques [17], the use of which has moreover changed very little since the Middle Ages.

The difference between oil gilding and water gilding lies mainly in the nature of the mordant, i.e., the layer underlying the gold leaf (Fig. 2). In the first case, the mordant is an oil-based mixture. It is laid on a thin sealer layer of shellac which has an insulating and saturating function. In the second case, it is a bole, a preparation based on clay or natural soil. This layer is placed on a yellow size which can be made of different preparations and creates a mechanical grip for the next layer and provides a first coloured shade under the gilding.

In the case of oil gilding, the mordant with oil must be left to partially dry. When it is tacky, it is ready to receive the gold leaf, which adheres immediately. Regarding water gilding, the bole is moistened with water; the gold leaf adheres to it immediately. After drying, the gold leaf can be burnished, that is, smoothed on the bole with a hard tool like an agate stone, to make it shiny and smooth. Unlike water gilding, the gold leaf in oil gilding cannot be burnished, so it remains matte and relatively rough.

Removal of varnish in gilded surfaces

Removal of varnish is a widely studied and documented restoration intervention, particularly in the field of painting restoration. In recent decades, this field has benefited from the contribution of substantial scientific research [18–20] which has made it possible to better understand the mechanisms of solubilisation of

organic films, and to introduce new cleaning methods. These always aim to find the best compromise between cleaning efficiency and harmlessness in relation to the artwork. However, unlike mechanical cleaning [21, 22], chemical cleaning methods have not been vastly studied on a gilded wood substrate. The study closest to this subject concerns the chemical removal of a brass-based overpaint on gilded wood [23] and cleaning soiled gilded wood [24]. Another study deals with the chemical cleaning of a brass object [25]. A survey of restorers specialising in this field reveals a relatively empirical practice, for lack of publications on the subject.

The Getty Conservation Institute devoted a study day [26] to the problem of cleaning gilded wood. The report describes the methods used by gilding conservators as well as the specific constraints of gilding on wood. Gilding is a surface treatment with a complex stratigraphy (Fig. 2). It is widely present on heritage objects and can exist on substrates other than wood. There are great differences between gilding on varied substrates, each requiring a different surface preparation and a different restoration approach. It is therefore essential to better understand its behaviour to adapt restoration practices accordingly. The authors of the report raise three problems induced by cleaning: the persistence of cleaning residues (especially in the case of gels), the penetration of solvents under the gold leaf (which can then partially solubilise or alter the substrate), and finally weathering of the gold leaf. The persistence of residues is a phenomenon studied in the field of painted surfaces [27]; its consequences, whatever the nature of the surface, seem to be the same: the residues can cause irreversible damage to the artwork, modify the surface appearance, and are quick to clog up or retain moisture.

Gold leaf, which is extremely thin (0.1 to 10 μm), is fragile [28] and can be altered in different ways: by mechanical abrasion, i.e. the loss of material during cleaning, and by modifying the surface appearance, in particular its gloss and colour. Cleaning is, in its general definition, the removal of all secondary debris and soiling which distract the perception and interpretation of the original surface. The secondary debris and soiling can sometimes form a film if deposited in the form of a layer, but they can be also be found in the form of uneven accretions on the surface. For the sake of clarity, this study refers to the removal of varnish, even though it is desirable that a thin layer of varnish is left on the surface. This paper focuses on the alteration of the surface appearance of gilding caused by varnishing and its subsequent removal.

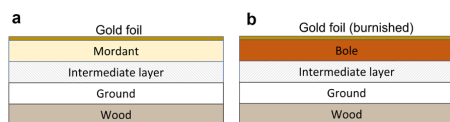


Fig. 2 General stratigraphy of (a) oil gilding and (b) water gilding. In the case of water gilding, the gold foil is burnished

Appearance measurement of gilded surfaces

Gilded surfaces present very interesting appearance properties. While the appearance of diffuse and opaque surfaces such as mineral pigments can easily be described by their colour, specular surfaces such as gilding require complex BRDF measurements in order to correlate them with their perceived appearance. These appearance measurements provide macroscopic characteristics, represented as a statistical aggregation of the reflection of light from many microfacets on the materials surface. Gilded or golden surfaces in cultural heritage objects pose technical imaging challenges.

In order to evaluate the influence of lighting conditions on spectral reconstruction and image stitching using multispectral images, a traditional Japanese painting was imaged with a multispectral camera [29]. The spectra were well estimated for the regions with an orange mineral pigment. However, the gilded region which exhibited high specular reflection presented a poor spectral reconstruction. None of the lighting configurations provided an accurate reconstruction of the reflectance spectrum. The lighting parameters were not optimised for this object and the authors conclude that to achieve better spectral reconstruction, specular reflection issues must be solved.

In the assessment of multispectral and hyperspectral imaging systems, a Round Robin Test assessed the performance of different systems for their spectral digitisation of artworks [30]. The artwork chosen was a polychrome Russian icon from the 19th century, fabricated in Moscow. The icon depicts the subject of the Virgin of Kazan and is printed in chromolithography onto a substrate of tinned steel. This icon was chosen because of its physical and material characteristics. It has a medium gloss on the painted areas and the gold areas have a shiny metallic finish. In the case of the gold area, the authors found significant differences in the reflectance spectra. The shape of the spectra was the same for all imaging systems, however the difference in magnitude varied by a factor of as much as 3x either higher or lower than the reference measurement. This was attributed to the granular nature of the surface and the breadth of the specular peak, characteristic to golden surfaces, which caused the image intensity to be critically dependent on its illumination geometry. The authors conclude that the imaging geometry plays a vital role on glossy surfaces, and it is essential to have some flexibility in the position of the light source and object relative to the camera so the operator can modify the setup according to judgement.

According to the recommendations given in [30], a multi-focus high-dynamic range (HDR) visible/near-infrared (VIS/NIR) hyperspectral imaging set-up is

presented for its application to works of art [31]. In this work, the authors present a complete framework for capturing and processing hyperspectral images of works of art in situ. This framework is applied to a facsimile of *The Golden Haggadah* from the British Library of London which presents gilded areas with high specular reflection. The authors propose a framework in which an HDR hyperspectral image is obtained. Although the final HDR image of the manuscript did not necessarily contain HDR information, the HDR was present in radiances where powerful light sources or dim shadowy areas are present in the same scene which is the case of paintings with gilded areas. The authors segmented gilded from non-gilded areas in the image, based on the spectral reflectance, and compared it to manual segmentation performed by a conservator. The HDR cube had a much better segmentation performance of 95.5% compared to that of the low-dynamic range (LDR) cube of 83.78%. Moreover, while the LDR cube was saturated in some golden areas, the HDR cube was correctly exposed throughout the scene.

In the case of measuring the appearance of gilded surfaces, the most common method is colorimetry. Dumazet et al. [32] used Kubelka-Munk's two flux theory to model the influence of the substrate's colour on the reflected light from the gold leaf, in order to study correlations between gold leaf's imperfections and appearance. The authors made oil gilding mock-ups on stone and measured the back-scattered light at normal incidence of the samples. They have found a red shift in the spectrum when the concentration of holes is higher. Mounier et al. [33] also present colorimetric observations on the appearance of gold leaf on white, red, and black substrates. Oil and distemper gilding mock-ups representative of mural paintings were fabricated and artificially aged. The transmission spectra of different thicknesses of gold leaf were measured and the CIE $L^*a^*b^*$ coordinates were compared individually.

Wu et al. [15] study the influence of substrate colour on the visual appearance of gilding. Gilding mock-ups were fabricated using different methods such as oil gilding, water gilding, and ground gilding. The authors used colorimetry and interferometric microscopy to characterise the mock-ups and conclude that the colour of the substrate does not alter the visual appearance of the gilding. However, they report that burnishing the gilding produces a significant change in appearance.

Finally, Sandu et al. [3] study the surface behaviour of water gilding and imitation gilding using liquid gold. The mock-ups were analysed before and after burnishing (for the water gilded samples), and varnishing. The authors have measured the mock-ups' colour in a

diffuse geometry of 0/0. They report that the CIE L^* value decreases after burnishing and imply a decrease in lightness which contradicts the hypothesis that burnishing increases gloss. The authors contribute these discrepancies to a poor burnishing and/or a different behaviour from the gold leaf imitation. While this may be true, it must be stressed that colorimetry measurements in a diffuse domain are not adequate for evaluating gloss. They also report that varnishing the surfaces, increases the L^* value of the water gilded samples but decreases it in the case of liquid gold.

Bidirectional reflectance of polychrome wood composed of a silver leaf and yellow pine resin which gives it a golden appearance was measured using a spectroradiometer to detect changes in appearance due to accelerated ageing [34]. The authors measured small colour changes due to ageing but significant gloss changes and more specifically a shift in the specular peak. The unaltered samples looked considerably glossier than the aged samples. The goniometric measurements showed that the reflectance peaks which originally were symmetrical, become asymmetrical as an effect of ageing.

Bidirectional reflectance measurements of gold leaves used for gilding are performed in an attempt to model their BRDF [35]. A multi-angle spectrophotometer was used to measure the reflectance of the samples at 12 different combinations of incidence and observation directions. The authors find that the colour change of the gold leaves at different angles of incidence and reflection is significant. Moreover, they conclude it is necessary to properly sample measurement angles close to the specular peak to obtain accurate BRDF models.

The literature review shows there is a lack of research in appearance capturing of gilded surfaces. Multispectral and hyperspectral imaging systems are presented to digitise and capture objects where there are gilded or golden areas present on the scene [29–31]. The three authors emphasise the necessity of appropriate illumination and viewing directions for accurate image capture. However, the focus is on the imaging device's advantages and limitations, as well as the spatial and spectral quality of the data, not the appearance of the gilding. In the case of evaluating the appearance of gilded surfaces more specifically [3, 15, 32, 33], studies are limited to colorimetric measurements which are not sufficient to describe the complete visual appearance of gilding. Moreover, these do not evaluate the effect of removing varnish from gilded surfaces. Thus, it is necessary to measure the appearance of gilded

surfaces accounting for viewing and illumination directions to provide a more complete evaluation [34, 35].

Materials and methods

Fabrication of gilding mock-ups

The gilding studied in this paper are common types of gilding found in the Middle Ages [17]. Water and oil gilding mock-ups were made by professional restorers using traditional techniques. The gold foil used for the gilding mock-ups is 22 karat or *Versailles* from Dauvet goldbeaters.

Four sets of mock-ups are produced using a plywood base. Two reference mock-ups with dimensions 11 x 6 cm, which are not varnished, and two test mock-ups with dimensions 22 x 11 cm (Fig. 3). The test mock-ups are varnished and then cleaned following the four methods described below. As part of the original investigation, two different varnishes were studied. However, in this paper, only one varnish is analysed. The preparation of each mock-up is detailed in Table 1.

The mock-ups are fabricated following traditional gilding techniques, with the same ground layer based on a chalk ground bound with diluted rabbit skin glue. In the case of oil gilding, an intermediate layer of shellac is applied on the ground and then, an oil-based gold size called mordant is used as substrate and adhesive. When the surface is tacky but not completely dry, the gold leaf is applied. For water gilding, an intermediate layer of rabbit skin glue and yellow ochre is applied, followed by a red bole. A mixture of ethanol and water is used as a wetting agent before applying the gold leaf. The gold leaf is burnished manually using an agate burnishing tool which is applied in one direction to produce a highly metallic gloss.

For each gilding technique, one reference sample is kept unvarnished. The test samples are varnished with a combination of dammar and colophony resins in equal proportions. This varnish was found on the artwork as part of past conservation work (see Appendix). To avoid any premature damage to the gold leaf, the varnish is sprayed on the mock-ups using an Ecospray at 10 cm. Each surface is varnished five consecutive times. To accelerate the polymerisation of the resin, the mock-ups are placed inside a Suntest XLS / XSL + UV chamber, with 840780 kJm^{-2} power and energy flux of 765 Wm^{-2} for 311 h, at 35° C. The polymerisation of the resin impacts the adhesion and ductility of the materials as well as the cohesion of the stratigraphy. It aims to replicate as close as possible a real, aged, varnished, gilded surface, since these properties could influence the solubility of the varnish.

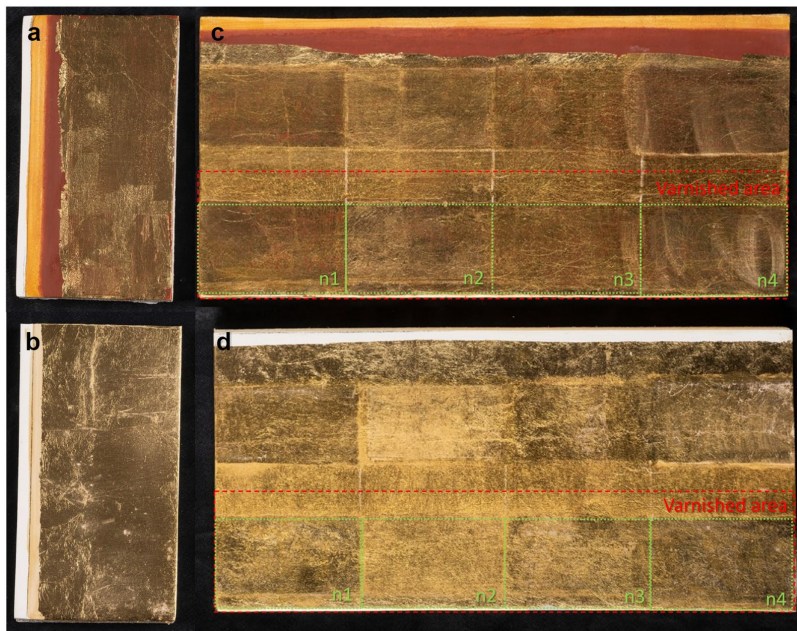


Fig. 3 Picture of the mock-ups fabricated. **a** Reference unvarnished water gilding. **b** Reference unvarnished oil gilding. **c** Varnished and cleaned water gilding. **d** Varnished and cleaned oil gilding. The red rectangle shows the varnished area with dammar and colophony. The green rectangles show the cleaned area for each method. ©Angèle Dequier/Inp

Varnish removal methods

Four chemical methods are tested to remove the varnish from the mock-ups. The methods chosen are commonly used in domains of conservation and restoration. The main principle is to use a solvent mixture of isooctane and ethanol in a 70:30 ratio [36], in four different ways. The varnish removal methods and their advantages and disadvantages are described below (Fig. 4).

Method 1: Solubilisation with a cotton swab (n1) This method is traditionally used when removing an organic film in paintings. The cotton swab is dipped in the mixture of solvents and applied on the surface with no pressure. When the cotton is saturated with varnish, a new cotton swab is used. The advantages of this method are the good control of the solubilisation action and the absence of residue on the surface. On the other hand, cotton is an abrasive material which can damage sensitive substrates since there is little control over the diffusion into the substrate and the evaporation of the solvent.

Method 2: Solubilisation by applying a compress (n2) This technique is widely used in the restoration and conservation of artworks. A compress of the same dimensions as the desired area to clean is placed on

Table 1 Structure and material composition of the mock-ups

Sample name	Type of gilding	Varnish	Type of cleaning
OG	Oil	No	N/A
OG-V	Oil	Yes	N/A
OG-V-n1	Oil	Removed	Method 1
OG-V-n2	Oil	Removed	Method 2
OG-V-n3	Oil	Removed	Method 3
OG-V-n4	Oil	Removed	Method 4
WG	Water	No	N/A
WG-V	Water	Yes	N/A
WG-V-n1	Water	Removed	Method 1
WG-V-n2	Water	Removed	Method 2
WG-V-n3	Water	Removed	Method 3
WG-V-n4	Water	Removed	Method 4

the surface and soaked with the solvent. The compress used here is an Evolon CR textile due to its absorbing qualities, simple use, and satisfying results [37, 38]. A Melinex plastic film is placed over the compress to avoid evaporation and a piece of glass is placed on top

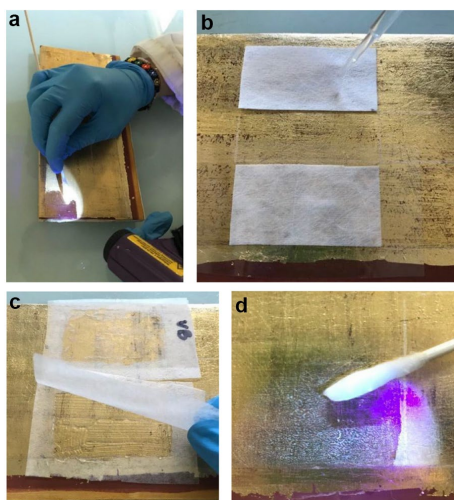


Fig. 4 Cleaning methods. **a** Solubilisation with a cotton swab under UV light. **b** Solubilisation by applying a compress. A pipette is used to soak the compress with the solvent. **c** Solubilisation by use of a gel. The gel is between two layers of hemp paper. **d** Rinsing the surface using a cotton swab

to apply pressure on the surface. The advantages of this method are that it does not require rubbing the surface, it does not leave fibrous residues, and it is an isotropic and resistant material [39]. However, there is little visual control over its action on the varnish and it can only be used on flat surfaces.

Method 3: Solubilisation by use of an aqueous gel (n3)
A solvent gel is fabricated following the technique developed by Richard Wolbers [19]. The gelling agent is a polyacrylic acid, a long-chain synthetic polymer (Carbopol type), which is neutralised by an organic base from the amine family with surfactant properties (Ethomeen type). A hemp paper interface is used to manipulate the gel and avoid unnecessary rinsing and rubbing. After two minutes the gel is removed, and the surface is rinsed with isooctane using a cotton swab. The advantage of using a gel is that there is little penetration of solvents compared to free-handed methods like n1. Moreover, it can be applied to a specifically defined area and requires little rubbing as this is only necessary in the final rinsing stage. Nonetheless, the water content in the gel might alter water-sensitive surfaces such as oil gilding.

Method 4: Solubilisation by use of a silicon-based gel (n4)
This method is applied in the same way as n3 but the gel chosen is silicon-based. The gel used here is a Shin Etsu KSG-350Z. It can be coupled with silicone solvents with different molecular weights, called cyclomethicones.

These are apolar solvents whose surface tension is very low. Their immiscibility with water, as well as their slow evaporation time, allow them to be used as a temporary “pore filler”; and thus, protect the substrate from the migration of other solvents. These evaporate more or less rapidly. The advantage of this method is that due to the silicon nature of the solvent, the substrate is temporarily protected. Also, this method is favourable for water-sensitive surfaces, and due to its high viscosity, the penetration of the solvent into the substrate is limited.

Conventional colour and gloss measurements

Colour measurements were carried out with a Konica Minolta CM-2600d spectrophotometer, at specular component excluded (SCE) mode to have only the diffuse light. 20 measurements were taken for each area, moving the device a few millimetres each time. Gloss measurements were taken with a Rhopoint Instruments Novo-Gloss glossmeter. The glossmeter measures at three angles of reflection (20° , 60° , and 85°). The measured area is 6.4×6 mm at 20° , 6×12 mm at 60° , and 4.4×4.4 mm at 85° . Since the measurement area is rather large, only three successive measurements at the same place were carried out, and the values were averaged in order to ensure their reproducibility. Both measurement systems are designed for flat surfaces. In the case of curved surfaces present in real objects, a different choice of noncontact device would be necessary.

Flexible HDR multispectral-imaging BRDF system

As previously explained in *Appearance measurement of gilded surfaces*, conventional colour and gloss measurements are insufficient to fully characterise the appearance of gilding. Thus, in this subsection, an alternative bidirectional reflectance acquisition and processing pipeline are presented.

The imaging system used in this paper has been described in [40]. It is composed of a five-joint robotic arm which holds the illumination source, a multispectral snapshot camera, and a tilted stage with an angle of elevation of 22.5° (Fig. 5). The multispectral camera captures eight narrow bands centred at 440 nm, 473 nm, 511 nm, 549 nm, 585 nm, 623 nm, 665 nm, and 703 nm. The camera is positioned vertically over the sample at 30 cm. The images are acquired at maximum zoom of 3x and maximum aperture size. The effective pixel size is 0.0377 mm. The robotic arm is capable of moving in a 70° arch on the y-z plane. Thus, the sample is tilted so it is illuminated at a fixed angle of observation, $\theta_r = -22.5^\circ$, and the illumination angles cover an arch of 35° from both sides of the mirror angle, ranging from $\theta_i = -57.5^\circ$ to $\theta_i = 12.5^\circ$, with a total of 63 angles.

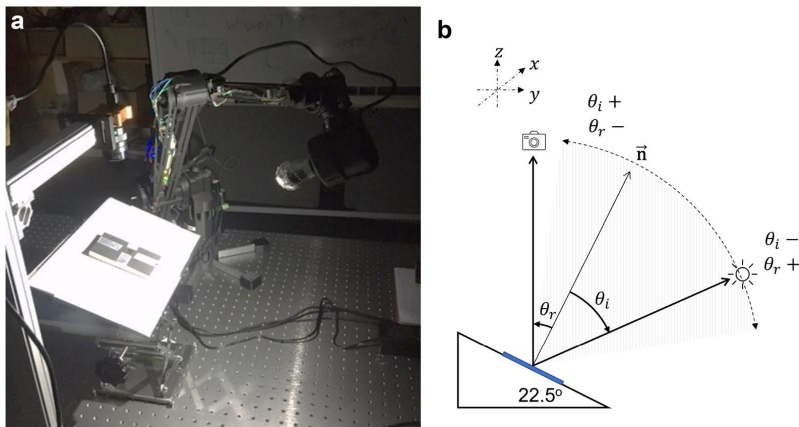


Fig. 5 Side view of the imaging system. The sample is placed on a tilted stage, the camera is above the sample and the light is held by a robotic arm. **a** Picture of the imaging system. **b** Schematic of the imaging system. (Robotic arm not illustrated). Taken from [40]

HDR acquisition pipeline

Due to the specularity of the samples and as suggested in [31], an HDR acquisition pipeline is developed. For each angle of illumination, ten images are taken at exposure times 1 ms, 2 ms, 4 ms, 8 ms, 16 ms, 32 ms, 64 ms, 125 ms, 250 ms, and 499 ms. Thus, for 63 angles of illumination, a total of 630 images are taken with an average time of 30 min per sample.

For each acquisition, a dark-current set of images is obtained at the same exposure times. The non-uniformity of the light source is corrected by performing a flat-field correction. This is done by acquiring a set of images of a uniform white reference target [41]. To perform the spectral reconstruction, a 30-patch ColorGauge Nano Target colour chart [42] which was measured using the HySpex VNIR-1800 hyperspectral imaging system at 45/0 measurement geometry, is also acquired using the

imaging system. The reflectance factors are interpolated to the range 400 nm - 700 nm in steps of 10 nm in order to calculate a transformation matrix for each angle of illumination. The colour chart is made of a diffuse material so it is assumed that the reflectance spectra of the patches will not change significantly at different illumination directions.

Data processing pipeline

The data is processed to obtain an HDR BRDF of the sample, and has been described in [40] (Fig. 6). The HDR multispectral image is created following the method proposed by Brauers, et al. [43].

For each sample, at each angle of illumination, ten raw images with 10-bit depth are taken with different exposure times. The dark current is subtracted for each exposure time. Each image is linearised using a look-up-table,

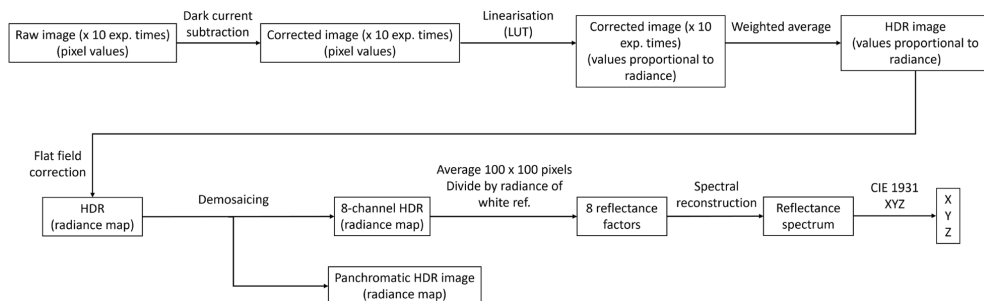


Fig. 6 Processing pipeline to obtain HDR BRDF of the samples as described in [40]

to obtain values proportional to the object's radiance. At this stage, the HDR image is created by performing a weighted average across exposure times using a modified Tukey window. A flat-field HDR image of a uniform nearly-Lambertian reference white calibration surface is generated following the same steps to correct for non-uniformity in the illumination. The flat-field correction is performed by multiplying the flat-field image with the HDR image. The HDR radiance map is demosaiced using bilinear interpolation where a multispectral image of 8 bands is obtained and a panchromatic image as the ninth channel.

An area of 100 x 100 pixels is averaged to obtain the discrete reflectance factors, \mathbf{Q} , at each spectral band. The spectral radiant power incident on the camera sensor is given by:

$$\phi = k\mathbf{H}\mathbf{S}\beta. \quad (1)$$

$k = Aa$ is a camera specific factor, where A is the area of the sensor and a is the aperture of the optics. \mathbf{H} are the spectral characteristics of the sensor filter array, \mathbf{S} is the light source spectral irradiance, and β is the spectral reflectance.

Since H cannot be inverted, Equation 1 is re-arranged:

$$\phi = k\mathbf{S}'\mathbf{H}\beta. \quad (2)$$

By using the camera response values from the uniform nearly-Lambertian reference white calibration surface, ϕ_{ref} , the discrete spectrum of the light source, \mathbf{S}_{ref} , is approximated, where the reflectance spectrum of the white balance card, β_{ref} , is assumed to be that of a Lambertian surface.

Dividing $\phi \div \phi_{\text{ref}}$ is the equivalent of a multispectral white balance, cancelling out the specific camera factor k , and giving the discrete reflectance factors for each spectral band \mathbf{Q} :

$$\mathbf{Q} = \mathbf{H}\beta. \quad (3)$$

Given that \mathbf{H} cannot be inverted, a transformation matrix, \mathbf{T} , is calculated using the known reflectance spectra, β_{cc} , and reflectance factors, \mathbf{Q}_{cc} , of the reference colour chart:

$$\mathbf{T} = \beta_{\text{cc}}\mathbf{Q}'_{\text{cc}}\text{inv}(\mathbf{Q}_{\text{cc}}\mathbf{Q}'_{\text{cc}} + \lambda\mathbf{I}), \quad (4)$$

where \mathbf{I} is an identity matrix and $\lambda = 0.0003$ is a regularisation factor which avoids overfitting and guarantees smooth curves.

Thus, the reflectance spectrum, β_{est} , can be estimated using the following equation:

$$\beta_{\text{est}} = \mathbf{T}\mathbf{Q}. \quad (5)$$

Bidirectional reflectance modelling

The bidirectional reflectance of the material is modelled using the BRDF defined by Nicodemus [44] as the ratio between the differential irradiance, E , along \mathbf{l} at point x and the differential outgoing radiance, L , along \mathbf{v} :

$$f(x, \mathbf{l}, \mathbf{v}) = \frac{dL_r(x, \mathbf{v})}{dE(x, \mathbf{l})}. \quad (6)$$

Cook-Torrance BRDF

Cook and Torrance describe a physically based BRDF model based on geometrical optics [45]. This model is a well-established physical model and is used extensively to model specular materials like gold [35, 45–47]. The BRDF is separated into a specular, R_s , and a diffuse, R_d component:

$$f = k_d R_d + k_s R_s, \quad (7)$$

where k_d and k_s are weighting parameters and $k_d + k_s = 1$. The specular term is based on micro-facet theory, which dictates that only the micro-facets on the surface with orientations in between the viewing vector and the incident vector, called half-vector, $\mathbf{h} = \mathbf{l}, \mathbf{v}$, will contribute to the reflected light.

The general form of the Cook-Torrance specular term is:

$$R_s = \frac{1}{\pi} \frac{FDG}{(\mathbf{n}, \mathbf{l})(\mathbf{n}, \mathbf{v})}, \quad (8)$$

where F is the Fresnel term [48], G is the geometrical attenuation factor accounting for shadowing and masking of micro-facets, D is the distribution of normals facing \mathbf{h} , and \mathbf{n} is the surface normal.

In this paper a simplified isotropic Cook-Torrance BRDF model is used:

$$I_p = \begin{bmatrix} I_{px} \\ I_{py} \\ I_{pz} \end{bmatrix} = I_a R_a + I_i \cos \theta_i \left(k_s R_s + (1 - k_s) \begin{bmatrix} R_{dx} \\ R_{dy} \\ R_{dz} \end{bmatrix} \right), \quad (9)$$

where I_p is the CIE tristimulus value at point P with incident angle θ_i and at fixed reflection angle $\theta_r = -22.5^\circ$. $I_a R_a$ is the ambient light term which is assumed to be zero as the experiment is performed in a dark environment. I_i is the incident light intensity, R_d are the spectral diffuse reflectance components. The specular components, R_s , are given by the Cook-Torrance GGX specular term (Eq. 15). (For more details on BRDF models refer to the Appendix.)

For each measurement, the CIE XYZ tristimulus values are calculated using the reflectance spectra, $S(\lambda)$, D65 illuminant, $I(\lambda)$, and CIE 1931 colour matching functions, $\bar{x}(\lambda)$, $\bar{y}(\lambda)$, and $\bar{z}(\lambda)$, according to:

$$\begin{bmatrix} X \\ Y \\ Z \end{bmatrix} = \frac{1}{N} \int_{\lambda} S(\lambda) I(\lambda) \begin{bmatrix} \bar{x}(\lambda) \\ \bar{y}(\lambda) \\ \bar{z}(\lambda) \end{bmatrix} d\lambda, \quad (10)$$

where

$$N = \int_{\lambda} I(\lambda) \bar{y}(\lambda) d\lambda. \quad (11)$$

The CIE XYZ colour space is chosen because the Y channel is representative of the M cone's spectral sensitivity for photopic vision; and thus, describes the luminance of the scene. The X channel contains a combination of the three CIE RGB curves, and the Z channel is related to the blue channel in RGB. Therefore, at a given Y value, the XY plane contains all chromaticities at that luminance. Moreover, the luminance is related to gloss as it can be defined as the sum of the distributions of the volume diffusion and the surface reflection caused by the microfacets [16].

These values are used to fit and optimise the parameters k_s , R_d , and α_g into the BRDF model. Using a genetic algorithm [49–51], the cube root cosine weighted root mean squared (RMS) formula is used as an objective function, defined as:

$$ost = \sqrt{\frac{\sum ((M(\theta_i, \theta_r) \cos \theta_i - E(\theta_i, \theta_r, p) \cos \theta_i)^2)^{1/3}}{n}}, \quad (12)$$

where M are the measured CIE XYZ values (Eq. 10) and E are the estimated BRDF values obtained using the Cook-Torrance GGX BRDF model (Eq. 9), with the parameters p , calculated for the n pairs of incident and reflected directions. The minimum and maximum values for the BRDF coefficients to be optimised and the initial parameters used in the genetic algorithm optimisation problem are presented in Tables 2 and 3, respectively. Each CIE XYZ channel is optimised individually, giving a set of three models per surface. The cube root cosine weighted RMS function is used because the cosine weight compensates for the reflectance increase towards grazing angles and the cube root compressive metric is used to avoid overemphasising the importance of BRDF peaks in the mirror angle [52].

Perceptual dimensions of gloss

Gloss is a function of a surface's directional reflectance. Hunter defines at least six visual phenomena related to apparent gloss [53]. In this paper, focus is given to contrast gloss and distinctness of image (DOI) gloss as they have been defined as perceptual dimensions of glossy appearance [54].

Contrast gloss is defined as the perceived relative brightness of specularly and diffusely reflecting areas, defined by Ferwerda et al. [54], and given by:

$$c = \sqrt[3]{k_s + \frac{R_d}{2}} - \sqrt[3]{\frac{R_d}{2}}, \quad (13)$$

where k_s is the specular weighted parameter and R_d is the diffuse component of the BRDF (Eq. 7). DOI gloss is defined as the perceived sharpness of images reflected in a surface and is given by:

$$d = 1 - \alpha, \quad (14)$$

where α is the width parameter for the specular lobe used to model the specular component, R_s (Eq. 15).

Table 2 Minimum and maximum values for the BRDF coefficients to be optimised

	α	k_s	R_d
Min	0.05	0.01	0
Max	0.99	0.5	5

Table 3 Initial parameters used for the optimisation problem

Max iterations	# population	Beta	pC	Gamma	Mu	Sigma
100	1000	1	1	0.01	0.05	0.01

Multivariate analysis

Multivariate analysis provides a statistical evaluation of various simultaneous observations. In this

subsection, multivariate methods used in this paper will be presented.

Principal component analysis

Principal component analysis (PCA) [55, 56] is a popular method of dimensionality reduction. PCA looks for a projection which transforms the data into a new coordinate space where most of the variation in the data can be described in fewer dimensions than the original data. Here, PCA is applied to the fitting parameters, α , k_s , and R_d , obtained to model the BRDF of the surfaces, and to the gloss attributes, c and d , using 5 principal components (PCs). The data is preprocessed by performing scaling and centring.

Mahalanobis distance metric

The Mahalanobis distance is a measure of distance between a point, P , and a distribution, D . When P is at the mean of D , the distance is zero, and increases as P moves away from the mean along each principal component axis [57]. The Mahalanobis distance is favoured since it is unitless, scale-invariant and takes into account the correlations of the dataset.

Results and discussion

In this section, conventional colour and gloss results, widely used in restoration-conservation studies, are presented. Then, appearance classification results obtained

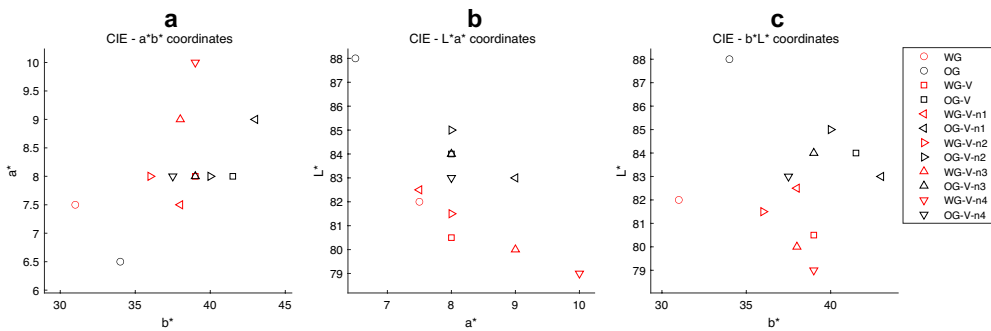


Fig. 7 Average L^* , a^* , b^* values for oil gilding (black) and water gilding (red), unvarnished (round marker), varnished (square marker), n1 (left pointing marker), n2 (right pointing marker), n3 (top pointing marker), and n4 (bottom pointing marker). **a** CIE a^*b^* coordinates. **b** CIE L^*a^* coordinates. **c** CIE L^*b^* coordinates

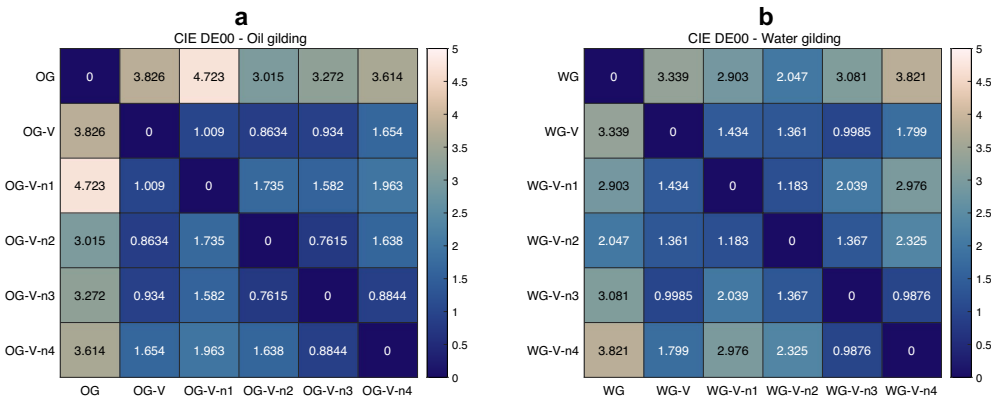


Fig. 8 CIE DE00 values calculated for **a** oil gilding and **b** water gilding. Values lower than 1 are below the JND

from bidirectional reflectance measurements are discussed as an alternative to the former.

Conventional colour and gloss measurements

Colour was measured following the method presented in *Conventional colour and gloss measurements* and the average CIE $L^*a^*b^*$ coordinates are calculated using CIE standard illuminant D65 and CIE 10° standard observer colour matching functions (Fig. 7). The colour difference between all the samples was calculated using CIE ΔE_{2000} (DE00) colour difference formula (Fig. 8), where values lower than 1 are below the just noticeable difference (JND).

Two clusters can be identified, water gilding samples have higher L^* values than oil gilding (Fig. 7). Varnishing is expected to saturate both types of gilding, L^* decreases and b^* increases, producing a perceptible colour change as the luminance decreases and the chroma shifts to higher values of b^* (Fig. 8).

Each varnish removal method changes the colour of the gilded surfaces differently. In the case of oil gilding, the colour difference between the four cleaned samples and OG-V is lower than the JND in the case of n2 and n3, suggesting an unperceivable colour difference, and just above the JND for n1 and n4 (Fig. 8). All varnish removal methods reduce the colour difference between the surface and the unvarnished reference, except for n1. For water gilding, the colour difference between the cleaned surfaces and the varnished surface is just above the JND for all methods except n3 (Fig. 8). Like oil gilding, removing the varnish reduces the colour difference between them and the reference, with exception of n4. In general, removing varnish from gilded surfaces has a more significant effect on water gilding than oil gilding.

Gloss was measured three times for each surface at 20° , 60° , and 85° and the results were averaged for each measurement angle (Fig. 9). For oil gilding, at 20° , the reference sample has the highest gloss. The varnished and cleaned surfaces have a similar gloss. At 60° , the varnished surface has lower gloss than the reference but, n2 has a slightly higher gloss than the reference. At 85° , the varnished surface has the highest gloss, n1 and the reference have similar values of gloss. The other three cleaning methods have lower gloss values than the reference.

In the case of water gilding, the relative differences in gloss are similar at the three measurement angles. In general, the unvarnished sample has the highest gloss. Varnishing decreases the gloss by almost two orders of magnitude in the case of 20° and 60° , and by a factor of 5 at 85° . Cleaning the varnish increases the gloss at all angles. Method n3 has the highest effect, at 20° and at 60° , n1, n2, and n4 are very similar. At 85° , n1 has gloss values closer to n3, then n2 and finally n4.

The glossmeter measurements show that varnishing decreases the gloss of the gilded samples, except for oil gilding at 85° . In the case of water gilding, the effect of varnishing decreases the gloss almost by a factor of 7 for all measurement angles. These results contradict empirical knowledge which states that varnishing increases the gloss of surfaces. It must be emphasised that gloss measurements are not easily correlated to human perception; and thus, when evaluating appearance changes caused by conservation methods, traditional gloss measurements must be interpreted with caution.

Conventional colour and gloss measurements are insufficient to fully understand appearance changes in gilded surfaces caused by varnishing. Colour measurements

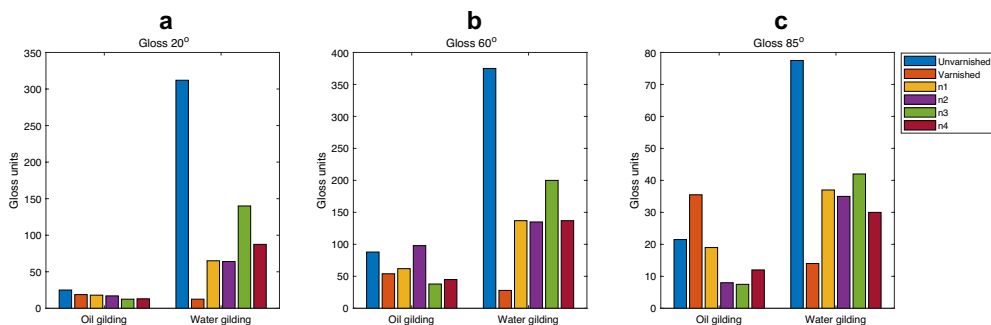


Fig. 9 Average gloss at **a** 20° , **b** 60° , and **c** 85° . Values for oil gilding (left) and water gilding (right), unvarnished (blue), varnished (orange), n1 (yellow), n2 (purple), n3 (green), and n4 (maroon)

provide a starting point in characterising the effects of varnishing and removing varnish. Yet, the colour differences calculated here are not correlated to perception. While some surfaces have colour differences of less than a JND, a clear difference in appearance is perceived by visual inspection. Gloss measurements are harder to interpret as gloss units are not easily correlated to perception. Moreover, the gloss measurements obtained above contradict empirical knowledge and experience. An evaluation of cleaning methods based on gloss measurements is not possible as the results oppose visual perception. Therefore, the appearance of gilded surfaces must be measured using alternative methods to have a better understanding of how it is affected by varnishing and the removal of varnish.

Bidirectional reflectance measurements

In this subsection, the results obtained with the bidirectional imaging system are presented. The samples were measured following the methodology proposed in *Flexible HDR multispectral-imaging BRDF system*, and the data was processed accordingly, to obtain CIE 1931 XYZ values as a function of the angle of incidence, θ_i , for the

fixed angle of reflection, $\theta_r = -22.5^\circ$. The data is modelled to the Cook-Torrance BRDF model and GGX distribution, using a genetic algorithm.

The BRDF parameters estimated for each surface at each CIE XYZ channel and the minimum error obtained are presented in Table 4. The mean and maximum error values achieved were 0.178 and 0.262 respectively. These values are within the acceptable quality range; thus, the models represent well the measured data.

The BRDF coefficients are used to model the BRDF of the surface at the fixed angle of viewing, $\theta_r = -22.5^\circ$, as a function of the angle of illumination, θ_i (Fig. 10). The left column shows the BRDF obtained for oil gilding, and the right column shows the BRDF obtained for water gilding.

For all the samples, the coefficients fitted for CIE Z are different from those fitted for CIE X and Y (Table 4). This implies that the goniochromatism in the CIE X and Y channels has a similar BRDF, but the BRDF in the CIE Z channel is different. The CIE Z channel is representative of the blue channel in the RGB space, which could explain this difference. The polar plots (Fig. 10) show similar specular lobes for CIE X and Y, but different for CIE Z, in the case of both types of gilding. In the

Table 4 BRDF model estimated coefficients and cosine cubic weighted RMS cost obtained using a genetic algorithm

	Oil gilding				Water gilding			
	α	k_s	R_d	cost	α	k_s	R_d	cost
Unvarnished								
CIE X	0.651	0.074	4.915	0.262	0.897	0.062	0.923	0.245
CIE Y	0.650	0.077	5.000	0.260	0.852	0.067	0.753	0.240
CIE Z	0.808	0.122	1.234	0.175	0.490	0.052	0.124	0.250
Varnished								
CIE X	0.343	0.060	2.218	0.193	0.462	0.052	1.751	0.175
CIE Y	0.371	0.066	2.130	0.190	0.480	0.057	1.584	0.173
CIE Z	0.222	0.054	0.471	0.183	0.192	0.037	0.430	0.166
n1								
CIE X	0.729	0.110	4.815	0.185	0.659	0.083	4.785	0.226
CIE Y	0.768	0.116	5.000	0.180	0.688	0.089	4.923	0.219
CIE Z	0.518	0.152	0.268	0.147	0.489	0.110	0.534	0.169
n2								
CIE X	0.724	0.128	4.382	0.158	0.728	0.082	4.755	0.192
CIE Y	0.770	0.134	4.831	0.155	0.759	0.088	4.916	0.190
CIE Z	0.497	0.161	0.427	0.142	0.451	0.091	0.560	0.148
n3								
CIE X	0.865	0.177	4.131	0.129	0.781	0.094	4.261	0.155
CIE Y	0.873	0.181	4.019	0.128	0.817	0.099	4.400	0.150
CIE Z	0.542	0.215	0.134	0.124	0.250	0.082	0.598	0.152
n4								
CIE X	0.764	0.112	4.889	0.170	0.826	0.075	4.380	0.200
CIE Y	0.776	0.115	4.838	0.170	0.859	0.082	4.312	0.183
CIE Z	0.472	0.134	0.383	0.147	0.243	0.058	0.516	0.198

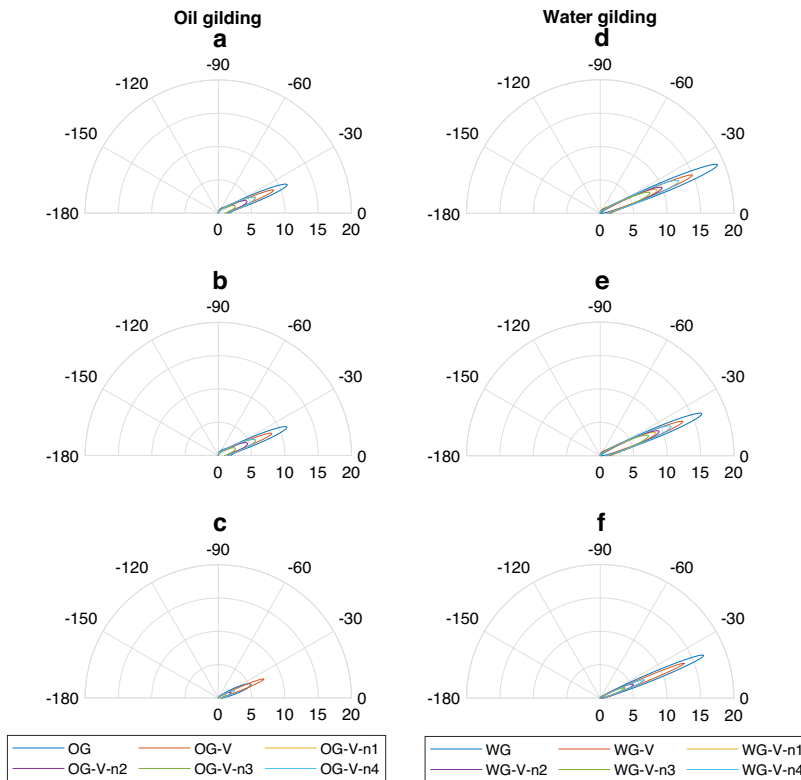


Fig. 10 Polar plot of modelled CIE XYZ values of each surface as a function of illumination angle, at fixed angle of viewing, $\theta_v = -22.5^\circ$. Oil gilding **a**: CIE X, **b**: CIE Y, **c**: CIE Z. Water gilding **d**: CIE X, **e**: CIE Y, **f**: CIE Z

case of oil gilding, the varnished sample has the highest magnitude in the Z coordinate.

The specular lobe of the three CIE XYZ coordinates for the oil gilding samples is smaller than that of the water gilding samples, suggesting water gilding is glossier than oil gilding. This is also suggested by the values of k_s , which in general are lower for water gilding than oil gilding (Table 4).

The BRDF coefficients are used to render the Adobe RGB visualisation of the surfaces at angle of viewing $\theta_v = -22.5^\circ$, and angles of illumination ranging from -57° to 12° . (Fig. 11). The left column displays the visualisations of the oil gilding samples, and the column on the right shows the water gilding samples. The order from top to bottom is reference, varnished, n1, n2, n3, and n4.

The appearance of the Adobe RGB rendered images of the modelled BRDF is representative of the visual

appearance of the varnished gilded surfaces (Fig. 11), these visualisations provide supplementary visual information which discriminates an oil-based gilded surface, from a water-based gilded surface, and indicates the presence (or not) of a varnish layer on the gold leaf. Moreover, in the context of varnish removal, the images allow to visualise the impact of the different treatments on a gilded surface, and to classify the types of gilding and to discriminate their characteristics. The visualisations allow to discriminate the various levels of gloss of the different surfaces and are similar to the gilded surfaces of the mock-ups. These nuances give a visual scale, which allows, in this case, to control the varnish removal and define the limits of acceptability.

Perceptual gloss attributes

The BRDF coefficients obtained for the CIE Y channel, representative of luminance, are used to calculate

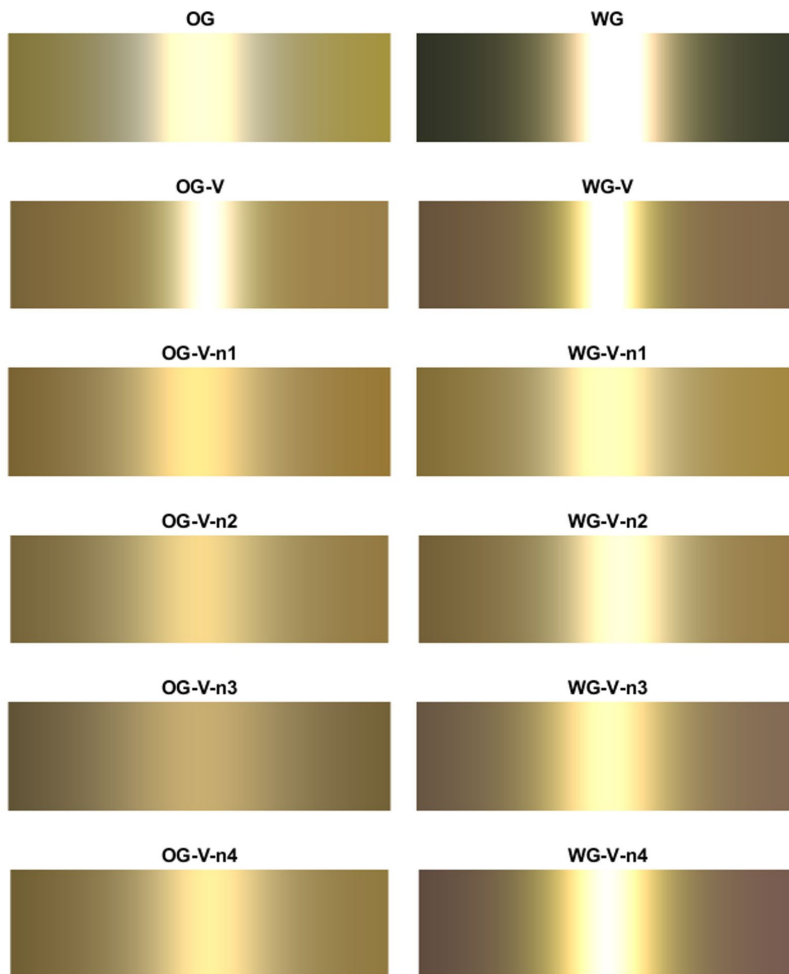


Fig. 11 Adobe RGB rendered images of the modelled BRDF of each surface at fixed viewing angle, $\theta_v = -22.5^\circ$. Each 10 pixels on the horizontal axis represent a step of one degree in angle of incidence

contrast gloss, c , and DOI gloss, d , values according to Eq. 13 and Eq. 14 respectively. (Fig. 12). The CIE Y channel is chosen since the luminance is correlated to the gloss BRDF [16].

Varnishing increases the contrast gloss, c , for both gilding techniques. The four varnish removal methods decrease c compared to the varnished area. In the case of oil gilding, n1 and n4 have the weakest effect on c , and n2 decreases the value of c the most. For water gilding, the

varnish removal methods have a value of c from higher to lower in the order n1, n2, n3, and n4.

Unvarnished water gilding has a value of DOI gloss, d , 8 times higher than unvarnished oil gilding. The DOI gloss, d , is also affected by varnishing. The two varnished samples, oil and water gilding, have the same value of d . In the case of oil gilding, d increases by a factor of 4. While for water gilding, varnishing decreases the value of d by half. Varnish removal methods n1, n2, and n4 decrease

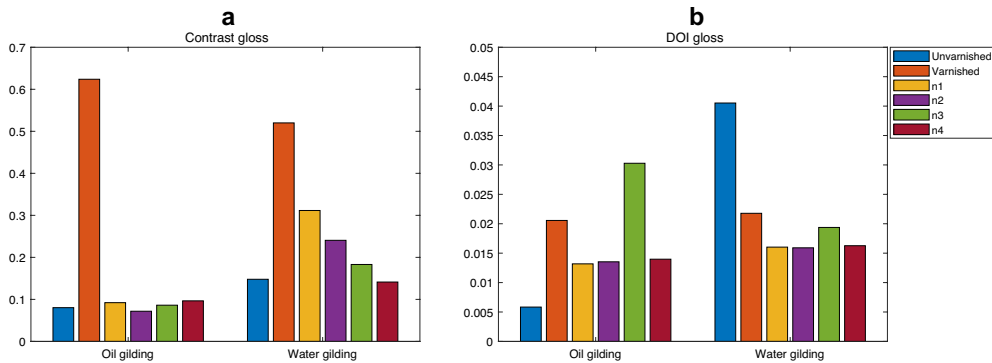


Fig. 12 **a** Contrast and **b**DOI gloss values obtained from BRDF coefficients modelled for oil gilding (left) and water gilding (right) for unvarnished (blue), varnished (orange), n1 (yellow), n2 (purple), n3 (green), and n4 (maroon)

the value of d by the same amount for both types of gilding. In the case of oil gilding, n3 increases the value of d .

These results are consistent with visual perception and empirical knowledge, and can be explained by the translucent nature of varnish. Varnishing the surface implies adding an interface in the stratigraphy of the gilding. Gold has a very high extinction index ($0.37 + 2.82i$ at 600 nm [58]), making it very opaque and reflecting. Varnish, on the other hand, is a refractive medium. In the case of unvarnished oil gilding, both contrast gloss and DOI gloss are lower than that of water gilding. This is expected since both surfaces have very different roughness; being smoother water gilding is glossier. However, once varnished, both oil and water gilded surfaces are very similar in appearance. The varnish has a saturating effect which is reflected in an increase in contrast gloss for both types of gilding. It also increases the DOI gloss of oil gilded surfaces; however, it has the opposite effect on water gilding. The varnish smooths the surface roughness of oil gilding, increasing its DOI gloss. In the case of water gilding, varnishing decreases the DOI gloss because the varnish acts as an interface where refraction and scattering decrease the perceived sharpness of the reflected image. The effect of refraction and scattering of varnish on oil gilding is lower than the effect of its surface roughness. However, for water gilding, the opposite is true since its original surface is smoother.

The contrast and DOI gloss values, unlike traditional gloss measurements, are consistent with the visual perception of the gilded surfaces as well as empirical knowledge and experience of conservators. These results

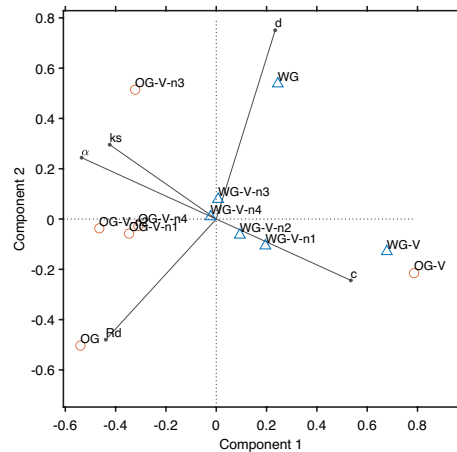


Fig. 13 Biplot of the PCA for the first two PCs, calculated using the coefficients obtained for the BRDF model in the CIE Y coordinates (α , k_s , and R_d) and gloss attributes (c and d). Oil gilding samples are displayed in orange (round markers), and water gilding samples are displayed in blue (triangle markers). PC1 and PC2 are representative of c and d respectively. Surfaces are clustered depending on their varnish level (reference or no varnish, varnished, and cleaned)

suggest that varnishing gilded surfaces increases both contrast and DOI gloss in the case of oil gilding, and only contrast gloss in the case of water gilding; which is expressed as a general increase in gloss by conservators.

Clustering based on perceptual gloss attributes

The BRDF coefficients obtained for all the samples at the CIE Y channel, as well as the corresponding c and d values for the same channel are used to perform a principal component analysis (PCA) with 5 principal components (PCs), with scaling and centring of the data. The first three PCs give a cumulative explained variance of 96%.

The first two PCs can be interpreted as perceptual axes. PC1 is strongly correlated to contrast gloss, c , which by definition is inversely proportional to α . PC2 is strongly correlated to the difference between distinctiveness of image gloss, d , and R_d (Fig 13).

Based on the PCA, clear clusters are formed. Firstly, the reference surfaces are at opposite ends of the PC space. OG lies in the negative quadrant of both PC1 and PC2, whereas WG lies in the positive quadrant for both PCs. This implies that both surfaces are the most different in terms of their appearance. WG has a high DOI gloss and relatively high contrast gloss, OG has a low DOI gloss and lower contrast gloss. This confirms common knowledge that oil and water gilding have very different appearance, since water gilding is burnished, it has a glossy effect, unlike oil gilding.

The varnished samples are also clustered in one group. They have a positive PC1 value and negative PC2 value. Varnishing the samples increases the contrast for both types of gilding. However, the DOI gloss of water gilding decreases whilst for oil gilding it increases. These changes produce a similar appearance for both types of gilding when varnished, which is consistent with empirical knowledge and experience.

Finally, the cleaned surfaces are clustered in two groups, dependent on their gilding type. Oil gilding samples are on the negative scale of PC1 and near 0 for PC2. Water gilding on the other hand, are closer to the origin, in the positive scale of PC1. This implies that oil gilding samples in general have lower contrast and DOI gloss than water gilding samples. OG-V-n3 does not belong to any cluster, as it lies on the negative scale of PC1 but positive scale of PC2.

While the different varnish removal methods (except for OG-V-n3) give each type of gilding a similar appearance, none of them restore the original appearance of the gilding before varnishing, nor maintain the appearance of the originally varnished surface.

The Mahalanobis distance [57] is calculated between each surface to evaluate the varnish removal methods, using the first three PCs which have a cumulative explained variance of 96%. (Fig. 14). The varnish layer is considered a part of the stratigraphy of the artwork, thus, the most desirable method is the one which produces an appearance closest to that of the varnished sample. The varnish removal methods are ranked from closest to furthest in appearance compared to the varnished layer. For oil gilding, the method which gives the closest appearance is n2, followed by n1, n4, and finally n3. For water gilding the order is n2, n3, n4, and finally n1.

Varnish removal method n2, which produces the closest appearance to that of the original varnished surface, involves the application of the solvent by applying a compress. This method does not involve any mechanical action on the surface and does not leave residues on the

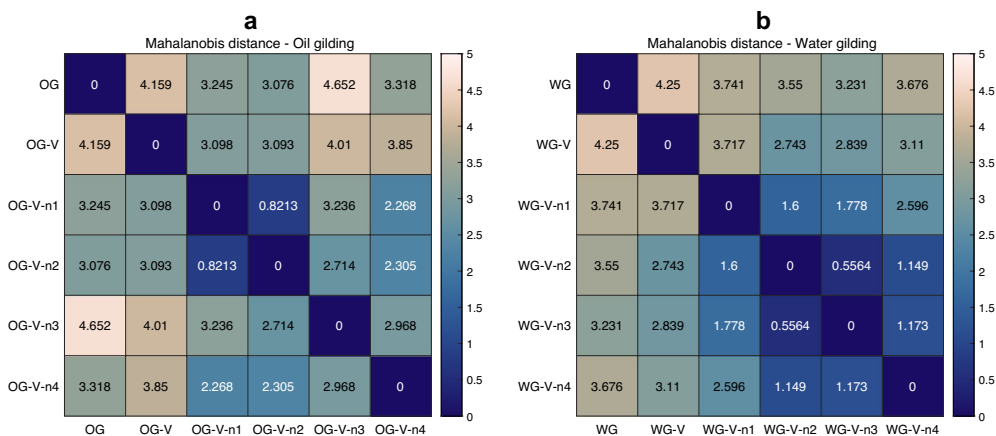


Fig. 14 Mahalanobis distance calculated between each surface in the PC space (Fig. 13) using the first three PCs for **a** oil gilding and **b** water gilding

surface, which could be the main reasons why it gives the best results. Method n1 requires mechanical action with a cotton swab to remove the varnish which can result in abrasion of the gold leaf. Methods n3 and n4 differ in the nature of the gel used, but both methods require the solvent to be rinsed with a cotton swab which is abrasive in nature. Moreover, method n3 is a water-based gel, which due to its water content can alter water sensitive surfaces, such as oil gilding. This could explain why in the case of oil gilding, n3 causes the strongest appearance change, while in the case of water gilding it gives a satisfying result.

Visual examination by a professional conservator

A professional conservator specialised in gilded surfaces was consulted to provide a visual examination of the mock-ups and the effect the different conservation procedures have. They stated that the varnished oil gilding sample had a glossier appearance than the reference oil gilding, and an appearance closer to that of varnished water gilding which is consistent with the results presented above.

Regarding the varnish removal methods, in the case of oil gilding, method n1 produced a strong cleaning. However, there were residues of varnish on the surface distributed in a non-homogeneous way. Method n2 produced a homogeneous cleaning, leaving a thin film of varnish on the surface. Method n3 gave a very aggressive stripping of the varnish, even to the point of damaging the gold foil. This could be the reason why n3 is not clustered with the other cleaned oil gilded samples (Fig. 13). Finally, n4 produced an aggressive and non-homogeneous removal leaving some varnished as well as unvarnished areas on the sample.

For the water gilding samples, method n1 produced a non-homogeneous, slightly aggressive clearance of the varnish, most likely due to the mechanical action of the cotton bud required to remove the varnish. Method n2 gives out a homogeneous clearing of the varnish. Method n3 also generated a homogeneous clearing of the varnish with a fine layer of varnish residue. In the case of method n4, the varnish was cleaned but not completely cleared. These comments confirm the results obtained by the cluster analysis (Fig. 14). The conservator concluded that for them, the best method to remove varnish from an oil gilded surface was method n2, while for a varnished, water gilded surface methods n2 and n3 were the most appropriate.

The results obtained by measuring the BRDF of the surfaces provide additional visual information on the appearance of the metal surface (Fig. 11), as well as a quantified approach to discriminate the gloss of water gilding and oil gilding, and indicates the presence or not of surface coatings on the gilding. In addition, this analysis in the context of varnish removal, makes it possible to characterise the presence of a layer of varnish on the gold leaf, not visible to the naked eye. Therefore, the varnish removal approach can be influenced by these results and controlled quantitatively. For example, in the case of oil gilding, method n3, has damaged the gold leaf due to the aqueous nature of the gel. This can be visualised in the render of the BRDF of the surface as OG-V-n3 has a distinct visual appearance, very different from both the unvarnished and varnished visualisations.

Conservation of the *Vierge de douleur/Virgin of sorrows*

As part of the conservation work carried out at the National Heritage Institute, the *Vierge de douleur/Virgin*

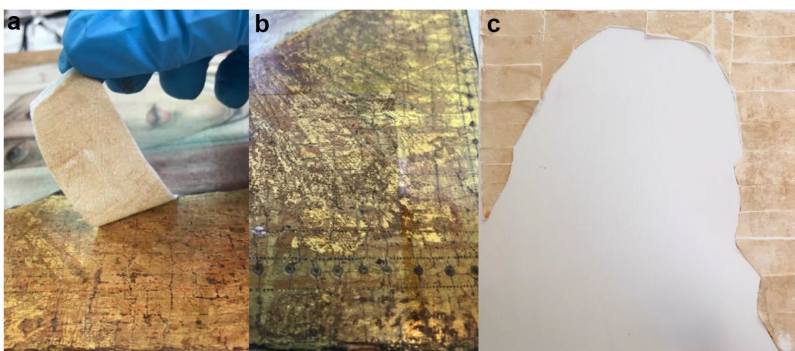


Fig. 15 Conservation of the *Vierge de douleur/Virgin of sorrows*. **a** Removal of varnish using Evolon CR compress soaked with solvent. **b** Detail of an area of the painting after removing the varnish. **c** Entire counterform of the gilding, in Evolon CR, after the varnish removal process

of sorrows underwent a restoration campaign. Kept in storage since its acquisition by the Jacquemart-André Museum, it was until now unknown to the public. Its study and conservation enable to re-appreciate this work, rich in values.

The conservation work consisted of a structural securing of the panel and the frame, and seeks to harmonise the appearance of the whole, mainly through a cleaning work. Targeted research on the cleaning of varnished gilding has been carried out, in order to guide the restoration treatments. Following the results presented above, as well as complementary analyses, the painting was cleaned by solubilisation by applying a compress, with particular attention against the use of cotton for this operation. (Fig. 15). Moreover, removing the varnish by applying a compress, not only produces the smallest change in gloss and causes no abrasion, but also is the most reproducible and homogeneous method, maintaining a very thin layer of varnish which is beneficial for the protection of the gilding from external degradation factors.

Conclusions and future work

This paper presents a framework for characterisation, classification, and evaluation of oil gilded and water gilded surfaces as well as the effect on appearance of varnish, and varnish removal methods.

It is shown that conventional colorimetric and gloss measurement and analysis are insufficient to properly characterise the appearance of gilded surfaces, and evaluate the appearance changes induced by different restoration processes such as varnishing and varnish removal methods.

To overcome this issue, an imaging system is used to measure the bidirectional reflectance of mock-ups of unvarnished oil gilding and water gilding, varnished mock-ups, and mock-ups cleaned with four different chemical varnish removal methods. By performing a PCA on the BRDF model coefficients as well as perceptual gloss attributes, clear groups can be identified. The evaluation of cleaning methods based on the PCA clusters are consistent with visual inspection by a professional conservator.

In particular, the results show that the varnishing effect is irreversible on the appearance of gilding. As expected, water gilding has the highest DOI gloss, and oil gilding has the lowest DOI gloss. It is found that varnishing modifies the appearance of both types of gilding, making their appearance more similar to each other. Furthermore, either for water or oil gilding, none of the varnish removal methods restore the gilding to its original appearance due to the fragility of the gold foil.

For future studies, this methodology could be applied on investigating the effects of ageing on the appearance of gilded surfaces and the effects of varnish removal methods on aged, gilded surfaces. It must be clarified that the method presented here focuses only on appearance changes induced by varnishing gilded wood, as well as effects due to varnish removal methods. A broader evaluation on cleaning methods must also consider other factors such as the uniformity of the cleaning, remnants of varnish on the surface, lacunas, stripping of the gold foil, absorption of the solvents by the surface, etc.

The methodology presented in this paper allows to not only characterise and cluster different gilded surfaces accurately, but does so in a coordinate space which is correlated to human perception, by using perceptual gloss attributes. Gloss attributes are necessary to explain the changes in appearance, whether due to different gilding techniques, varnishing, or different cleaning methods, and these are accurately represented in the component space. Moreover, this methodology can evaluate cleaning methods with results consistent to those of visual examination by experts.

Finally, a 15th-century panel painting and its 19th-century neo-gothic frame were restored, involving a cleaning campaign guided by the results obtained by this framework. Solubilisation by applying an Evolon CR compress has proven to be an effective method which creates the minimum change in appearance, as well as being homogeneous, maintaining a thin layer of varnish which protects the gilding from external degradation factors.

Appendix

Technological study of the artwork

To guide the conservation of the painted panel a technological study was conducted to identify its materials and fabrication methods [59]. Macro XRF showed that only pure gold leaf was used in the gilding. The contracts from this time period suggest the use of a 23 karat gold leaf [60]. Water gilding would be the most appropriate technique for this type of work. However, the stratigraphic cross-section reveals the presence of an extremely thin orange layer under the gold leaf, composed of ochre. Due to the lack of lead pigments almost systematically used as driers in the mordant [60], oil gilding is dismissed as a possible fabrication technique. A third technique, less known and less documented, could have been used. It is a water-based gilding that does not use a bole, but only a charged preparation. This is bound with fish glue and egg white or honey, and coloured with cinnabar and saffron. The gold leaf is placed directly on this preparation, or dry by reapplying water [4]. It is

difficult to know whether the gold leaf was burnished or not: the absence of a bole as well as the great finesse of the gold leaf would make this process difficult [60]. Moreover, binocular microscopic observation revealed the presence of a translucent orange film over the gold, most likely a glaze applied uniformly over the gold leaf to create a “vermillionage” [4].

Gas chromatography coupled with mass spectrometry analysis of the varnish on the painted panel reveals the presence of colophony pine resin, oil, and dammar resin. While it is hypothesised that the colophony and oil found on the painting belong to the original varnish, the dammar resin must be a product of previous conservation campaigns since it was first used in Europe in 1829 [61].

Bidirectional reflectance modelling

GGX distribution Walter et al. [62] propose a Bidirectional Scattering Distribution Function (BSDF) called GGX. This GGX BRDF is inspired by the micro-facet model proposed by Cook and Torrance. The general form of the GGX is given by:

$$R_s = \frac{1}{4} \frac{FDG}{(\mathbf{n}\cdot\mathbf{l})(\mathbf{n}\cdot\mathbf{v})}, \quad (15)$$

The GGX normal distribution function of micro-facets is given by:

$$D = \frac{\alpha_g^2 \chi^+(\mathbf{h}\cdot\mathbf{n})}{\pi \cos^4 \theta_h (\alpha_g^2 + \tan^2 \alpha_h)}, \quad (16)$$

where α_g is a width parameter for the specular lobe, θ_h is the angle between the half-vector, \mathbf{h} , and the surface normal, \mathbf{n} , and χ^+ is a positive characteristic function which equals to one if its parameter is greater than zero and zero if its parameter is lesser or equal to zero.

The geometrical attenuation factor which describes the shadowing and masking effects is derived from the GGX distribution, D (Eq. 16). This is given by the monodirectional shadowing term defined as:

$$G_1(\mathbf{v}) = \chi^+ \left(\frac{\mathbf{v}\cdot\mathbf{h}}{\mathbf{v}\cdot\mathbf{n}} \right) \frac{2}{1 + \sqrt{1 + \alpha_g^2 \tan^2 \theta_v}}, \quad (17)$$

where θ_v is the angle between the viewing vector, \mathbf{v} , and the surface normal, \mathbf{n} .

Abbreviations

BRDF	Bidirectional reflectance distribution function
HDR	High-dynamic range
VIS/NIR	Visible/Near-infrared
LDR	Low-dynamic range

SCE	Specular component excluded
RMS	Root mean squared
DOI	Distinctiveness of image
PCA	Principal component analysis
PC	Principal component
DE00	ΔE 2000
JND	Just noticeable difference

Acknowledgements

The authors would like to thank Pierre Curie from the Jacquemart-André Museum who granted confidence and trust in this project, Agnès Lattuat-Derieux for her supervision in the chemical analysis, Vlado Kitanovski for his invaluable help with the data acquisition, and Doctor Malgorzata Sawicki for her revision and suggestions.

Author contributions

DM prepared the gilding mock-ups, DM and YA designed the experiments, DM and YA conducted the experiments, YA computed the results, all authors interpreted the results, YA wrote the manuscript. All authors read and approved the final manuscript.

Funding

This work has received funding from the European Union's Horizon 2020 research and innovation program under the Marie Skłodowska-Curie grant agreement No. 813789 as part of the CHANGE (Cultural Heritage Analysis for New Generations) ITN project.

Availability of data and materials

The data used and/or analysed during the current study are available from the corresponding author on reasonable request.

Declarations

Competing interests

The authors declare that they have no competing interests.

Received: 5 August 2022 Accepted: 17 January 2023

Published online: 14 February 2023

References

- Mastrotheodoros GP, Beltsios KG, Bassiakos Y, Papadopoulou V. On the metal-leaf decorations of post-byzantine greek icons. *Archaeometry*. 2018;60(2):269–89. <https://doi.org/10.1111/arc.12287>.
- Sandu I, Murta E, Ferreira S, Pereira M, Kuckova S, Valbi V, Dias L, Prazeres C, Cardoso A, Mirão J. A comparative multi-technique investigation on material identification of gilding layers and the conservation state of 7 portuguese mannerist altarpieces. *Int J Conserv Sci*. 2015;6:439–54.
- Sandu IA, Busani T, de Sá MH. The surface behavior of gilding layer imitations on polychrome artefacts of cultural heritage. *Surf Interface Anal*. 2011;43(8):1171–81.
- Neven S. The Strasbourg Manuscript: A Mediaeval Tradition of Artists' Recipe Collections (1400–1570). London: Archetype Publication; 2016.
- Kollandsrud K, Plahter U. Twelfth and early thirteenth century polychromy at the northernmost edge of europe: past analyses and future research. *Medievalista*. 2019. <https://doi.org/10.4000/medievalista.2303>.
- Chaban A, Lanterna G, Gigli MC, Becucci M, Fontana R, Striova J. Multi-analytical approach to the study of mecca gilding technique. *Microchem J*. 2021;168: 106415.
- Todd JT, Norman JF. The visual perception of metal. *J Vision*. 2018;18(3):9. <https://doi.org/10.1167/18.3.9>.
- Vernardakis TG. *Pigment Handbook, Vol. I, Properties and Economics*. 2nd ed. New York: Wiley; 1988.
- Saris H, Gottenbos R, Van Houwelingen H. Correlation between visual and instrumental colour differences of metallic paint films. *Color Res Appl*. 1990;15(4):200–5.

10. Billmeyer FW, Davidson JG. Color and appearance of metallized paint films. I. Characterization. *J Paint Technol.* 1974;46(593):31–7.
11. Baba, G., Arai, H.: Gonio-spectrophotometry of metal-flake and pearl-mica pigmented paint surfaces. In: 4th Oxford Conference on Spectroscopy (2003), vol. 4826, pp. 79–86. SPIE
12. Wills J, Agarwal S, Kriegman D, Belongie S. Toward a perceptual space for gloss. *ACM Trans Graph (TOG).* 2009;28(4):1–15.
13. Obein G, Knoblauch K, Viéot F. Difference scaling of gloss: Nonlinearity, binocularity, and constancy. *J vision.* 2004;4(9):4.
14. Rhopoint Instruments: Appearance Measurement (2022). <https://www.rhopointinstruments.com/faqs/appearance-measurement/> Accessed 18 July 2022
15. Wu Q, Hauldenschild M, Rösner B, Lombardo T, Schmidt-Ott K, Watts B, Nolting F, Ganz D. Does substrate colour affect the visual appearance of gilded medieval sculptures? Part I: colorimetry and interferometric microscopy of gilded models. *Herit Sci.* 2020;8:118. <https://doi.org/10.1186/s40494-020-00463-3>.
16. Obein, G., Leroux, T., Vienot, F. 2001. Bidirectional reflectance distribution factor and gloss scales. In: *Human Vision and Electronic Imaging VI.* 2001. vol. 4299, pp. 279–290. SPIE. <https://doi.org/10.1117/12.429491>
17. Courrier S, Dubost M. Lor et la manière : les techniques de la dorure sur bois à travers le temps. In: Mailho L, de Reyder D, Catillon R, Leroux L, Bruhiere N, Bourges A, Cabilliac I, editors. *Coré - Conservation Restauration du Patrimoine Culturel.* 1st ed. France: SFIC; 2021. p. 10–29.
18. Learner, T.J., Smithen, P., Krueger, J.W., Schilling, M.R.: *Modern Paints Uncovered: Proceedings from the Modern Paints Uncovered Symposium.* The Getty Conservation Institute, Los Angeles. 2007. http://hdl.handle.net/10020/gci_pubs/paints_uncovered
19. Wolbers RC, Stavroudis C, Cushman M. Aqueous methods for the cleaning of paintings. In: Stoner JH, Rushfield R, editors. *Conservation of Easel Paintings.* 2nd ed. London: Routledge; 2020. p. 526–48.
20. Mecklenburg, M.F., Charola, A.E., Koestler, R.J.: *New Insights Into the Cleaning of Paintings: Proceedings from the Cleaning 2010 International Conference, Universidad Politécnica de Valencia and Museum Conservation Institute.* Smithsonian Institution Scholarly Press, Washington DC. 2013. <https://doi.org/10.5479/si.19492359.3.1>
21. Sawicki M, Bramwell-Davis V, Dabrowa B. Laser cleaning from a practical perspective: Cleaning tests of varied gilded-wood surfaces using Nd:YAG Compact Phoenix laser system. *AICCM Bull.* 2011;32(1):44–53.
22. Boonrat P, Dickinson M, Cooper M. Initial investigation into the effect of varying parameters in using an Er:YAG laser for the removal of brass-based overpaint from an oil-gilded frame. *J Inst Conserv.* 2020;43(1):94–106.
23. Sawicki M, Rouse E, Bianco SL, Kautto S. An investigation of the feasibility of the use of gels and emulsions in cleaning of gilded wooden surfaces. Part A: removal of brass-based overpainting. In: Nevin A, Sawicki M, editors. *Heritage Wood.* 1st ed. Cham: Springer; 2019. p. 1–36.
24. Sawicki M, Rouse E, Bianco SL, Kautto S. An investigation of the feasibility of the use of gels and emulsions in cleaning of gilded wooden surfaces. part b: cleaning of soiled oil-gilding. In: Nevin A, Sawicki M, editors. *Heritage Wood.* 1st ed. Cham: Springer; 2019. p. 37–64.
25. Albano M, Grassi S, Fiocco G, Invernizzi C, Rovetta T, Licchelli M, Marotti R, Merlo C, Comelli D, Malagodi M. A Preliminary Spectroscopic approach to evaluate the effectiveness of water-and silicone-based cleaning methods on historical varnished brass. *Appl Sci.* 2020;10(11):3982. <https://doi.org/10.3390/app10113982>.
26. Auffret, S., Nikolaus, S.B.: *Cleaning of Wooden Gilded Surfaces: An Experts Meeting Organized by the Getty Conservation Institute, March 12-14, 2018.* The Getty Conservation Institute, Los Angeles. 2019. http://hdl.handle.net/10020/gci_pubs/gilded_surfaces
27. Stulik D, Miller D, Khanjian H, Carlson J, Khandekar N, Wolbers R, Petersen WC. Solvent Gels for the Cleaning of Works of Art: the Residue Question. Los Angeles: The Getty Conservation Institute; 2004.
28. Darque-Ceretti E, Felder E, Aucouturier M. Foil and leaf gilding on cultural artifacts: forming and adhesion. *Matéria (Rio de Janeiro).* 2011;16:540–59. <https://doi.org/10.1590/S1517-70762011000100002>.
29. Toque, J.A., Komori, M., Murayama, Y., Ide-Ekessabi, A.: *Analytical Imaging of Traditional Japanese Paintings Using Multispectral Images.* In: Ranchordas, A. (ed.) *VISIGRAPP: International Joint Conference on Computer Vision, Imaging and Computer Graphics Theory and Applications.* 2010. pp. 119–132
30. MacDonald LW, Vitorino T, Picollo M, Pillay R, Obarzanowski M, Sobczyk J, Nascimento S, Linhares J. Assessment of multispectral and hyperspectral imaging systems for digitisation of a Russian icon. *Herit Sci.* 2017;5:41. <https://doi.org/10.1186/s40494-017-0154-1>.
31. Martinez MA, Valero EM, Nieves JL, Blanc R, Manzano E, Vilchez JL. Multifocus HDR VIS/NIR hyperspectral imaging and its application to works of art. *Optics Express.* 2019;27(8):11323–38. <https://doi.org/10.1364/OE.27.011323>.
32. Dumazet, S., Genty, A., Zymla, A., De Contencin, F., Texier, A., Ruscassier, N., Bonnet, B., Callet, P.: Influence of the substrate colour on the visual appearance of gilded sculptures. In: Georgopoulos, A. (ed.) *XXI International CIPA Symposium.* 2007. pp. 01–06
33. Mounier A, Daniel F. The role of the under-layer in the coloured perception of gildings in medieval mural paintings. *Open J Archaeom.* 2013;1(1):16. <https://doi.org/10.4081/arc.2013.e16>.
34. Sidorov, O., Hardeberg, J.Y., George, S., Harvey, J.S., Smithson, H.E.: Changes in the Visual Appearance of Polychrome Wood Caused by (Accelerated) Aging. In: Hebert, M. (ed.) *Proceedings of the IS & T International Symposium on Electronic Imaging: Material Appearance.* 2021. vol. 32, pp. 1–8. Society for Imaging Science and Technology. <https://doi.org/10.2352/ISSN.2470-1173.2020.5.MAAP-060>
35. Arteaga, Y., Sole, A., Hardeberg, J.Y., Boust, C.: Characterising appearance of gold foils and gilding in conservation and restoration. In: Sole, A., Guarnera, D. (eds.) *Proceedings of the 11th Colour and Visual Computing Symposium, Gjøvik.* 2022
36. Feller, R.L.: The relative solvent power needed to remove various aged solvent-type coatings. In: *Congress of the International Institute for the Conservation of Historic and Artistic Works, Lisbon.* 1972
37. Baij L, Astefanei A, Hermans J, Brinkhuis F, Groenewegen H, Chassouant L, Johansson S, Corthals G, Tokarski C, Iedema P. Solvent-mediated extraction of fatty acids in bilayer oil paint models: a comparative analysis of solvent application methods. *HeritSci.* 2019;7:31.
38. Baij L, Liu C, Buijs J, Alvarez Martin A, Westert D, Raven L, Geels N, Noble P, Sprakel J, Keune K. Understanding and optimizing Evolon CR for varnish removal from oil paintings. *Herit Sci.* 2021;9:155.
39. Tauber G, Smelt S, Noble P, Kirsch K, Siejek A, Keune K, van Keulen H, Smulders-De Jong S, Erdman R. Evolon CR: Its use from a scientific and practical conservation perspective. *AIC Paintings Specialty Group Postprints.* 2018;31:45–50.
40. Arteaga, Y., Hardeberg, J.Y., Boust, C.: HDR multispectral imaging-based BRDF measurement using flexible robot arm system. In: *Proceedings of the 30th Color and Imaging Conference, Scottsdale.* Society for Imaging Science and Technology. 2022.
41. x-Rite: *ColorChecker white balance* (2022). <https://www.xrite.com/en/categories/calibration-profiling/colorchecker-white-balance> Accessed 18 Oct 2022
42. Image Science Associates: *ColorGauge Nano Target* (2022). <https://www.imagescienceassociates.com/colorgauge-nano-target.html>. Accessed 18 Oct 2022
43. Eschbach, R., Brauers, J., Marcu, G.G., Schulte, N., Bell, A.A., Tominaga, S., Aach, T. Multispectral high dynamic range imaging. In: *Color Imaging XIII: Processing, Hardcopy, and Applications.* SPIE, 2008. pp. 26–37. <https://doi.org/10.1117/12.761105>
44. Nicodemus, F.E., Richmond, J.C.: *Geometrical considerations and nomenclature for reflectance.* National Bureau of Standards. 1977
45. Cook RL, Torrance KE. A reflectance model for computer graphics. *ACM Transactions Graph.* 1982;1(1):7–24.
46. Sole A, Farup I, Nussbaum P, Tominaga S. Bidirectional reflectance measurement and reflection model fitting of complex materials using an image-based measurement setup. *J Imaging.* 2018;4(11):136. <https://doi.org/10.3390/jimaging4110136>.
47. Sole A, Guarnera GC, Farup I, Nussbaum P. Measurement and rendering of complex non-diffuse and goniochromatic packaging materials. *Visual Comput.* 2021;37(8):2207–20.
48. Torrance KE, Sparrow EM. Theory for off-specular reflection from roughened surfaces. *J Opt Soc Am.* 1967;57(9):1105–12.
49. Bremermann HJ. *The Evolution of Intelligence: The Nervous System as a Model of Its Environment.* Department of Mathematics. Seattle: University of Washington; 1958.

50. Fraser AS. Simulation of genetic systems by automatic digital computers II Effects of linkage on rates of advance under selection. *Aust J Biol Sci.* 1957;10(4):492–500.
51. Holland JH. *Adaptation in Natural and Artificial Systems: an Introductory Analysis with Applications to Biology, Control, and Artificial Intelligence.* Massachusetts: MIT press; 1992.
52. Fores, A., Ferwerda, J., Gu, J. Toward a perceptually based metric for BRDF modeling. In: 20th Color and Imaging Conference, vol. 2012, pp. 142–148. Society for Imaging Science and Technology
53. Hunter RS. Gloss investigations using reflected images of a target pattern. *J Opt Soc Am.* 1936;26(4):190–6.
54. Ferwerda, J.A., Pellacini, F., Greenberg, D.P. Psychophysically based model of surface gloss perception. In: *Human Vision and Electronic Imaging VI*, (8 June 2001). 4299: 291–301. SPIE. doi: <https://doi.org/10.1117/12.429501>
55. Jolliffe IT, Cadima J. Principal component analysis: a review and recent developments. *Philos Trans R Soc A.* 2016;374(2065):1–16.
56. Jackson JE. *A User's Guide to Principal Components.* New York: Wiley; 2005.
57. Mahalanobis, P.C.: On the generalized distance in statistics. In: *Proceedings of the National Institute of Science of India.* 1936. vol. 2, pp. 49–55
58. Palik ED. *Handbook of Optical Constants of Solids.* Boston: Academic Press; 1985.
59. Marchioni, D.: *Conservation-restauration d'une vierge de douleur, panneau peint et doré de la fin du XVème siècle, et de son cadre doré et polychromé (Musée Jacquemart-André, Paris).* Recherche de provenance et datation de l'oeuvre. Etude comparative de différentes méthodes de nettoyage d'une dorure sur bois vernie. Master thesis, National Heritage Institute, Conservation Department. Paris, France. 2021
60. Kroustallis S, Gomez Gonzalez M, Miquel Juan M, Bruquetas Galan R, Perez Monzon O. Gilding in Spanish panel painting from the fifteenth and early sixteenth centuries. *J Mediev Iberian Stud.* 2016;8(2):313–43.
61. Fisher, S.L. *Introduction to the Painting Conservation Catalogue. Introduction to Volume I: Varnishes and Surface Coatings.* Washington DC: American Institute for Conservation; 1997.
62. Walter, B., Marschner, S.R., Li, H., Torrance, K.E. Microfacet models for refraction through rough surfaces. In: *Eurographics Conference on Rendering Techniques.* 2007, pp. 195–206. Eurographics Association

Publisher's Note

Springer Nature remains neutral with regard to jurisdictional claims in published maps and institutional affiliations.

Submit your manuscript to a SpringerOpen[®] journal and benefit from:

- ▶ Convenient online submission
- ▶ Rigorous peer review
- ▶ Open access: articles freely available online
- ▶ High visibility within the field
- ▶ Retaining the copyright to your article

Submit your next manuscript at ▶ [springeropen.com](https://www.springeropen.com)

Article E

Yoko Arteaga, Clotilde Boust, and Jon Y. Hardeberg. Quantifying the appearance of gilded surfaces. To appear in *Cultural Heritage Analysis for New Generations*, Degrigny, C., George, S., Hardeberg, J.Y. & Østlien, A., Routledge, 2023

This paper is submitted for publication and is therefore not included.

ISBN 978-82-326-7001-7 (printed ver.)
ISBN 978-82-326-7000-0 (electronic ver.)
ISSN 1503-8181 (printed ver.)
ISSN 2703-8084 (online ver.)



NTNU

Norwegian University of
Science and Technology